THE MECHANICS OF DIAMOND CORE DRILLING OF ROCKS

A

Dissertation

Presented to the Faculty of the University of Alaska

in Partial Fulfillment of the Requirements

for the Degree of

Doctor of Philosophy

By

Zhengwen W. Wang, B.S., M.S.

Fairbanks, Alaska

May 1995

THE MECHANICS OF DIAMOND CORE DRILLING OF ROCKS

by

Zhengwen W. Wang

RECOMMENDED:

Advisory Committee Chair

Sukumar Bandopadhyay
Head, Dept. of Mining & Geol. Engr.

APPROVED:

Dean, School of Mineral Engineering

Dean of the Graduate School

April 27, 1995
Date

Abstract

In an attempt to study the mechanics of diamond core drilling in rocks, an investigation on rock drillability was conducted at the University of Alaska Fairbanks. A series of drilling and coring tests was conducted on six types of rock using several different diamond bits. Factors involved in a diamond coring and drilling process such as weight-on-bit, rotational speed, and rock type were identified and the effects of those parameters were experimentally evaluated based on the penetration rate, applied torque, and specific energy. Statistical techniques were used to design the drilling tests and to develop drilling models. Fundamentals of rock failure mechanics in relation to rock drilling were reviewed. Several existing rock drilling models were also examined with the data from this study.

Results indicated that all of the three drilling parameters, i.e., the penetration rate, applied torque, and specific energy, were significantly affected by the weight-on-bit and rock type. The penetration rate of a bit was also affected by the rotational speed. The effects of the rotational speed on the applied torque and specific energy, however, were found to be insignificant.

It was also found that the theoretical models can be used to predict the maximum effective weight-on-bit and penetration rate. Among the four theoretical models examined, the elastic model predicted the most accurate penetration rate. The maximum effective weights-on-bit predicted by the plastic model and the two fracture models, however, were

close to each other and in agreement with the experimental observation.

Statistical models developed in this study were used to predict the penetration rate in the *Rock Drilling under the Greenland Ice Sheet* project. The variation between the predicted value and the actual value was less than 10%.

Table of Contents

Abstract iii

Table of Contents v

List of Figures xii

List of Tables xvii

Acknowledgements xx

CHAPTER 1 INTRODUCTION 1

CHAPTER 2 DRILLIBILITY AND ROCK CUTTING MECHANISM 5

2.1 ROCK DRILLABILITY STUDIES 5

2.2 FUNDAMENTALS OF ROCK FAILURE 12

2.2.1 Elastic Deformation 12

2.2.2 Plastic Deformation 14

2.2.3 Brittle Fracture 17

2.2.3.1 Griffith's Theory 17

2.2.3.2 Fracture Mode 18

2.2.3.3 Stress Intensity Factor 20

2.3 ROCK CUTTING THEORIES 22

2.3.1 Tensile Failure 22

2.3.2 Shear Failure 24

2.3.3 Abrasive Wear Theory 26

2.3.3.1 Plastic Deformation 28

2.3.3.2 Compressive Crushing 32

2.3.3.3 Brittle Fracture 32

CHAPTER 3 STATISTICAL DESIGN AND ANALYSIS 40

3.1 LATIN SQUARE DESIGN 40

3.2 ANALYSIS OF VARIANCE 46

3.3 REGRESSION ANALYSIS 50

3.3.1 General Linear Model 50

3.3.2 Stepwise Regression 53

3.3.3 Nonlinear Model 54

CHAPTER 4 LABORATORY DRILLING EXPERIMENT 55

4.1 INTRODUCTION 55

4.2 DRILLING TEST DESIGN 55

4.2.1 The Preliminary Rock Coring Test 56

4.2.2 The 6×6 Latin Square Design Drilling Test 56

4.3 EQUIPMENT FOR DRILLING TEST 57

4.3.1 Core Bits 57

4.3.2 Drilling System 61

4.3.3 Measuring Devices 61

4.3.4 Data Acquisition System 63

CHAPTER 5 PHYSICAL PROPERTIES OF MATERIAL 67

5.1 INTRODUCTION 67

5.2 MINERAL AND GRAIN SIZE 67

5.2.1 Mineralogy 67

5.2.2 Grain Size 68

5.3 STRENGTH PROPERTIES 69

5.3.1 Uniaxial Compressive Strength 69

5.3.2 Splitting Tensile Strength 70

5.3.3 Point Load Strength 71

5.3.4 Fracture Toughness 72

5.4 HARDNESS 74

5.4.1 Schmidt Hardness 75

5.4.2 Shore Schleroscope Hardness 76

5.5 RESULTS AND COMPARISONS 78

5.5.1 Relationships among Hardness Indices 80

5.5.2 Relationships among Strengths 82

5.5.3 Strengths vs. Shore Scleroscope Hardness 86

5.5.4 Strengths vs. Schmidt Hardness 86

CHAPTER 6 RESULTS AND DISCUSSIONS - PART I 90

6.1 INTRODUCTION 90

6.2 SURFACE-SET BITS 98

6.2.1 Penetration Rate 99

6.2.1.1 AQ1 Bit 99

6.2.1.2 BQ1 Bit 103

6.2.2 Applied Torque 107

6.2.2.1 AQ1 Bit 107

6.2.2.2 BQ1 Bit 111

6.2.3 Specific Energy 111

6.2.3.1 AQ1 Bit 116

6.2.3.2 BQ1 Bit 120

6.3 IMPREGNATED BITS 120

6.3.1 Penetration Rate 124

6.3.1.1 AQ2 Bit 124

6.3.1.2 BQ2 Bit 126

6.3.2 Applied Torque 126

6.3.2.1 AQ2 Bit 126

6.3.2.2 BQ2 Bit 133

6.3.3 Specific Energy 139

6.3.3.1 AQ2 Bit 139

6.3.3.2 BQ2 Bit 143

6.4 COMPARISON 147

6.4.1 Penetration Rate 147

6.4.2 Applied Torque 147

6.4.3 Specific Energy 150

6.5 CHAPTER SUMMARY 153

CHAPTER 7 RESULTS AND DISCUSSIONS - PART II 155

7.1 INTRODUCTION 155

7.2 PENETRATION RATE 156

7.2.1 ANOVA Test 156

7.2.2 Newman-Keuls Test 156

7.2.2.1 Weight-on-Bit 158

7.2.2.2 Rock Type 160

7.2.2.3 Rotational Speed 162

7.2.3 Regression Analysis 162

7.2.3.1 Weight-on-Bit 164

7.2.3.2 Rock Type 164

7.2.3.3 Rotational Speed 166

7.2.3.4 Multi-variable Regression Analysis 166

7.3 APPLIED TORQUE 171

7.3.1 ANOVA Test 171

7.3.2 Newman-Keuls Test 171

7.3.2.1 Weight-on-Bit 171

7.3.2.2 Rock Type 173

7.3.3 Regression Analysis 176

7.3.3.1 Weight-on-Bit 176

7.3.3.2 Rock Type 178

7.3.3.3 Multi-variable Regression Analysis 178

7.4 SPECIFIC ENERGY 181

7.4.1 ANOVA Test 181

7.4.2 Newman-Keuls Test 183

7.4.2.1 Weight-on-Bit 183

7.4.2.2 Rock Type 186

7.4.3 Regression Analysis 186

7.4.3.1 Weight-on-Bit 186

7.4.3.2 Rock Type 189

7.4.3.3 Multi-variable Regression Analysis 189

7.5 CHAPTER SUMMARY 192

CHAPTER 8 DRILLING PERFORMANCE PREDICTION AND ENGINEERING APPLICATION 193

8.1 PENETRATION RATE 193

8.2 WEIGHT-ON-BIT 196

8.3 ROTATIONAL SPEED 200

8.4 GREENLAND UNDER ICE SHEET BEDROCK CORING 201

8.5 CONCLUSIONS 206

Bibliography 207

Appendix

Appendix 1: F-distribution at α=0.05 215

Appendix 2: Newman-Keuls q-Values at α=0.05 216

Appendix 3: An example of data sheet from the 6-488B data acquisition system 217

Appendix 4: The Basic program used to extract peer data from the data logger 222

Appendix 5: Result of the preliminary rock coring test 223

Appendix 6: Result of the 6×6 Latin square drilling test 225

List of Figures

Figure 2.1: An elastic sphere being pressed against a plane 13

Figure 2.2: Schematic drawing illustrating the three fundamental modes of fracture 19

Figure 2.3: Stress field and geometry of a mode I crack 21

Figure 2.4: Illustration of tensile breakage of rock by a pick cutter 23

Figure 2.5: Illustration of shear failure of rock by a pick cutter 25

Figure 2.6: Illustration of (a) two-body and (b) three-body abrasive wear 27

Figure 2.7: Geometry of contact between an idealized conical abrasive particle and a surface. 29

Figure 2.8: Diagram showing crack formation in a brittle material due to point indentation. 33

Figure 2.9: Schematic illustration of material removal in a brittle material by the extension of lateral cracks beneath a plastic groove. 36

Figure 4.1: Surface-set and impregnated diamond bits. 59

Figure 4.2: A 20-inch drill Clausing press and its modifications. 62

Figure 4.3: SHC 6-488B data acquisition system. 64

Figure 4.4: Schematic of the laboratory drilling test procedures. 66

Figure 5.1: Schematic of the Chevron Bend method and specimen geometry for fracture toughness test. 73

Figure 5.2: Vickers hardness vs. Shore scleroscope hardness. 77

Figure 5.3: Schmidt hardness of core specimen vs. Schmidt hardness of bulk specimen. 83

Figure 5.4: Schmidt hardness vs. Shore scleroscope hardness. 84

Figure 5.5: Point load strength and splitting tensile strength vs. uniaxial compressive strength 85

Figure 5.6: Strengths vs. Shore scleroscope hardness. 87

Figure 5.7: Strengths vs. Schmidt hardness of bulk specimens. 88

Figure 6.1: Drilling test of BQ1 bit on rock A, Trial No. 1. 91

Figure 6.2: Drilling test of BQ1 bit on rock B, Trial No. 1. 92

Figure 6.3: Drilling test of BQ1 bit on rock C, Trial No. 1. 93

Figure 6.4: Drilling test of BQ1 bit on rock D, Trial No. 1. 94

Figure 6.5: Drilling test of BQ1 bit on rock E, Trial No. 1. 95

Figure 6.6: Drilling test of BQ1 bit on rock F, Trial No. 1. 96

Figure 6.7: Penetration rate vs. rock properties for AQ1 bit in the preliminary rock coring test. 101

Figure 6.8: Penetration rate vs. rock properties for BQ1 bit in the preliminary rock coring test. 105

Figure 6.9: Applied torque vs. rock properties for AQ1 bit in the preliminary rock coring test. 109

Figure 6.10: Applied torque vs. rock properties for BQ1 bit in the preliminary

rock coring test. 113

Figure 6.11: Specific energy vs. rock properties for AQ1 bit in the preliminary rock coring test. 118

Figure 6.12: Specific energy vs. rock properties for BQ1 bit in the preliminary rock coring test. 122

Figure 6.13: Penetration rate vs. rock properties for AQ2 bit in the preliminary rock coring test. 127

Figure 6.14: Penetration rate vs. rock properties for BQ2 bit in the preliminary rock coring test. 130

Figure 6.15: Applied torque vs. rock properties for AQ2 bit in the preliminary rock coring test. 134

Figure 6.16: Applied torque vs. rock properties for BQ2 bit in the preliminary rock coring test. 137

Figure 6.17: Specific energy vs. rock properties for AQ2 bit in the preliminary rock coring test. 141

Figure 6.18: Specific energy vs. rock properties for BQ2 bit in the preliminary rock coring test. 145

Figure 6.19: Penetration rate vs. uniaxial compressive strength for all the four bits in the preliminary rock coring test. 148

Figure 6.20: Applied torque vs. uniaxial compressive strength for all the four bits in the preliminary rock coring test. 149

Figure 6.21: Specific energy (kerfing) vs. uniaxial compressive strength for all the four in the preliminary rock coring test. 151

Figure 6.22: Specific energy (core recovery) vs. uniaxial compressive strength for all the four bits in the preliminary rock coring test. 152

Figure 7.1: Penetration rate vs. weight-on-bit in the Latin square drilling test. . . 165

Figure 7.2: Penetration rate vs. uniaxial compressive strength in the Latin square drilling test. 167

Figure 7.3: Penetration rate vs. rotational speed in the Latin square drilling test. . 168

Figure 7.4: Applied torque vs. weight-on-bit in the Latin square drilling test. . . . 177

Figure 7.5: Applied torque vs. uniaxial compressive strength in the Latin square drilling test. 179

Figure 7.6: Specific energy (kerfing) vs. weight-on-bit in the Latin square drilling test. 188

Figure 7.7: Specific energy (kerfing) vs. uniaxial compressive strength in the Latin square drilling test. 190

Figure 8.1: Penetration rate predicted by theoretical models vs. actual experimental data. 195

Figure 8.2: Maximum effective weight-on-bit vs. uniaxial compressive strength of rock. 198

Figure 8.3: Normalized penetration rate vs. weight-on-bit for BQ1 bit on granite rock. 199

Figure 8.4: Maximum rotational speed vs. weight-on-bit for BQ1 bit. 202

List of Tables

Table 3.1: An example of a 6×6 Latin square. 41

Table 3.2: ANOVA table for a n×n Latin square. 44

Table 3.3: Mean difference arrangement for Newman-Keuls test. 48

Table 4.1: The 6×6 Latin square design for rock drilling test with BQ1 bit. 58

Table 4.2: Summary of diamond core bits. 60

Table 5.1: Rock physical properties. 79

Table 5.2: Coefficients of determinations among rock physical properties in the preliminary rock coring test. 81

Table 6.1: Regression analysis of penetration rate for AQ1 bit in the preliminary rock coring test. 100

Table 6.2: Regression analysis of penetration rate for BQ1 bit in the preliminary rock coring test 104

Table 6.3: Regression analysis of applied torque for AQ1 bit in the preliminary rock coring test. 108

Table 6.4: Regression analysis of applied torque for BQ1 bit in the preliminary rock coring test. 112

Table 6.5: Regression analysis of specific energy for AQ1 bit in the preliminary rock coring test. 117

Table 6.6: Regression analysis of specific energy for BQ1 bit in the preliminary rock coring test. 121

Table 6.7: Regression analysis of penetration rate for AQ2 bit in the preliminary rock coring test. 125

Table 6.8: Regression analysis of penetration rate for BQ2 bit in the preliminary rock coring test. 129

Table 6.9: Regression analysis of applied torque for AQ2 bit in the preliminary rock coring test. 132

Table 6.10: Regression analysis of applied torque for BQ2 bit in the preliminary rock coring test. 136

Table 6.11: Regression analysis of specific energy for AQ2 bit in the preliminary rock coring test. 140

Table 6.12: Regression analysis of specific energy for BQ2 bit in the preliminary rock coring test. 144

Table 7.1: Results of ANOVA test for penetration rate. 157

Table 7.2: Newman-Keuls test for weight-on-bit on penetration rate. 159

Table 7.3: Newman-Keuls test for rock type on penetration rate. 161

Table 7.4: Newman-Keuls test for rotational speed on penetration rate. 163

Table 7.5: Summary of regression analysis for penetration rate in Latin square drilling test. 170

Table 7.6: Results of ANOVA test for applied torque. 172

Table 7.7: Newman-Keuls test for weight-on-bit on applied torque. 174

Table 7.8: Newman-Keuls test for rock type on applied torque. 175

Table 7.9: Summary of regression analysis for applied torque in Latin square drilling test. 180

Table 7.10: Results of ANOVA test for specific energy. 182

Table 7.11: Newman-Keuls test for weight-on-bit on specific energy. 184

Table 7.12: Newman-Keuls test for rock type on specific energy. 187

Table 7.13: Summary of regression analysis for specific energy in Latin square drilling test. 191

Table 8.1: Geometry constants for the theoretical drilling models for BQ1 bit. . . 194

Table 8.2: Summary of drilling parameters of the GISP2 bedrock coring. 204

Acknowledgements

I would like to express my sincere appreciation to all the members of my graduate committee, Drs. Scott L. Huang, John J. Kelley, Robert C. Speck, William M. Sackinger, John P. Zarling, and Mr. Kerry L. Stanford for their helpful criticism in the preparation of this thesis.

I am particularly grateful to Dr. Huang, chairman of my advisory committee, who has given me the greatest help since I came to the University of Alaska Fairbanks. Without his generous support and understanding, this research project could not have been accomplished. Special thanks are also given to Dr. John Kelley, Director of Polar Ice Coring Office at the University of Alaska Fairbanks, for his continuous support and encouragement. Mr. Jesse T. Collins, an engineer of the Polar Ice Coring Office, was deeply involved in this research project. His work included drill system modification, fabrication of some machine parts, and purchase of a data acquisition system and monitoring devices. He also directly participated in some of the drilling and coring experiments.

During the course of my Ph.D. program, I received a lot of help from many individuals at the University of Alaska Fairbanks: Dr. Gang Chen, Mr. Edwin Baine Kroeger, and Ms. Lucy Trant.

Special thanks should be given to my fine wife, Hong Lee, for her gracious support and understanding during my study and assistance in the preparation of this thesis.

She has input a great amount of experimental data from my drilling experiments into the computer. The most noteworthy event during this period may be that Hong Lee gave birth to our first child -- Michael Lee Wang. That was a lot of work. But it was very rewarding, too.

Finally, I would like to express my gratitude to the people at the Polar Ice Coring Office of the National Science Foundation and the Department of Mining and Geological Engineering at the University of Alaska Fairbanks, and to the city of Fairbanks where we have been spent five wonderful years.

CHAPTER 1

INTRODUCTION

The first diamond drill was designed by a Swiss engineer, Jean Rudolphe Leschot, in 1862. Since then, diamond drilling has become one of the most common and effective ways for boring holes in hard rocks. The basic idea of diamond drilling, however, has not changed significantly, regardless of a wide variety of equipment used and strata drilled. Improvement of operation efficiency and better utilization of energy expended in rock drilling have been always the goal of drilling industry ever since the diamond rotary drill existed.

Drillability is the prediction of drilling performance based on the specifications of a drill system and the properties of rock to be drilled. Many investigations have been done on the drillability studies of diamond drilling since the 1950's. A variety of mathematical relationships have been developed to transform laboratory measurements into predictions of drilling rate and energy requirements in field operation. These relationships, often known as drillability equations, are derived from theoretical or empirical approaches.

A mathematical model (i.e., theoretical and empirical) is a functional relationship between causes and effects in a process. It defines the process and relates the dependent with independent variables in order to predict results and possibly provide control to that

process. The difference between an empirical model and a theoretical model lies in the element of drilling performance each method predicts. An empirical drillability model provides a formula to predict the drilling rate or energy requirements for a given system from one or more quantities which can be decided from laboratory tests. A theoretical model, however, describes the processes taking place at the rock-bit interface and cutting mechanism of the drill bit.

Either one of the theoretical model or the empirical model has its own merits and limitations as well. For example, a regressional analysis of the experimental results from a process produces an empirical relationship between dependent and independent variables. Most of the drillability equations in the literature fall in this category. The empirical model is useful to predict the performance of a specific drilling operation. It, however, can only be constructed using results from an established operation, and should only be used in connection with that operation. It is, however, of limited use when a drilling condition is changed. Its use for design of a drill is restricted as well, unless vast amounts of data are accumulated from many varying operations.

In contrast to the empirical approach, development of successful theoretical models needs an identification of all variables involved, a thorough understanding of the fundamentals of a process, and the appropriate mathematical tools. With these factors, an adequate and usable functional relationship can then be formulated. It may be relatively easy to express the overall form of a theoretical model of a process. Transformation of the model into usable information for field practice, however, can be difficult and can

result in an inaccurate prediction of an operation due to the over-simplified assumptions embedded in the theoretical models. Furthermore, theoretical evaluation of drilling parameters is virtually impossible, and the use of experimentally derived parameters with statistical techniques becomes a necessary supplement. This situation is especially common in such a complex process as drilling, and creates a situation in which most of the mathematical models are empirical.

This thesis presents the results of an investigation involving a diamond drilling experiment on six rock types. Rock failure mechanism, in relation to the diamond drilling process, was studied as well. The project focused on identification and evaluation of the variables involved in a diamond rock drilling, and provided a better understanding of the fundamentals of rock cutting mechanism with diamond bits.

In Chapter 2, literature in rock drillability and rock cutting mechanism is reviewed. This literature review includes not only diamond drilling but also several related drilling methods. Several rock failure mechanisms in relation to drilling are discussed. Theoretical relationships between drilling parameters and drill performance, developed for diamond coring bits, are discussed.

Because statistical techniques such as experimental design, variance analysis, and regression analysis were used throughout this research, it is necessary to review some of the relevant statistical fundamentals. Chapter 3 provides a brief summary of the basic statistical theories used.

Laboratory drilling and coring tests were the major portion of this research. The statistical models were developed from results of the drilling tests. Existing drilling and

rock cutting theories were also examined and compared with the experimental data obtained through this project. Two sets of rock drilling tests were performed in this research. One was a preliminary rock coring test and the other was a rock drilling test using a 6×6 Latin square design. In Chapter 4, those two types of drilling experiments and the equipment used in the tests are described.

Physical properties of testing materials are presented in Chapter 5. Six types of rocks were used in this study. Rock properties investigated in this work included mineralogy, grain size, strength properties, and hardness indices. Statistical comparisons of those properties are also presented in this chapter.

In Chapter 6, the results from the preliminary rock coring test are reported. This drilling test was designed to compare the performances of four diamond core bits. Discussions are focused on how the rock properties affected the bit performance.

The results of the rock drilling test are discussed in Chapter 7. Three independent drilling factors (i.e., weight-on-bit, rotational speed, and rock type) identified as parameters in a 6×6 Latin square design were evaluated. Observations noted in this evaluation included penetration rate, applied torque, and specific energy. The observations were correlated with the three independent variables. Statistical models were developed to predict the bit performance.

In Chapter 8, factors affecting drilling operations are discussed. Rock cutting theories and drilling models were evaluated based on the experimental data. Engineering applications of this study to the *Rock Drilling under the Greenland Ice Sheet* project are also presented.

CHAPTER 2

DRILLABILITY AND ROCK CUTTING MECHANISM

2.1 ROCK DRILLABILITY STUDIES

Studies of rock drilling mechanism stem from the attempt to predict drilling speed of a drill system. These studies have resulted in a number of drillability models which are applied in field operation with varying degrees of substantiation. Although most of these studies are empirical in nature, there are some generic rock failure mechanisms, explicitly or implicitly, behind them.

Early researchers attempted to use rock properties as a direct measure of the drillability. The earliest report on drillability was made by Gyss and Davis in 1927 (Paone and Bruce, 1963), who proposed a theory stating that speed of drilling was a function of rock hardness and toughness. Shepherd (1950) evaluated the critical load or thrust with abrasiveness, work hardening value, and Shore scleroscope hardness on rock drillability, and found that none of these factors were important to rotary drilling. Contrary to Shepherd's findings, in a parallel work Alpan (1950) correlated rock physical properties with penetration rates. He claimed that each of the factors of crushing strength, Shore hardness, toughness, and resistance to abrasion had a similar effect on penetration, and that any one of the properties could describe drillability.

Fransen (1950) developed a workability index by pressing an indenter into materials, and from the load-penetration curves a rough correlation was found between

the load and the penetration rates. Another drillability index, developed by Sievers (1950), was based on abrasiveness of rock by measuring the penetration depth in a fixed period of time using constant thrust and rotational speed. Head (1950), on the other hand, penetrated rock specimens of a fixed depth with a constant thrust and rotational speed and measured the time interval. He devised a similar drillability index. Kinoshita (1956) correlated the number and size of quartz grains in rocks and Shore hardness with penetration rate, and stated that the rock properties were insufficient as a measure of drillability.

Energy criteria were also used by researchers in earlier years. Harley (1926) first devised a method of hardness classification based on the energy required to cut a unit volume of rock in a drill hole. This idea was advanced by Teale (1965) as a means of drillability measurement and he named it the *Specific Energy*. Opolski (1956) determined drillability of coal by the amount of energy required to produce 1 cm^3 of coal. Goodrich (1956) reported a drillability concept based on the depth of hole drilled in a unit time per bit weight at a constant rotational speed. Mechanical energy input to rock and the drilling strength of rock were correlated by Simon (1956) to predict penetration rate for rock drilling. He concluded that the penetration rates were directly proportional to mechanical power input of a drill.

It was in the late 1950's that compressive and tensile strengths were combined into drillability models. Shimomura and Takato (1958) conducted diamond drilling tests and concluded that the compressive and tensile strengths were related to the penetration rate. For impregnated bits they found that abrasive hardness showed an even better correlation

with penetration rate than did the correlation with the compressive and tensile strengths.

Fish (1961) conducted extensive investigations on a small hole rotary drill. He noted that the most important rock properties in drillability were strength properties that could significantly influence the drilling forces during a drilling process, the abrasive properties that determine rate of bit wear, and the structure properties that determine the nature of drill cuttings.

A laboratory drop-test was conducted by Hartman (1962) to study the relationship between crater volume and the principal variables involved in a percussive drilling process. He suggested that the general crater-volume relation would appear to be valid for any rock type and, thus, developed a drillability model based upon the above parameters.

Sasaki et al. (1962) performed a diamond drillability study by changing thrust, rotational speed, and torque. Their result showed that the penetration rate and maximum thrust could be predicted from measurements of Shore scleroscope hardness, indentation depth, and compressive strength of rock.

A drillability study of a diamond core bit was conducted by Paone and Bruce (1963) on various types of rock. Compressive strength, tensile strength, Young's modulus, and shear modulus were correlated with the penetration rate. They concluded that the penetration rate was directly related to the drilling strength of rock, which approximates its uniaxial compressive strength. They developed a semi-theoretical drillability equation for surface-set diamond bits. In their equation, thrust force, uniaxial compressive strength, frictional resistance of rock, and applied torque were combined to calculate the penetration depth per revolution of rotation.

Laboratory and field drillability studies on impregnated diamond bits were carried out by Paone and Madson (1966), and their results were compared with the results for surface-set bits by Paone and Bruce (1963). They found that the penetration rates correlated well with the compressive and tensile strengths of rock. The penetration rates achieved by surface-set bits were substantially higher than that achieved by the impregnated bits. Furthermore, penetration rates achieved by the surface-set bits in the field did not show significant difference from rates measured in the laboratory.

Results from the above two studies were statistically analyzed by Paone et al. (1966). They concluded that the drilling capability (i.e., penetration rate) of both surface-set and impregnated bits depended on the thrust force, rotational speed, compressive strength of rock, Shore hardness, and quartz content of the rock. For impregnated diamond bits, they found that the most significant parameters were thrust, Young's modulus, shear modulus, abrasiveness, quartz content, and compressive strength. A statistical regression analysis indicated that all the physical properties were highly correlated with each other.

A study similar to Paone et al.'s (1963 and 1966) work was conducted by Tsoutrelis (1969) with a rotary diamond bit and comparable results were produced. It was found that the penetration rate was significantly correlated with the compressive strength of rock. They also demonstrated that the drillability equation could be used to accurately predict the compressive strength of an unknown rock. Based on the experiences from open pit mining, Bauer and Calder (1967) took into account the thrust force and rotational speed and showed that a correlation could be obtained by comparing the penetration rate

to the uniaxial compressive strength of rock.

Duklet and Bates (1981) developed an empirical equation for predicting the penetration rate of diamond bits for oil well drilling. Five parameters were included in their equation: average load per diamond, rotary speed, hydraulic horsepower per unit area, mud fluid loss rate, and a rock strength index called *Effective Formation Strength*, which is the sum of the compressive strength and the hydrostatic pressure below the bit.

Brown et al. (1981) reviewed the influence of rock anisotropy on hole deviation in rotary drilling for oil well drilling. They discussed a drilling rate prediction equation which considered the torque, thrust, bit diameter and a drillability strength index which was not fully defined.

Leighton et al. (1982) studied a rotary blasthole drill with carbide-tipped tricone bits and stated that if the same equipment and rotational speed were applied in the drilling processes, the ratio of thrust to penetration rate reflected the changes in formation strength.

Attempts have also been made to relate the specific energy with rock brittleness. Conflicting conclusions, however, exist among different sources. For example, the experimental work of Pozin et al. (1979) produced a conclusion that higher specific energy was attributed to a less brittle coal. Singh (1987) showed that a directly proportional relationship existed between *in-situ* specific energy and brittleness of three Utah coals. Göktan (1991), however, reviewed rock brittleness and specific energy for chisel picks from five different sources, and concluded that there were no reliable relationships which could be found between these two measurements.

Controversial conclusions also exist for the specific energy as a drillability index. Rabia (1982) compared the specific energy of percussive and rotary drilling in the laboratory and in the field. He stated that the specific energy was sensitive to the type of drill and drilling conditions.

Rock fracture theories were introduced into the drillability studies more recently. A rock fracture model of rotary drilling with a cone bit developed by Eronini et al. (1982a) assumed that the bit action was made up of independent indentation by each of the individual teeth. The subsequent fragmentation process in the rock was determined by the rotary power and the axial and lateral forces. They (1982b) also described a dynamic model of rotary drilling with a cone bit. They stated that the vibration arising upon the pulsation of the mud flow might introduce a percussive effect in the bit forces and improve the penetration rate.

Another rock cutting theory concerning rock fracture was proposed by A. G. Cherepanov and G. P. Cherepanov in 1990. In their model, the maximum cutting force was predicted based upon a rock property, namely, *sliding viscosity*, in a brittle mode. The invariant Γ-integral was used to derive the equation, and rock cracking was considered. However, the rock property employed in the equation could not be measured.

A systematic approach was used to develop a kinematic model of the roller cone bit by Umez-Eronini (1983). This model was integrated with a rock fracture description to simulate the test data from a study on the effects of bit offset. Other drillability studies concerning the kinematics can be found in the work of Ma and Yang (1985), Schumacher et al. (1983), and Feng and Schumacher (1983).

Besides drilling rate, energy requirements, and cutting force prediction in drillability studies, some researchers have used applied torque as a drillability criterion. For example, the relationships between applied torque and other drilling parameters of a percussive drill were investigated by Unger and Fumanti (1972), Pearse (1985), and Sinkala (1991). A common observation is that when other conditions are the same, the minimum applied torque required to rotate a percussive bit decreases with the increasing hardness of rock.

Conclusions from these wide aspects of drillability studies indicate that drilling rate and energy requirements of a diamond drill depend on many factors. Two types of influential factors can be distinguished. The bit type, bit diameter, bit geometry, diamond quality, diamond size and geometry, weight-on-bit, rotational speed, and circulating fluid are the controllable design and operation variables in a diamond drilling system. Formation properties, including rock properties and geological conditions are, however, the uncontrollable factors in drilling. The subjects of a drillability study can be one or more of the following topics: 1) identification of the influential drilling parameters; 2) evaluation of the influential factors on drilling performance, using different criteria; 3) correlation between influential factors and drillability; and 4) prediction of drilling performance for a certain ground condition and a drill system.

2.2 FUNDAMENTALS OF ROCK FAILURE

Theories of rock cutting originate from metal cutting. A common assumption in metal cutting is that chips are formed by shearing the surface material. Action of diamond cutting can be described as a hard particle of arbitrary shape being pressed into a solid half-space by a specific normal force, and then moving under the action of a tangential force along the boundary of the half-space. Breaking of the surface layer of the solid material consequently occurs, and the broken fragments of the material is then removed by circulating fluids. The rock failure mechanism under a diamond bit, however, is not as clear because of the lack of research on this aspect.

2.2.1 Elastic Deformation

The elastic contact between a sphere and a plane has been extensively studied in the past. When a sphere of an elastic material is pressed against the host plane of a second elastic material (Figure 2.1) under a normal load w, a contact will occur between two bodies over a circular area of radius a, given by Hertz's equation (1881):

$$a = \left(\frac{3wr}{4E}\right)^{1/3} \qquad (2.1)$$

$$\frac{1}{E} = \frac{(1-\nu_1^2)}{E_1} + \frac{(1-\nu_2^2)}{E_2} \qquad (2.2)$$

where:

r is the radius of the sphere,

E_1, E_2 are Young's moduli of the materials of the sphere and plane, respectively, and

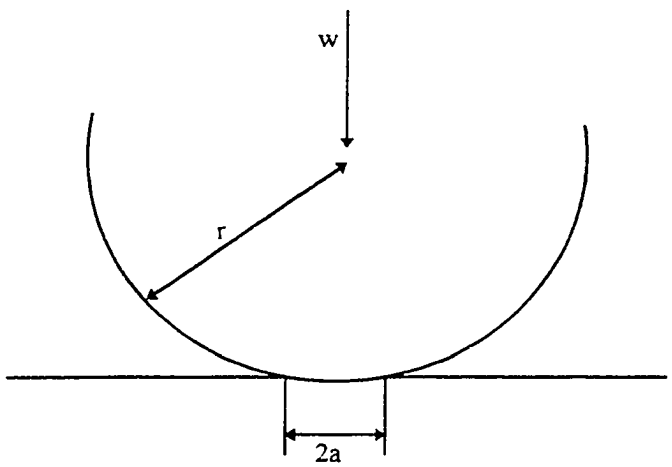

Figure 2.1: An elastic sphere being pressed against a plane

υ_1, υ_2 are Poisson's ratios of the materials of the sphere and the plane, respectively. The area of contact between the sphere and the plane, πa^2, is thus given by:

$$A=\pi a^2=\frac{9\pi}{16}\left(\frac{Wr}{E}\right)^{2/3} \qquad (2.3)$$

In this case, when the deformation is purely elastic, the area of contact is proportional to $w^{2/3}$. The mean pressure (i.e., mean normal stress) over the contact area is $P_{mean}=w/\pi a^2$, and thus is proportional to $w^{1/3}$. This normal stress is not uniformly distributed over the circular area of contact, but has a maximum value of $1.5P_{mean}$ at the center and falls to zero at the edges.

Under an elastic compressive stress field, rock will eventually fail when strain developed in the rock body exceeds a yield value. In such a case, the maximum stress on the stress-strain curve defines the compressive strength of material for this specific condition.

2.2.2 Plastic Deformation

Pure elastic compressive deformation is rarely the case in the deformation of a natural material. When the normal load between the sphere and the plane is increased, some components of the system may start to deform plastically. In the case of diamond rock drilling, the modulus of elasticity of diamond is so much larger than the modulus of elasticity of the rock (440-589 GPa vs. 10-60 GPa), that the diamond can be considered rigid and plastic deformation will occur only in the rock surface. Kragelskii (1965) proposed an equation to express the transition from elastic deformation to plastic

deformation as follows:

$$d=240\frac{\sigma_Y^2}{E^2}r \qquad (2.4)$$

where:

d is the penetration depth of the sphere,

r is the radius of the sphere,

σ_Y is the uniaxial yield strength of the surface material, and

E is the Young's modulus of the surface material.

Indentation tests are extensively employed in studying the hardness of metals (Tabor 1951, Mott 1956). The indentation of a rock surface by chisel bits has also been studied in relation to rock failure (Cheatham and Gnirk, 1967; Jaeger and Cook, 1976). Hertz's analysis (Durelli et al., 1958) of the elastic stress field due to a spherical indenter on a flat surface showed that the maximum shear stress beneath the indenter occurs at a depth of about 0.47 times the radius of the contact circle. This is the point where plastic flow first occurs. If shear failure occurs, the shear stress which initiates plastic flow is one-half of the uniaxial yield strength of the material.

If the normal load is increased further, the zone of plastic deformation extends from underneath the indenter until it eventually reaches the surface. At this point, Tabor (1951) indicated that the mean pressure over the contact area has risen at this stage to a constant value and remains at nearly the same value for further increases in load. In other

words, once the plasticity has been fully developed the mean contact pressure becomes independent of load. The constant proportionality between the pressure and the yield stress of the indented material provides the basis for indentation hardness testing.

Observations from Prandtl and Hencky (Tabor, 1951) in the studies of plastic deformation of material during the indentation test indicated that hydrostatic pressure itself plays no part in producing a plastic flow. The cause of plastic flow is the maximum shear stress or the maximum shear strain energy. Tabor (1956) further found that two-thirds of the mean contact pressure is in the form of hydrostatic pressure, and only one-third remains to cause plastic deformation,

$$P_{mean}=3\sigma_Y \tag{2.5}$$

For fully plastic deformation, the yield strength σ_Y is approximately the magnitude of the uniaxial tensile strength (σ_t). For rock materials, Zhao et al. (1994) argued σ_Y approximates the uniaxial compressive strength (σ_c).

Johnson (1970) considered an indenter to be encased in a hemispheric cone and assumed that a hydrostatic uniform pressure exists throughout the cone, which is equal in magnitude to the mean contact pressure:

$$\frac{P_{mean}}{\sigma_Y}=\frac{1}{\sqrt{3}}\left[1+\ln\left(\frac{4E}{3\pi\sigma_Y\tan\frac{\theta}{2}}\right)\right] \tag{2.6}$$

where θ is the angle of the indenter cone and E is Young's modulus of the surface material.

2.2.3 Brittle Fracture

Apart from the plastic deformation one may consider brittle fracture, in which the material behaves elastically until failure. In conventional rock strength testing devices, due to the instability of the machine-specimen system, brittle fracture occurs spontaneously at the peak stress in a stress-strain curve. The loading capacity of the material drops to a minimum rapidly after the failure. In cases like this, strength failure and fracture become synonymous.

However, in a stiff testing machine, some rock can withstand a partial load after the peak stress is reached. In a carefully designed experiment, it is possible to observed all the phenomena beginning with crack initiation, followed by crack propagation, partial loss of loading capacity, gradual damage of the material, to total failure.

2.2.3.1 Griffith's Theory

Fracture mechanics is originally derived from Griffith's work. Griffith (1920) postulated that the presence of small cracks or flaws in material may cause stress concentration at the tips of pre-existed cracks when the material is stressed. The crack would start to extend when tensile stress at the crack tip attains a certain value. It was believed that this critical value represented the molecular cohesion strength of the material (Orowan, 1949). Because this molecular cohesion strength is difficult to determine by direct measurement, this critical tensile stress at a crack tip is expressed by relating the principal stress components of applied stress field to the uniaxial tensile strength of the material at the stage of fracture initiation, as follows:

$$(\sigma_1-\sigma_3)^2=-8\sigma_t(\sigma_1+\sigma_3) \qquad (2.7)$$

where σ_1 and σ_3 are the major and minor principal stresses, and σ_t is the uniaxial tensile strength of the material.

Griffith's theory does not consider the effect of closure of cracks under a compressive stress field. McClintock and Walsh (1963) modified Griffith's hypothesis by introducing a coefficient of internal friction (μ) between crack faces. Their expression is in the following form:

$$\sigma_1=\frac{4\sigma_t}{(1-\frac{\sigma_3}{\sigma_1})\sqrt{1+\mu^2}-(1+\frac{\sigma_3}{\sigma_1})} \qquad (2.8)$$

Since the uniaxial compressive strength is easier to determine in a laboratory experiment than is the tensile strength, it is also used as the critical quantity in place of the uniaxial tensile strength. Bieniawski (1967) gave a modified Griffith criterion by using the uniaxial compressive strength and the coefficient of internal friction:

$$\sigma_1=\sigma_3(\sqrt{1+\mu^2}+\frac{\mu}{\sqrt{1+\mu^2}}-\mu)+\sigma_c \qquad (2.9)$$

where σ_c is the uniaxial compressive strength of a rock.

2.2.3.2 Fracture Mode

More recently three basic modes of crack tip displacement have been distinguished in fracture mechanics of rock. Figure 2.2 shows the three fracture modes. In problems concerning crack loading the superposition of these three basic modes is sufficient to

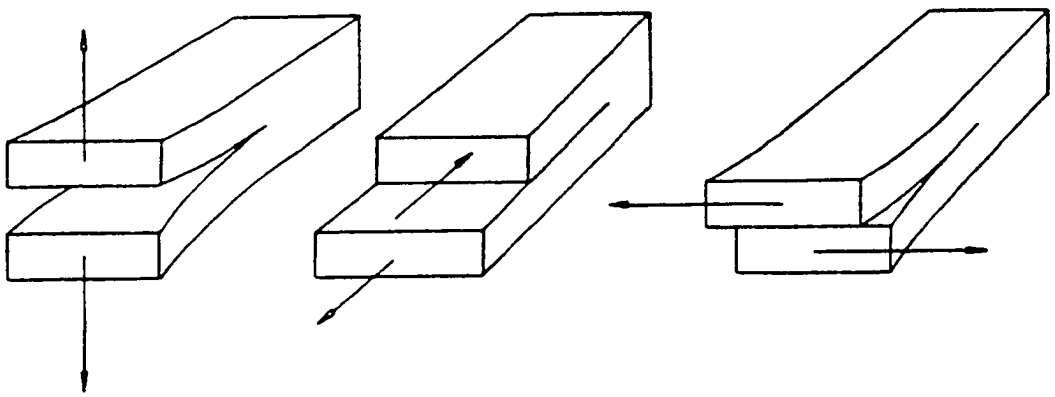

Figure 2.2: Schematic drawing illustrating the three fundamental modes of fracture: a-mode I, tensile or opening mode; b-mode II, in-plane shear or sliding mode; c-mode III, anti-plane shear or tearing mode (from Evans and Pomeroy, 1966)

describe most cases of crack tip deformation and stress field. Among them the mode I is most common and the majority of experimental data are also focused on this mode of fracture.

2.2.3.3 Stress Intensity Factor

Stress intensity analysis aims to give a measure of the real forces applied to a crack tip, which will determine whether a crack will grow or remain stable. Stress intensity factor K is, at least in the linear elastic fracture mechanics (LEFM), the governing parameter. The basic relationship equates K to a critical value, which is often taken as a material property, and called the plane strain *fracture toughness*, K_c. When K reaches K_c at the crack tip, the crack is assumed to grow until the rock fails, if $K \geq K_c$ holds true throughout loading. The growth stops if and when K drops below K_c. Figure 2.3 presents the stress field and geometry of a crack. The stresses near the tip of a crack are given by:

$$\sigma_x = \frac{K}{(2\pi r)^{1/2}} \cos\frac{\theta}{2}\left(1+\sin\frac{\theta}{2}\sin\frac{3\theta}{2}\right) \qquad (2.10)$$

$$\sigma_y = \frac{K}{(2\pi r)^{1/2}} \cos\frac{\theta}{2}\left(1-\sin\frac{\theta}{2}\sin\frac{3\theta}{2}\right) \qquad (2.11)$$

$$\tau_{xy} = \frac{K}{(2\pi r)^{1/2}} \cos\frac{\theta}{2}\sin\frac{\theta}{2}\cos\frac{3\theta}{2} \qquad (2.12)$$

where:

K is mode I stress intensity factor,

r is the distance measured from the crack tip, and

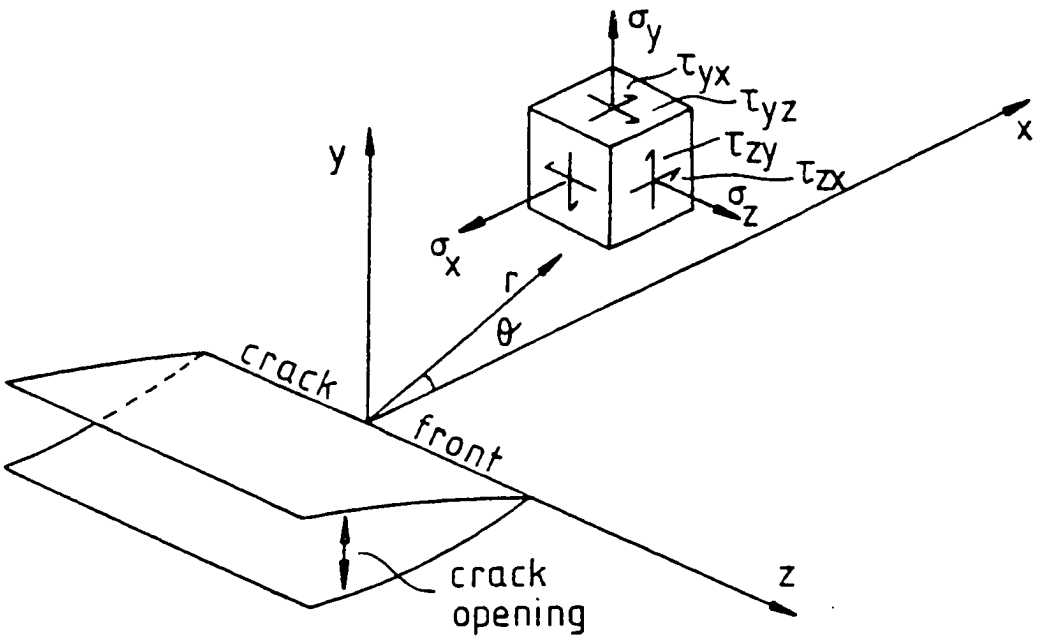

Figure 2.3: Stress field and geometry of a mode I crack (from Evans & Pomeroy, 1966)

θ is the angle between vector **r** and plane xz.

For a two-dimensional crack, the stress intensity factor is given by:

$$K=\sigma_r(\pi C)^{1/2} \qquad (2.13)$$

where σ_r is the applied remote stress, and c is one half length of a crack.

2.3 ROCK CUTTING THEORIES

2.3.1 Tensile Failure

One of the fundamental rock cutting theories based on tensile failure of rock was proposed by Evans (1966). It was originally developed to describe coal cutting by picks, and later research by Roxborough (1973) and Whittaker and Szwilski (1973) indicated that Evan's model is also applicable to the general field of rock cutting.

Figure 2.4 illustrates the Evans' model. It describes the penetration of a wedge into rock. According to Evans, the breakage is caused by tearing along a circular path, fh. The assumption is that the rock fails basically by brittle fracturing with the dominating tensile strength. In Figure 2.4, R is the force acting normal to the wedge's leading edge, T is the tensile force resulting from tearing along the circular path, and S is the force required to maintain an equilibrium in rock. When a wedge with a 2θ angle attacks a rock with tensile strength σ_t at cutting depth d, the total cutting force required, F_c, is:

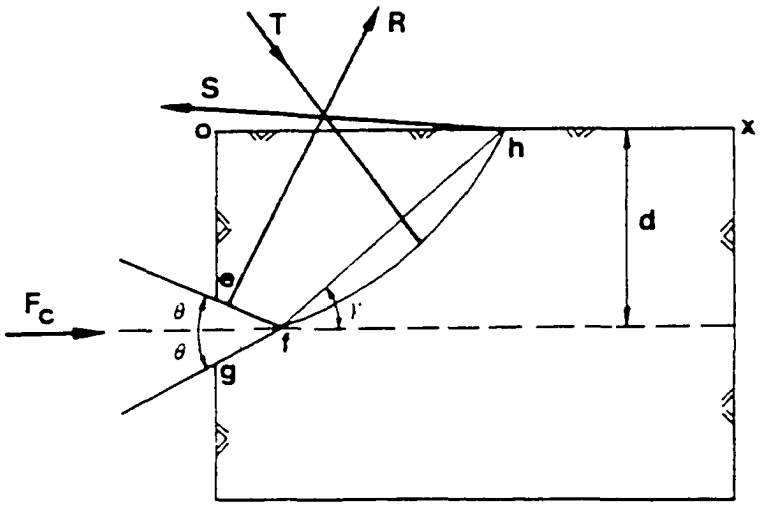

Figure 2.4: Illustration of tensile breakage of rock by a pick cutter (from Evans, 1966)

$$F_c = \frac{d\sigma_t \sin\theta}{\sin\gamma\cos(\theta+\gamma)} \qquad (3.14)$$

2.3.2 Shear Failure

Coulomb failure criterion can be employed to describe cutting models based on shear failure. As a cone or a pick is pushing into rock (Figure 2.5), the rock will fracture in some preferred failure angle, β. Nishimatsu (1972) studied this failure mechanism and incorporated shear failure into a chisel pick cutting equation to predict the required cutting force:

$$F_c = \frac{2\tau d W \cos\phi\cos(\psi-\alpha)}{(n+1)\,[1-\sin(\phi-\alpha+\psi)]} \qquad (2.15)$$

where:

τ is the shear strength of the rock,

d is the depth of cut,

W is the width of the pick,

ϕ is the angle of internal friction of the rock,

ψ is the angle of friction between the rock and the pick material,

α is the rake angle, a nd

n is the stress distribution factor.

Evans' tensile breakage theory and Nishimatsu's shear failure theory were examined by Göktan (1990), based on the experimental data for pick cutters from Bilgin (1977). Results revealed a similar trend with both theories. At zero or negative rake angle,

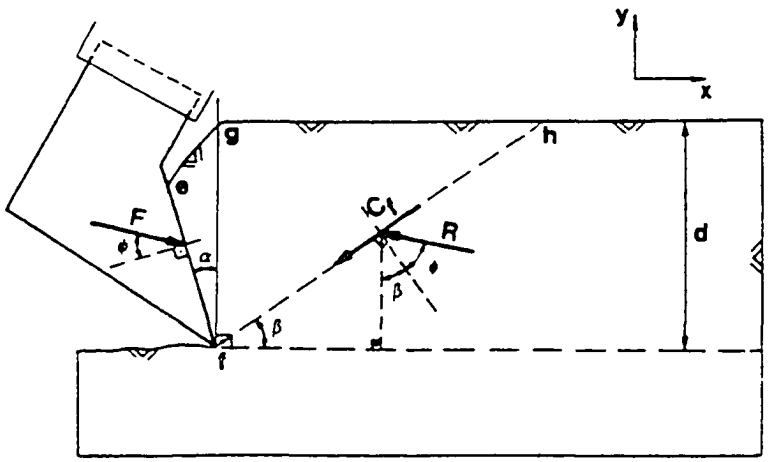

Figure 2.5: Illustration of shear failure of rock by a pick cutter (from Nishimatsu, 1977)

Nishimatsu's model gave a better prediction than did the Evan's model, although neither could produce a reasonably accurate result.

It is the author's opinion that application of the above theories to diamond drilling is limited. Diamond cutters are relatively small compared to the pick cutters. The size of diamond particles in a diamond core bit is about the same size as the mineral grains in rocks, or even smaller. When a rock material is broken under a diamond core bit, the failure is more likely to be along the grain boundary instead of a shear surface through the mineral grains. Furthermore, in diamond coring drilling, there is no free surface (*oh* in Figure 2.4 and *gh* in Figure 2.5) allowing the rock to fail in tension or in shear.

2.3.3 Abrasive Wear Theory

A close view of diamond bits reveals that the diamond particles protrude from the bit matrix. When the bit is forced against and slides on the rock surface, small rock particles are produced and removed from the rock surface. In such a case, abrasive wear might be experienced by the bit and the rock.

For abrasive wear in drilling, a distinction can be made between two-body abrasive wear by diamonds, illustrated in Figure 2.6(a), and three-body abrasive wear by rock debris shown in Figure 2.6(b). In the case of two-body abrasion, wear is caused by hard diamond particles on the bit, while in three-body wear, abrasive particles (i.e., rock cuttings) are produced by the drilling process itself and are free to roll and slide between bit and rock surface. Generally, the rate of three-body wear is much lower than that of two-body wear, given the same abrasive particles and surface material.

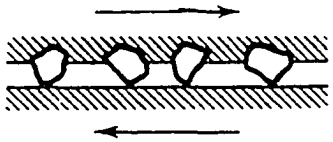

(a) Two-body abrasion

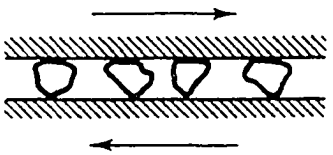

(b) Three-body abrasion

Figure 2.6: Illustration of (a) two-body abrasive and (b) three-body abrasive wear (from Hutchings, 1992)

The hardness of abrasive particles and surface material involved in a wear process influence the rate of wear. Moore (1978) indicated that for an effective wear, the relative hardness of the particles should be at least 1.25 times the hardness of the surface material.

Mechanisms of the rock failure in diamond drilling process can involve both plastic flow and brittle fracture. In most cases both may occur conrrently depending on the individual drilling conditions. For the sake of simplicity, however, separate models described each mechanism have been developed.

2.3.3.1 Plastic Deformation

Hutchings (1992) described a simple model of abrasive wear by hard particles for general materials in which only plastic deformation is involved (Figure 2.7). In this model an abrasive particle is idealized as a cone with an inclusive angle of 2θ. This particle is dragged across the surface of a ductile material which flows under an indentation pressure, P. A groove along the particle path is formed, and a proportion of the surface material is removed from the groove due to the displacement of the surface material by the cone. It is assumed that the normal load on that particle is supported by plastic flow beneath the particle, which causes a pressure P to act over the area of contact between the particle and the surface. Since the cone is moving forward only the front surface of the particle is in contact with the surface material. When the normal load the particle carries is w, then

$$w = P\frac{\pi a^2}{2} = \frac{1}{2}P\pi x^2 \tan^2\theta \qquad (2.16)$$

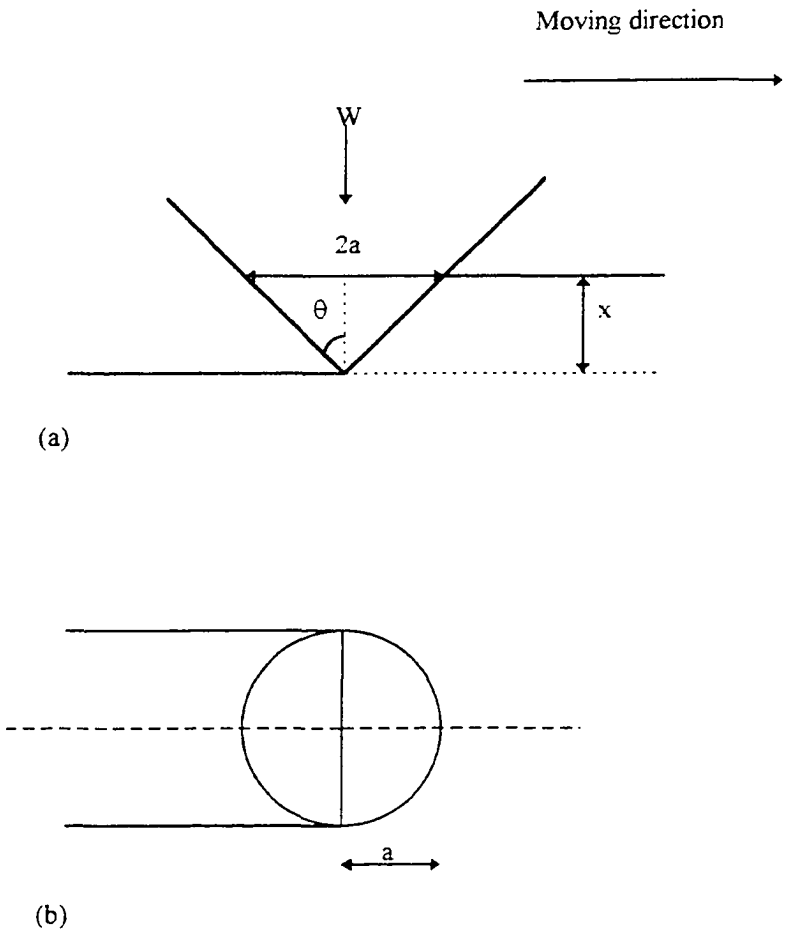

Figure 2.7: Geometry of contact between an idealized conical abrasive particle and a surface: (a) in cross-section; (b) in plane view (after Hutchings, 1992)

where x is the depth of protrusion of the particle into the rock surface, and a is the radius of the cone at the intersection of the rock surface. The volume of material displaced by the cone in moving a unit distance along the surface is, therefore $2xa$. If all of the material displaced from the groove is removed as debris, then the volume of debris removed by this single particle, q, is

$$q=x^2\tan\theta \qquad (2.17)$$

Assuming that only a portion of the material, η, in the groove will actually be removed as drilling debris, then, combining the above two equations gives

$$q=\frac{2\eta W}{\pi P\tan\theta} \qquad (2.18)$$

The above model can be further modified to describe a diamond drilling process in which only plastic deformation is involved. It is assumed that the hardness, shape, and size of the diamond particles on a bit are identical, and that the total bit weight W, is uniformly distributed among those n diamonds. It is further assumed those diamonds are uniformly distributed in the cross-sectional area of the bit surface, and thus the average distance from the center of the bit to the center of the n diamonds, r, can be expressed as $r=(D_o-D_i)/2$. Here D_o and D_i are the outer and inner diameters of the bit barrel, respectively. If the rotational speed of the bit is N, then the distance a diamond travels is $2\pi rN$ in a unit time. The volume of rock debris removed by a single diamond particle is

$$Q=\frac{4\eta WrN}{nP\tan\theta} \qquad (2.19)$$

The total volume of rock removed by the bit is

$$Q=\frac{2\eta WN(D_o+D_i)}{P\tan\theta} \qquad (2.20)$$

Note that the cross-sectional area of a diamond core bit is $A=\pi(D_o^2-D_i^2)/4$. Then the penetration rate PR of the bit is calculated as follows:

$$PR=\frac{8\eta WN}{\pi P(D_o-D_i)\tan\theta} \qquad (2.21)$$

Substituting $3\sigma_Y$ for P and one finds that

$$PR=\frac{8\eta WN}{3\pi\sigma_Y(D_o-D_i)\tan\theta} \qquad (2.22)$$

The specific energy (kerfing), SE_k, can be calculated as:

$$SE_k=\frac{3T\sigma_Y\tan\theta}{2\eta W(D_o+D_i)} \qquad (2.23)$$

Here T is the measured applied torque during drilling. For ideal plastic material, $\sigma_Y\approx\sigma_t$, and therefore, Equation 2.22 becomes:

$$PR=\frac{8\eta WN}{3\pi\sigma_t(D_o-D_i)\tan\theta} \qquad (2.24)$$

Analysis of Equation 2.22 indicates that the penetration rate is a function of the bit weight, rotational speed, yield strength of the rock material, kerf thickness of the bit, and sharpness of each individual diamond. A direct proportional relationship between the

penetration rate and the weight-on-bit, or with the rotational speed, is predicted by this equation. The yield strength of the rock material, the thickness of the kerf, and the inclusive angle of the diamond, on the other hand, all have an inverse relationship with the penetration rate. It is also noted from Equation 2.23 that the specific energy is not a function of the rotational speed. Instead, it is dependent upon the applied torque.

2.3.3.2 Compressive Crushing

If the rock underneath the diamond particles is assumed to fail elasticaly instead of plastically, and if other conditions are the same, then the compressive crushing (elastic) drilling model can be derived. In such a case, Equation 2.22 will be in the following form:

$$PR=\frac{8\eta \bar{W}N}{\pi\sigma_c(D_o-D_i)\tan\theta} \qquad (2.25)$$

2.3.3.3 Brittle Fracture

The third type of rock failure model in hard particle abrasion is the brittle fracture model. In the brittle fracture model, material removed by plastic flow is only a portion of the total material removed.

Lawn and Swain (1975) discussed a cracking process of brittle material subject to point indentation. This fracture mechanism, which is usually caused by sharp rigid conical, pyramidal, or hard irregular grit particles, generates an elasto-plastic stress field underneath. In Figure 2.8, the stress field and crack process caused by the indentation of

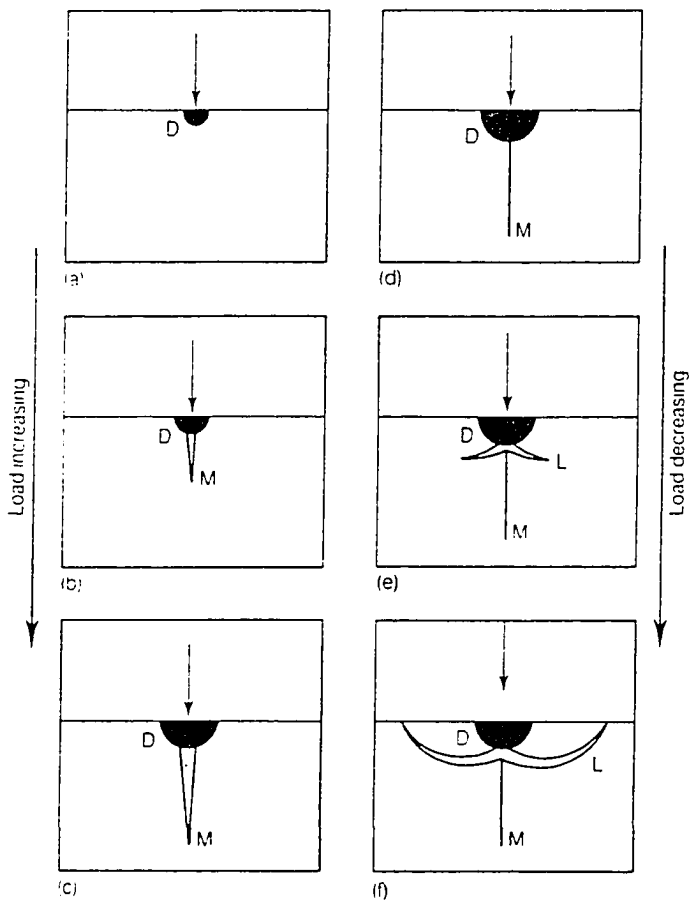

Figure 2.8: Diagram showing crack formation in a brittle material due to point indentation (from Lawn and Swain, 1975). The normal load increases from (a) to (c), and is then pregressively reduced from (d) to (f).

a perfectly sharp (i.e., with zero radius of curvature) indenter is illustrated. At the point of initial contact, very high stresses occur at the tip of the indenter, with the combination of shear stress and hydrostatic compressive stress. These intense stresses, in turn, cause local plastic flow and material densification around the tip of the indenter. The zone of deformed material is indicated by the letter D in Figure 2.8. If the load on the indenter increases to a critical value, tensile stress across the vertical mid-plane will initiate a *median vent* crack (indicated by letter M in Figure 2.8). Further increase of the normal load will result in an extension of the median vent crack (Figure 2.8(c)). Once the normal load is reduced, the median vent crack will close (Figure 2.8 (d)) and initiation and growth of *lateral vent* cracks (indicated by letter L in Figure 2.8 (e)) will occur. The formation of these lateral cracks is driven by residual elastic stresses, caused by relaxation of the deformed material around the region of contact. These lateral cracks will curve upwards and eventually reach the free surface of the material.

The median cracks, like the Hertzian cone cracks due to a blunt indenter, grow downward into the bulk of the material with an increasing normal load, and close when the normal load decreases. They do not contribute to the removal of surface material in a drilling process. The lateral cracks, to the contrary, may actually lead to the removal of the surface material.

Because formation of the lateral cracks is derived by the residual elastic stresses when the load is released, the normal load on the indenter has to exceed a critical value, w^*, for the lateral cracks to form. The value of w^* depends on the fracture toughness of the surface material, K_c, and its hardness (i.e., Vicker hardness), H. According to Evans

(1979), the following relationship exists:

$$W' \propto \left(\frac{K_c}{H}\right)^3 K_c \qquad (2.26)$$

where K_c is the mode I plane strain fracture toughness, which can be measured by conventional notched tensile or bending tests.

Evans (1979) also proposed a model to describe material removed by brittle fracture based on the concept of lateral cracks. As a sharp particle slides over the surface forming a plastic groove, lateral cracks propagate upwards to the free surface from the base of the subsurface deformed region (Figure 2.9). It is assumed that material is removed as chips from the region bounded by the lateral cracks and the free surface. The sideways length of the lateral crack, c, is given by

$$c=\alpha_1 \frac{(E/H)^{3.5} W^{5.8}}{K_c^{1.2} H^{1.8}} \qquad (2.27)$$

where w is the normal load on a particle, E and H are the Young's modulus and hardness of the surface material, respectively. K_c is the fracture toughness of the surface material and α_1 is a constant which depends on the shape of the particle. The depth of the lateral cracks, b, is assumed to be proportional to the radius of the plastic zone,

$$b=\alpha_2 \left(\frac{E}{H}\right)^{2.5} \left(\frac{W}{H}\right)^{1.2} \qquad (2.28)$$

where α_2 is another geometrical constant determined by the shape of the particle. The maximum volume of material removed by this particle over a unit distance is $2bc$, then

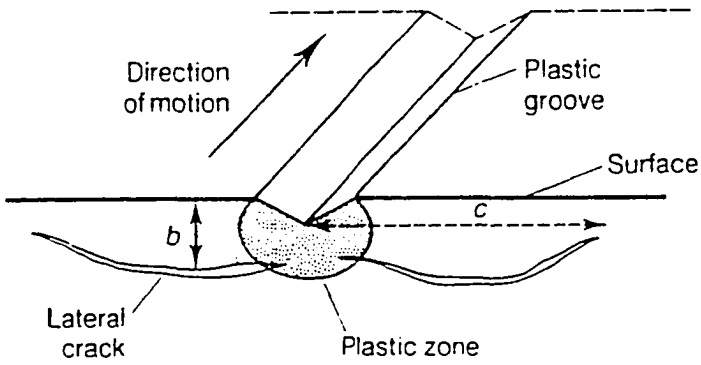

Figure 2.9: Schematic illustration of material removal in a brittle material by the extension of lateral cracks beneath a palstic groove (from Evans, 1979)

$$Q=\alpha_1\alpha_2\frac{(E/H)\,W^{9/8}}{K_c^{1/2}H^{5/8}} \qquad (2.29)$$

If the same assumptions for Equations 2.22 and 2.23 are employed to develop a drilling model, and the concept of brittle fracture of rock is used, the penetration rate takes the following form:

$$PR=2\alpha_1\alpha_2\frac{(E/H)\,W^{9/8}N}{K_c^{1/2}H^{5/8}(D_o-D_i)} \qquad (2.30)$$

Here the constants α_1 and α_2 are geometrical constants determined by the shape of the diamonds of a bit. Theoretical determination of these constants has not yet been developed. The corresponding specific energy in the brittle fracture model is;

$$SE_f=\frac{2T}{\alpha_1\alpha_2\pi(D_o-D_i)}\frac{K_c^{1/2}H^{5/8}}{(E/H)\,W^{9/8}} \qquad (2.31)$$

A comparison among Equations 2.24, 2.25, and 2.30 indicates that the three models give virtually the same functional relationship between penetration rate, specific energy, and drilling factors. For the brittle model, because the ratio E/H does not vary greatly between different hard brittle solids, the material is represented by $K_c^{1/2}H^{5/8}$ instead of by H as in the plastic/elastic models. It is also worth noting that the weight-on-bit in the fracture model is more significant than is the rotational speed. They have the same degree of importance as in the plastic/elastic models, however.

Equations 2.26 through 2.31 were derived from single cutter conditions. In fact, the diamond core bits contain more than one cutter, and the spacing distance between diamond cutters may play an important role in rock cutting. When the ratio of spacing

distance to penetration depth, *s / l*, is small, cracks generated by one cutter may interact with those produced by other cutters. In this case, propagation of cracks may occur at much lower stress. As the s/l ratios becoming larger than a critical value, the cutters are too far apart for the interaction to occur, and cracks are formed independently.

Laboratory experiments have shown that the effects of spacing are limited when spacing to penetration ratio approaches a critical value. Ozdemir et al. (1977) found that this ratio was from 20 to 50 for multiple pass disc cutting. For a single pass test, Snowdon et al. (1982) found that the critical value of this ratio was about 20. In a similar single pass disc cutting test, Zhao et al. (1994) concluded that the value of this ratio could be as low as 10. When the s/l ratio is lower than the critical value, the length of cracks is simply a function of the cutter geometry. Sanio (1985) gave the equation:

$$c=\frac{sa}{2\sqrt{2rx-x^2}} \qquad (2.32)$$

where:

c is the half length of the crack,

s is the cutter spacing distance,

a is the radius of crater,

r is the radius of the indenter curvature, and

x is the penetration depth.

For a diamond shown in Figure 2.1, if one assumes that the crater size is the size of diamond cone being pressed into the rock surface, then $a/x=\tan\theta$ and the radius of the

crater, a, is equal to the square root of $(2rx-x^2)$. Therefore, the crack length is simply the diamond spacing distance. Equations 2.30 and 2.31 become

$$PR=\alpha_2 \frac{2NSX}{(D_o-D_i)} \left(\frac{E}{H}\right)^{2/5} \left(\frac{W}{H}\right)^{1/2} \qquad (2.33)$$

and

$$SE_k=\frac{2T}{\alpha_2 \pi (D_o+D_i) SX} \left(\frac{H}{E}\right)^{2/5} \left(\frac{H}{W}\right)^{1/2} \qquad (2.34)$$

CHAPTER 3

STATISTICAL DESIGN AND ANALYSES

Modern statistics began about 1925 when Fisher's *Statistical Methods for Research Workers* was published. Statistics applies now virtually to all fields of scientifical endeavor--engineering, business, social sciences, physical sciences, biological sciences, education, and so on.

Experimental design is a field of statistics. In order to yield the most applicable results and the maximum possible information, a researcher should properly design an experiment and analyze the results. Basically, statistical design is derived from the concept of randomization. The function of randomization is to ensure a valid and unbiased estimate of the experimental error, means of factors investigated, and differences among them.

3.1 LATIN SQUARE DESIGN

The random block design technique was employed to statistically design the laboratory experiment in this study. The construction of a Latin square was detailed by Fisher (1956). The purpose of using the Latin square design was to remove unwanted variation as it might occur in the experimental procedures while maximizing information from a limited number of experiments. Table 3.1 illustrates an example of a 6×6 Latin square. There are three mutually independent variables in the 6×6 Latin square, namely:

Table 3.1: An example of a 6-by-6 Latin square

	Column					
Row	A	F	E	B	D	C
	C	B	D	A	F	E
	F	C	B	D	E	A
	B	E	F	C	A	D
	D	A	C	E	B	F
	E	D	A	F	C	B

Row-factor, Column-factor, and L-treatment (A, B, C, D, E, and F). These three factors are randomized so that each treatment occurs only once in each row and in each column, and the combination of the three variables is unique for each condition (Davies, 1979).

Several assumptions are made when a Latin square design is used. Apart from the experimental errors, they are:

a. The true effect of changing from one treatment to another is the same in every row and in every column;
b. The true effect of changing from one row to another is the same in every column and for every treatment; and
c. The true effect of changing from one column to another is the same in every row and for each treatment.

The above assumptions mean that all of the three variables affect the results independently. Divergence of the results from the true value is caused by experimental errors only. The model can, thus, be expressed as:

$$Y_{ijk}=\mu+R_i+C_j+L_k+e_{ijk}; \quad i,j,k=1,2,3,\ldots,n \qquad (3.1)$$

where

i, j, k is the location of observation in i^{th} row, j^{th} column, and k^{th} treatment,

Y_{ijk} denotes the observed result from the i^{th} row, j^{th} column, k^{th} treatment,

μ is the overall mean of all results if there were no experimental errors,

R_i is the difference between the average of the i^{th} row and the average over all rows

if the column and treatments were the same and if there were no experimental errors,

C_j is the difference between the average of j^{th} column and the average over all columns if the row and the treatments were the same and if there were no experimental errors,

L_k is the difference between the average of k^{th} treatment (L-treatment) and the average over all L-treatments if the row and column were the same and if there were no experimental errors,

e_{ijk} is the experimental error from the i^{th} row, j^{th} column, and k^{th} treatment, and

n is the size of the square.

The *Sums of Squares* (i.e., SS) corresponding to the changes in Row-factor, Column-factor, L-treatment, and the experimental errors, can be calculated from the above equation. The analysis of variance (ANOVA) table for a n×n Latin square is shown in Table 3.2.

The *Sum of Squares for Total* (i.e., SST) is computed by the following equations:

$$SST = \sum_{j=1}^{n}\sum_{i=1}^{n} (Y_{ij} - \bar{Y})^2 = \sum_{j=1}^{n}\sum_{i=1}^{n} Y_{ij}^2 - CM \qquad (3.2)$$

Table 3.2: ANOVA table for a n×n Latin square

Source	Degree of freedom	Sum of squares	Mean sum of squares	F-test
Row	n-1	SSR	SSR/(n-1)	MSR/MSE
Column	n-1	SSC	SSC/(n-1)	MSC/MSE
L-treatment	n-1	SSL	SSL/(n-1)	MSL/MSE
Error	(n-1)(n-2)	SSE	SSE/(n-1)(n-2)	

where

$$CM=\frac{1}{n^2}\left(\sum_{j=1}^{n}\sum_{i=1}^{n}Y_{ij}\right)^2 \qquad (3.3)$$

is the correction for overall mean. The Y_{ij} denotes the result of i^{th} row and j^{th} column, and $\overline{Y}$ represents the mean value of total observations. Similarly, the *Sum of Squares for Row-factor* (SSR), *Sum of Squares for Column-factor* (SSC), and *Sum of Squares for L-treatment* (SSL) are calculated by the following equations:

$$\begin{aligned} SSR &= n\sum_{i=1}^{n}\left(\overline{R}_i-\overline{Y}\right)^2 \\ &= \frac{1}{n}\left(\sum_{i=1}^{n}R_i^2\right)-CM \end{aligned} \qquad (3.4)$$

and

$$\begin{aligned} SSC &= n\sum_{j=1}^{n}\left(\overline{C}_j-\overline{Y}\right)^2 \\ &= \frac{1}{n}\left(\sum_{j=1}^{n}C_j^2\right)-CM \end{aligned} \qquad (3.5)$$

and

$$\begin{aligned} SSL &= n\sum_{k=1}^{n}\left(\overline{L}_k-\overline{Y}\right)^2 \\ &= \frac{1}{n}\left(\sum_{k=1}^{n}C_k^2\right)-CM \end{aligned} \qquad (3.6)$$

where R_i and $\overline{R}_i$, C_j and $\overline{C}_j$, and L_k and $\overline{L}_k$are the total and the average for all results in row i, column j, and L-treatment k, respectively. The *Sum of Squares for Error* (i.e. SSE) is:

$$SSE=SST-SSR-SSC-SSL \qquad (3.7)$$

This quantity measures variability unexplained by the differences in rows, columns, and treatments.

3.2 ANALYSIS OF VARIANCES

In a null hypothesis test, a variation in experimental conditions is first assumed to have no effect on the result of the trial. The essence of the Analysis of Variance (ANOVA) test is to compare the actual observed measurement of a test to that one would expect to observe if the null hypothesis were true. To do this, the first step is to divide each sum of squares by its *degrees of freedom* and obtain the *Mean Sum of Squares* (MSS) for a particular factor or treatment (i.e., MSR, MSC, MSL) and the *Mean Sum of Squares for Error* (MSE). In a n×n Latin sqaure, the *degrees of freedom* for row, column, and treatment are n-1, and the *degrees of freedom for error* is (n-1)(n-2). The ratio of the mean sum of squares for a particular factor or treatment to the *Mean Sum of Squares for Errors* (MSE) is known as the F-statistic. For example, the F-value for Row-factor is as follow:

$$F_{[v1,v2]} = \frac{MSR}{MSE} \qquad (3.8)$$

Here v1 and v2 are the *degrees of freedom for Row-factor* and the *degrees of freedom for error*, respectively. The critical values of the F-test at $\alpha = 0.05$ are listed in Appendix 1. Similar comparisons can be made to test the null hypothesis for Column-factor and

treatment by estimating the ratios of MSC, and MSL to MSE as shown in Table 3.2.

In F-statistic, when the null hypothesis is accepted (i.e., the computed F-value is smaller than the critical F-value at a given probability of acceptance, e.g., $1-\alpha = 0.95$ in this study), the differences among values of a factor are declared insignificant. The deviation between the overall mean and the observed result is considered due mainly to the residual error. This implies that there is no statistically significant effect on result caused by the analyzed variable. To the contrary, in a case for which the F-value calculated is larger than the corresponding critical value at a specific significant level (e.g, $\alpha = 0.05$), the null hypothesis is rejected. The differences among values of a factor is declared significant. It is, however, not clear where these differences exist among the values of this factor. If an investigated factor is found to have significantly affected the observation, further tests may be needed. One of such tests is a Newman-Keuls test. This is a statistical test which provides a multiple comparison technique to investigate the relative significance of that influential variable.

In order to perform the Newman-Keuls test, for each of the analyzed variables the means of the n^2 observations are averaged to form n groups according to an independent variable. These n groups are, then, arranged in a descending order as follows:

$$\bar{X}_1 > \bar{X}_2 > \bar{X}_3 > \bar{X}_4 > \bar{X}_5 > \ldots > \bar{X}_n \qquad (3.9)$$

The differences of those means are tabulated in a triangular arrangement as shown in Table 3.3. The least significant value of the Newman-Keuls test (R_k) is calculated by the equations:

Table 3.3: Mean difference arrangement for Newman-Keuls test

No. of Means Spanned	k	k - 1	k - 2	...	2
Test Significant Value	R_k	R_{k-1}	R_{k-2}	...	R_2
Mean Difference	$\overline{X}_1 - \overline{X}_2$	$\overline{X}_1 - \overline{X}_{n-1}$ $\overline{X}_2 - \overline{X}n$	$\overline{X}_1 - \overline{X}_{n-2}$ $\overline{X}_2 - \overline{X}_{n-1}$ $\overline{X}_3 - \overline{X}_n$	... ...	$\overline{X}_1 - \overline{X}_2$ $\overline{X}_2 - \overline{X}_3$ $\overline{X}_3 - \overline{X}_4$ ... $\overline{X}_{n-1} - \overline{X}_n$

$$R_k = q_\alpha(k, df)\, S_y \qquad (3.10)$$

and

$$S_y = \sqrt{MSE/n} \qquad (3.11)$$

where:

q_α is the entry value shown in Appendix 2,

k is the order of mean difference,

df is the *degree of freedom* of the experimental error. The df is equal to (n-1)(n-2) in a n×n Latin square,

S_y is the standard error of the mean, and can be calculated from Equation 3.11 in a Laitn square design, and

n is the size of the square.

The differences of means in Table 3.3 are compared with the least significant value, R_k. If a difference of means, for example, $\overline{X}_n - \overline{X}_1$, is larger than the standard value, R_{n-1}, it is concluded that the factor tested is not equivalent at level 1 and n. Then the Newman-Keuls test continues as though this were true. Once the differences of means are less than a given R_k, testing stops and the set of means is declared homogenous, that is, no significant differences among the remaining groups of factors.

3.3 REGRESSION ANALYSIS

A mathematical equation which describes the relationship between the observed results and the independent factors allows the prediction of a drill performance (i.e., penetration rate, applied torque, and specific energy). The best model fitting the data for each relationship was selected based on the accuracy of the formula, simplicity of the equation, and the consistency of the model as compared with the physical conditions.

To analyze the results of this experiment, the Statistical Analysis System (SAS) was used. The SAS package, available at the University of Alaska Fairbanks Computer Center, is capable of performing numerous statistical analysis from descriptive statistics to complex multivariate analysis.

3.3.1 General Linear Models

The General Linear Model (GLM) regression technique was used to formulate the relationships among influential factors and dependent variables observed in an experiment. The problem of fitting a straight line or a curve by the least squares technique can be handled through the use of matrices. In a GLM regression analysis, the relationship can be described as follows (Clarke, 1969):

$$\boldsymbol{Y}=\boldsymbol{XB}+\boldsymbol{E} \qquad (3.12)$$

where:

Y is an n×1 vector of observations,

X is an n×p matrix of factors,

B is a p×1 vector of coefficients for the factors,

E is an n×1 unobservable vector of random variables and normally distributed with mean zero. Elements of **E** are uncorrelated.

By transposing matrix **X** to a p×n matrix $\mathbf{X}^{\mathbf{T}}$, other basic forms of calculation in GLM can be obtained:

$$\boldsymbol{X}^{T}\boldsymbol{Y}=(\boldsymbol{X}^{T}\boldsymbol{X})\,\boldsymbol{B} \tag{3.13}$$

$$(\boldsymbol{X}^{T}\boldsymbol{X})^{-1}\boldsymbol{X}^{T}\boldsymbol{Y}=(\boldsymbol{X}^{T}\boldsymbol{X})^{-1}\boldsymbol{X}^{T}\boldsymbol{B} \tag{3.14}$$

$$\boldsymbol{B}=(\boldsymbol{X}^{T}\boldsymbol{X})^{-1}\boldsymbol{X}^{T}\boldsymbol{Y} \tag{3.15}$$

A GLM model can be expressed as the following general form of polynomial equation:

$$Y_i=\sum_{k=0}^{p-1} B_k X_{ik}+\varepsilon_i; \quad X_{i0}=1 \tag{3.16}$$

where:

Y_i is the dependent observation,

X_{ik} is either an independent variable or a set of different variables,

B_k is the best fitting coefficient for parameter X_{ik}, and

ε_i is the intercept.

The *degrees of freedom* (df) is a concept related to sample size. For a n×n Latin square, the sample size is n^2, and the *degrees of freedom for total* (df_t) is one less the sample size, e.g., $n^2 - 1$. When a regression model is considered, the *degrees of freedom for the regression model* (df_m) is the number of coefficients. Generally, a higher degree regression equation includes more coefficients than that of a lower degree regression equation. Therefore, the *degrees of freedom for a regression model* of higher order equation is larger than that of a lower order. In a regression analysis, the *degrees of freedom for total* is the result of the *degrees of freedom* for the regression model plus the *degrees of freedom for error* (df_e), i.e., $df_t = df_m + df_e$. The accuracy of a regression equation can be judged by its *coefficient of determination*, R^2, which is calculated by:

$$R^2 = 1 - \frac{SSE}{SST} \qquad (3.17)$$

The coefficient of determination measures the proportionate reduction of total variation in an observation associated with the use of a set of variables. It assumes the value of 0.0 when all values of the regression coefficients are of zero's, i.e., $B_{ik} = 0$. The R^2 assumes the value of 1.0 when all the observations match exactly on the predicted values (i.e., directly on the fitted response surface). The coefficient of determination, however, has a limitation on the evaluation of a regression model. As the *degrees of freedom for error* become small, the R^2 value may be quite close to one but the generality of the model may not be satisfied. Therefore, one should investigate the significance of the proposed equation by F-test:

$$F=\frac{MSS_m}{MSS_e} \qquad (3.18)$$

The MSS_m is the mean sum square for the regression model and the MSS_e is the mean sum for error. A smaller F-value suggests less contribution of the model toward prediction of the magnitude of a drilling parameter. The decision rule to accept or reject a variable based on Type I error at α is:

$$\begin{aligned} &If\ F \le F(1-\alpha; p-1, n-p),\ accepted\ Null\ hypothesis \qquad (3.19)\\ &If\ F > F(1-\alpha; p-1, n-p),\ rejected\ Null\ hypothesis \end{aligned}$$

In this study, the GLM analysis was first performed on each individual influential factor to describe the effect of that factor on the observation. Then the GLM procedures were conducted to include all significant influential factors to develop a prediction model for drill performance. A lower order equation is always preferred if its R^2 and F-value are high enough to ensure a considerably accurate and meaningful prediction.

3.3.2 Stepwise Regression

Models built by GLM procedure contain all the variables and their combinations at a given power of the equation. It is to the advantage of applications to eliminate some of the least significant variables or combinations of variables. An automatic search procedure, namely, *Backward Stepwise Elimination Method*, was used to perform the statistical regression in this study. The backward stepwise regression procedure begins with the model containing all potential variables and identification of the one with the

smallest F-value. If a variable is found to have the minimum F-value which is less than a predetermined limit, that variable is dropped. The model with the remaining variables is then fitted, and the next candidate for dropping is identified. This process continues until no further variables can be dropped.

3.3.3 Nonlinear Model

In a *Non-Linear Regression* (NLIN), the parameter **B** is also estimated by the least squares method. The computing technique for a NLIN analysis is as follow:

$$\boldsymbol{Y}=\boldsymbol{F}(\boldsymbol{B}_0,\boldsymbol{B}_1,\ldots,\boldsymbol{B}_p;\boldsymbol{X}_1,\boldsymbol{X}_2,\ldots,\boldsymbol{X}_n)+\boldsymbol{E} \qquad (3.20)$$

let

$$\boldsymbol{B}=(\boldsymbol{B}_0,\boldsymbol{B}_1,\ldots,\boldsymbol{B}_p)^T \qquad (3.21)$$

and

$$\boldsymbol{X}=(\boldsymbol{X}_1,\boldsymbol{X}_2,\ldots,\boldsymbol{X}_n)^T \qquad (3.22)$$

then

$$\boldsymbol{Y}=\boldsymbol{F}(\boldsymbol{B},\boldsymbol{X})+\boldsymbol{E} \qquad (3.23)$$

where both variable **X** and parameter **B** are functions of **B** and the solution cannot be obtained directly. Thus an iterative technique is required. In an iterative calculation, the initial values for the least squares are computed in a succession of stages until the *Sum of Square for Errors* (ESS) is minimized.

CHAPTER 4

LABORATORY DRILLING EXPERIMENT

4.1 INTRODUCTION

A laboratory drilling experiment, also as a part of the "*Rock Drilling under the Greenland Ice Sheet*" project by the Polar Ice Coring Office (PICO) at the University of Alaska Fairbanks, was performed in this study. The purpose of the PICO rock drilling program was to retrieve rock cores from formations beneath the 3,050 m (10,010 ft) thick ice sheet. Success of the project no doubt would contribute significantly not only to the understanding of the geology in Greenland, but also to the advancement of drilling technology in glacial areas. The extremely cold weather, the lack of information about the bedrock geology in Greenland, the great depth of the borehole, and the great difference in material properties of ice and rock made it a challenge to achieve this goal. It was thus necessary to conduct an experimental drilling and coring investigation in the laboratory to evaluate the performance of the intended coring bits and to optimize the drilling parameters. In the following sections of this chapter, the experimental design and the equipment for drilling and coring testing are described.

4.2 DRILLING TEST DESIGN

In the laboratory testing program, two independent drilling and coring experiments were designed and performed. The first experiment was a preliminary rock coring test with four

Longyear bits. The purpose of this drilling test was to compare the performance of the four Longyear diamond bits (i.e., AQ1, AQ2, BQ1, and BQ2). As a result of this preliminary testing, the best performing bit was selected for the second experiment, namely, 6×6 Latin square design drilling test. Purpose of the comprehensive test was to identify and evaluate the influential drilling factors.

4.2.1 The Preliminary Rock Coring Test

This experiment consisted of a set of 48 coring tests on six rocks (labelled as A, B, C, D, E, and F in the study) with four Longyear core bits (labelled as AQ1, AQ2, BQ1, and BQ2 in the study). Short descriptions of rock properties and bit characteristics are included in later sections of this chapter. In this test, all the four bits were tested at the same condition on each type of rock. Performance of any single bit on a given rock was compared with others and the best performing bit was chosen. In most of the tests, rock cores were also collected for the material property tests.

During the entire coring test, the weight-on-bit was kept at a constant load of 2,402 N (540 lb) and the rotational speed was set at about 500 rpm. The borehole was cleared by water and the flow rate was maintained at 5.68 $l\,min$ (1.5 gpm).

4.2.2 The 6×6 Latin Square Design Drilling Test

The second drilling experiment performed in this study was a set of 36 drilling tests using the chosen bit from the preliminary rock coring test. It was also conducted on the six types of rock (i.e., rocks A, B, C, D, E, and F). To maximize information from a limited

number of tests, a 6×6 Latin square design was employed in this test. Table 4.1 shows the testing conditions. Factors investigated in this test were weight-on-bit, rotational speed, and rock type. In this square design, the Row-factor was the weight-on-bit ranging from 890 N (200 lb) to 2,669 N (600 lb). The Column-factor was the rotational speed ranging from 200 to 600 rpm. The treatment (L-treatment) was designed as the six types of rock. To minimize the variation caused by repetitive use of the bit, the testing sequence was also randomized. This randomization process was intended to minimize the effect on observation because of bit wear. In addition, water was used as the flushing fluid in this test and the flow rate was maintained at a constant rate of 5.68 $l\ min$ (1.5 gpm).

4.3 EQUIPMENT FOR DRILLING TEST

4.3.1 Core Bits

In this laboratory drilling experiment, four types of diamond core bits were tested. Figure 4.1 shows these bits. AQ1 and BQ1 bits were surface-set diamond core bits, with three steps of diamond profiles. AQ2 and BQ2 bits were impregnated diamond core bits with a "V" groove at the face of the matrices. This "V" groove is designed to improve stability of a bit at the beginning of a new boring. The impregnated bits expose fewer cutting points to the rock surface. During the course of boring, the matrix is worn by the abrasiveness of the rock. Gradually, the bit exposes new cutting points and thus the bit life can be extended. The basic characteristics of these bits are summarized in Table 4.2.

Table 4.1: The 6×6 Latin square design rock drilling test for BQ1 bit

W \ N	200	300	400	450	500	600
200	A17	F6	E28	B14	D10	C25
300	C13	B12	D26	A9	F30	E3
400	F1	C33	C31	D7	E22	A21
450	B8	E32	F29	C2	A20	D16
500	D34	A19	C35	E23	B5	F24
600	E15	D27	A4	F11	C36	B18

W: Weight-on-bit, lb,
N: Rotational speed, rpm,
A-F: Six rock types, and
1-36: Sequence of test.

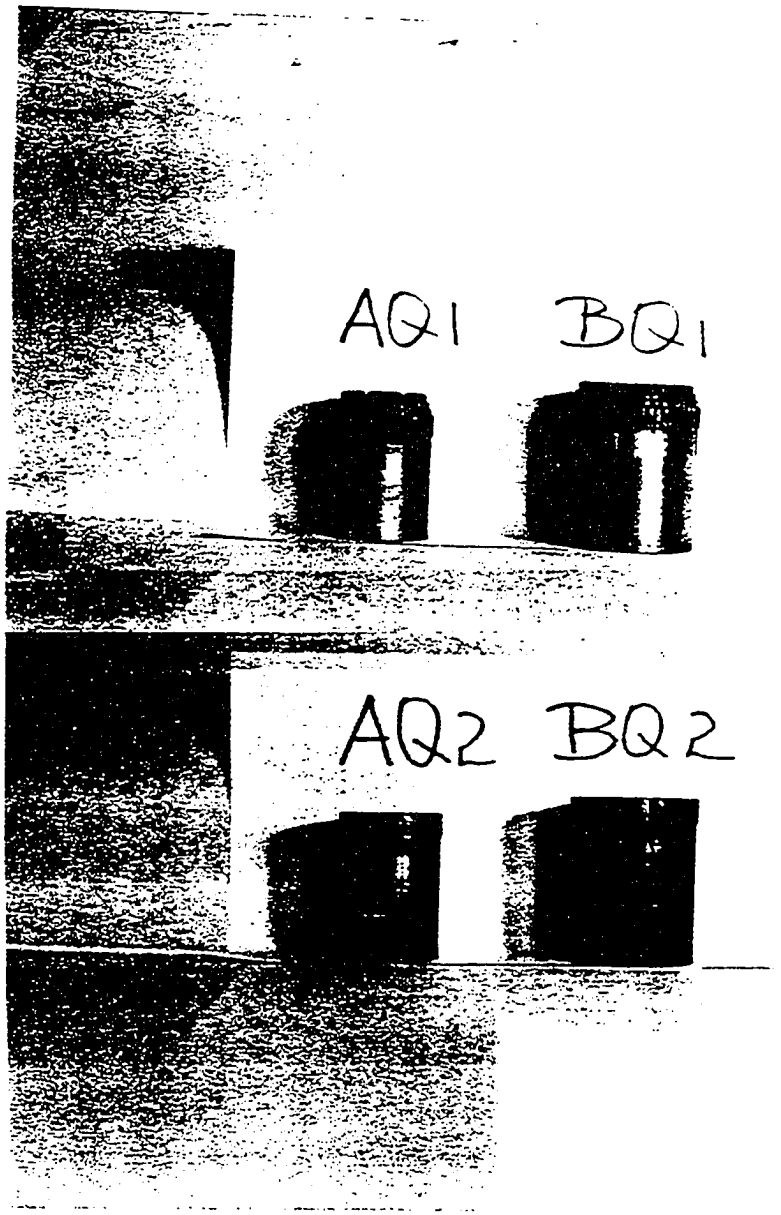

Figure 4.1: Surface-set and impregnated diamond bits

Table 4.2: Summary of diamond core bits

	AQ1	AQ2	BQ1	BQ2
Number of diamonds	180	n/a	224	n/a
Diamond size	10	n/a	12	n/a
Carat weight of diamonds	15/25	n/a	15/25	n/a
Number of waterways	6	5	8	6
Outer diameter (in)	1.875	1.875	2.375	2.375
Inner diameter (in)	1.187	1.187	1.625	1.625

4.3.2 Drilling System

In a laboratory operation, a core bit was mounted vertically on a 20-inch Clausing drill press (Figure 4.2) which was modified for this rock coring and drilling study. The maximum power output of the motor is 0.75 Hp (1.12 kW) at a low gear ratio and 1.5 hp (2.24 kW) at a high gear ratio. The rotational speed ranges from 150 to 2,000 rpm.

According to the experimental design, a constant load must be applied onto the rock surface throughout the test. To achieve this constant loading condition, a two-sheave block was employed (Figure 4.2). The top sheave was mounted at the top of a hollow-stem pile which is encased in the column of the drilling machine. The lower sheave was mounted on the feed handle of the drill. The two sheaves were connected by a steel cable. When a weight is hung to the cable, this two-sheave block system can exert a constant load to the rock surface.

4.3.3 Measuring Devices

Weight-on-bit, rotational speed, applied torque, and penetration rate were the four parameters needed to be measured during each test. Three load cells purchased from S. Himmelstein and Company (SHC) were utilized to measure the bit load. The capacity of each of those load cells was 8,896 N (2,000 lb). Those three load cells were mounted to the bottom plate of the drill press. The three load cells were connected to a joint-box and the load measured by each individual load cell was totalled. The maximum load capacity of the three load cells was 26,688 N (6,000 lb).

The actual rotational speed of the bit and applied torque were measured by a SHC

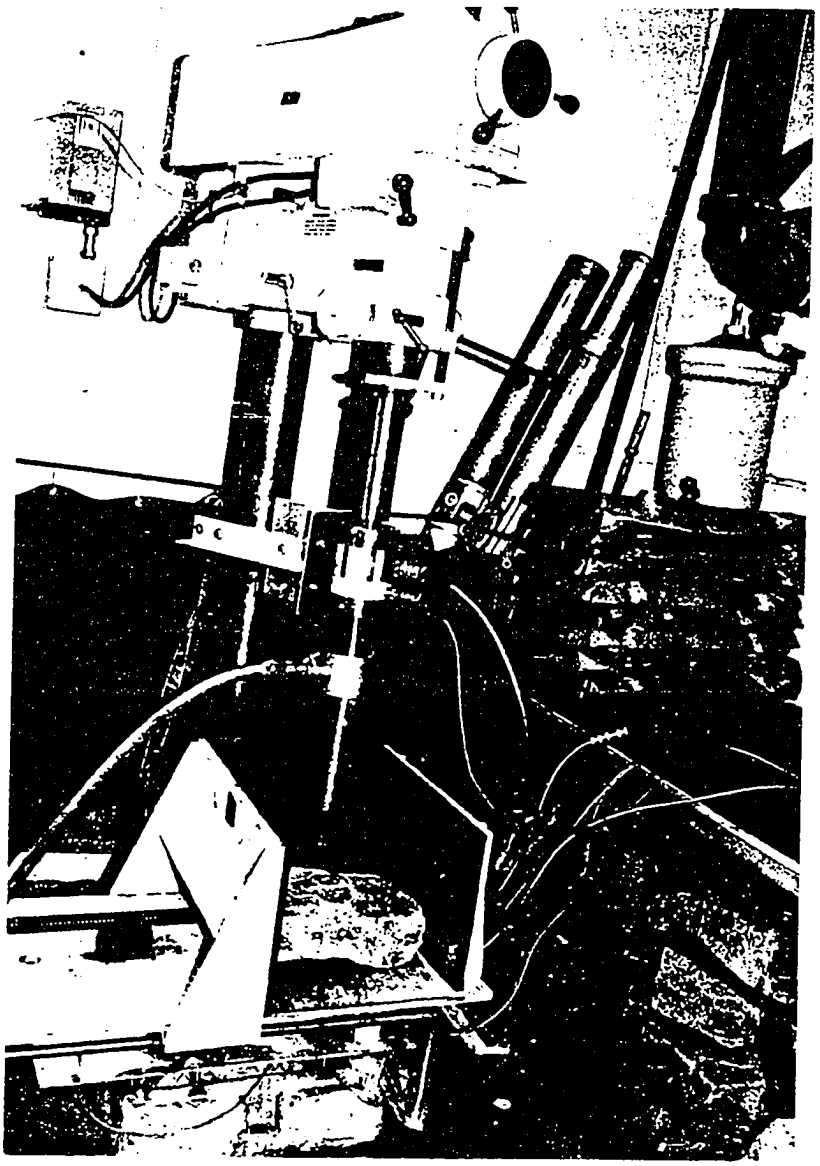

Figure 4.2: A 20-inch drill Clausing press and its modifications

MCRT 2900T tachometer. Two transducer units were contained in this tachometer. One was to measure the applied torque and the other was to measure the rotational speed. It was installed between the drill spindle and the core barrel. The full scale of the tachometer was 565 N-m (5,000 lb-in) and its speed rating was from 0 to 10,000 rpm.

The penetration depth of a bit is the distance from the rock surface to the cutting face of the hole. The travel of a bit was measured with a SHC LVGT-600 long stroke LVDT. The capacity of the LVDT was 61 cm (24 inch). The derivative of penetration depth with respect to time was defined as the *penetration rate.*

Two flow meters have been employed in this test to monitor the flow rate of circulating water. Their measurement ranged from 0 to 45.42 l/min (0 to 12 gpm).

4.3.4 Data Acquisition System

Measurements acquired by the four transducers were transmitted to a SHC 6-488B data acquisition system (Figure 4.3). The SHC 6-488B was an advanced multi-channel, programmable data logger which provided a fast, accurate data acquisition, processing and computer interfacing. It was housed in a standard System-6 cabinet. The two upper left module slots were occupied by LED numeric and alphanumeric displays, timers and interfaces. The keyboard occupied the two lower left slots. Four System-6 modules, namely, Transducer Amplifiers 6-201 and 6-205B, Digital Counter 6-260B.2, and LVDT Amplifier, were installed in the remaining space at the right. Data recorded by the SHC 6-488B could be transmitted to a computer or sent to a printer. Because each channel of the SHC 6-488B data logger was programmed with engineering units, a Basic program

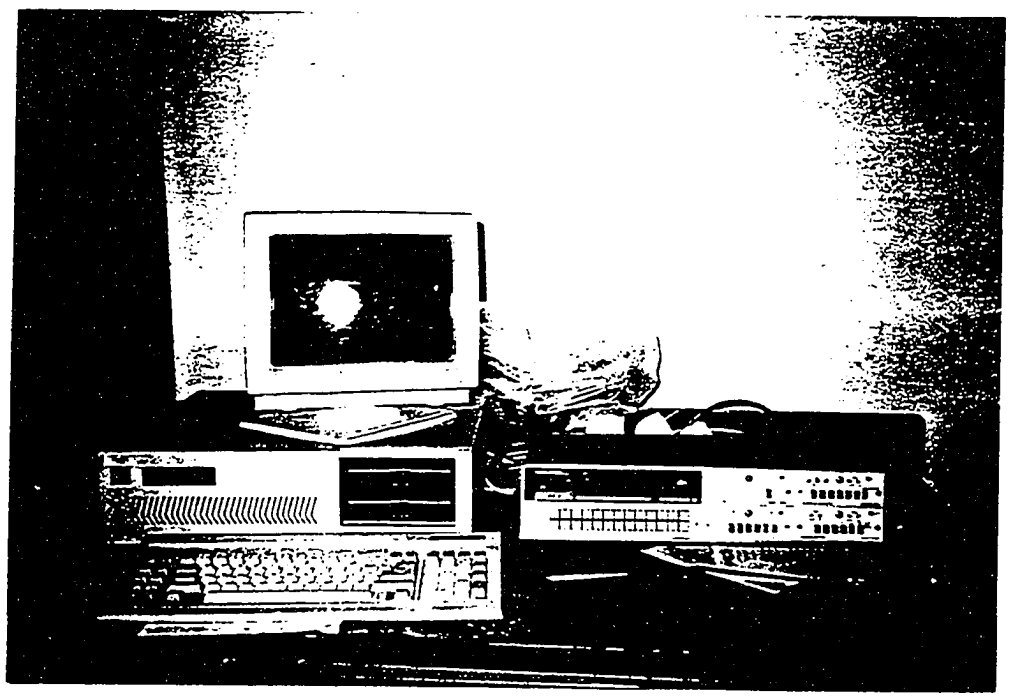

Figure 4.3: SHC 6-488B data acquisition system

was developed to extract data for the purpose of graphics and calculation. This program is included in Appendix D. Figure 4.4 presents the schematic of the laboratory drilling test procedures.

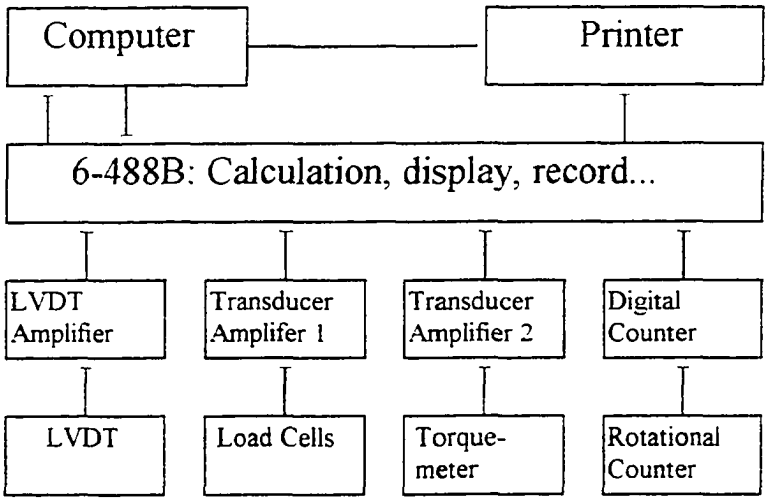

Figure 4.4: Schematic of the laboratory drilling test procedures

CHAPTER 5

PHYSICAL PROPERTIES OF MATERIAL

5.1 INTRODUCTION

In this research, six types of rock samples were collected and labeled as A, B, C, D, E, and F. In order to relate rock characteristics to drillability, a series of physical property tests was performed on rock samples. These tests included: 1) Shore scleroscope hardness test; 2) Schmidt hammer rebound hardness tests (on both bulk and core specimens); 3) point load strength test; 4) unconfined compression test; 5) splitting tensile strength test; 6) fracture toughness test; and 7) mineralogical analysis; and 8) grain size measurement.

5.2 MINERALOGY AND GRAIN SIZE

5.2.1 Mineralogy

Rock A was sandstone collected from Healy, Alaska. It was uniform, fine-grained, light brown in color. The major component of rock A was 70% quartz particles, cemented by calcite. It also contained about 5% feldspar and mica and 1-2% hornblende.

Rock B was diorite obtained from Aleutian Islands, Alaska. It contained 55% plagioclase, 40% hornblende, 2-3% potash feldspar, and a small amount of brown mica and quartz. Plagioclase and hornblende were intergrown, and formed a porphyraceous texture in the rock. The overall color of rock B was greenish grey.

Rock C was granite collected from the Silver Fox Mine, Alaska. It was brownish

grey in color. Rock C contained 25% quartz, 25% hornblende, 30% potash feldspar, and 20% plagioclase. The boundaries between quartz and hornblende particles were well defined. There was also a small amount of fine mica particles present.

Rock D was schist obtained from Aleutian Islands, Alaska. In rock D, large grained quartz and feldspar porphyroblasts were corrugated in a dark, green matrix. Boundaries of the large minerals were well defined. It also contained a small amount of mica and chlorite. Overall, rock D had s dark green color.

Rock E was limestone collected from Livengood, Alaska. It was composed of large pinkish-brown and some grey particles. The particles were large and the grain boundaries were distinguishable. Some edges of the mineral grains were dissolved, leaving voids of 1-2 mm in dimension.

Rock F was granodiorite also collected from the Silver Fox Mine, Alaska. It was light grey in color, consisted of equigranular, medium grained particles. It contained 30% quartz, 20% hornblende, 30% plagioclase, less than 20% feldspar, and a small amount of mica. Grain boundaries were not as clearly defined as in rock C.

5.2.2 Grain Size

Because individual minerals in a cemented rock are difficult to separate without destroying the particles, the measurement of grain size of a solid rock is usually made by viewing thin sections. Two major difficulties, however, are often associated with this method. First, grain boundaries are not always distinguishable under a microscope. Secondly, it is not possible for a thin section to cut through the longest axis of all the

grain particles. Therefore, the result from this time-consuming operation is usually not comparable with those obtained by sieve analysis (Moorhouse, 1959). In this study, a simplified method was developed to estimate the grain size of mineral particles. It was made by counting the number of mineral particles in a certain area of polished rock surface under a microscope. A grain size measurement, namely, the *Characteristic Dimension*, L_D, is obtained in this study. It is defined as:

$$L_D = \sqrt{\frac{4A}{\pi n}} \qquad (5.1)$$

where A is the total area of rock surface measured and n is the number of grain particles in that area. The Characteristic Dimension is the equivalent diameter of the average grain in a rock.

5.3 STRENGTH PROPERTIES

5.3.1 Uniaxial Compressive Strength

Among all rock strength properties and indices, the uniaxial compressive strength was the most frequently suggested by investigators (Karpuz, et al. 1990; Howarth, 1986) as a quantitative index of rock in drillability studies. In this research, the uniaxial compressive strength test was performed according to ASTM D2938-86 standard method.

The uniaxial compressive strength test requires appropriate specimen preparations. The specimens were prepared according to the ASTM D4543 standard method. To do so, cores from the preliminary rock coring test were cut with an electrical diamond saw. Then the specimen was ground with a diamond surface grinder until both ends were smooth and

perpendicular to the core axis. The length of the specimen, according to the ASTM D4543, was about twice of the diameter. The specimen was then air dried at room temperature for about 72 hours and loaded without a confining pressure under a compression testing machine until failure. A data acquisition system in the Rock Mechanics Laboratory at the Department of Mining and Geological Engineering, University of Alaska Fairbanks, was used to record the axial load and displacement continuously. The stress and strain at failure were determined from the load and displacement readings. The peak stress at failure was defined as the uniaxial compressive strength, also known as the unconfined compressive strength, σ_c.

5.3.2 Splitting Tensile Strength

Uniaxial tensile strength of rock is an important factor in coring, especially for a cable-suspended down-hole drill. In laboratory, the uniaxial tensile strength test is usually in the form of indirect methods such as Brazilian disc test or splitting tensile test. The splitting tensile strength test is much simpler and less expensive to perform than the direct tensile strength test. To do this test, a core specimen is compressed diametrically between two parallel platens. A normal compressive stress then is developed along the diameter across the upper and bottom contacts with the platens. When this compressive load reaches a critical point, the specimen will break in tension diametrically and a tensile strength, namely, the splitting tensile strength, can be obtained. The procedure of this test can be found in the ASTM D3967-86. In this study, the splitting tensile strength was used to give the indication of the uniaxial tensile strength (σ_t).

5.3.3 Point Load Strength

Both uniaxial compressive strength and splitting tensile strength tests require a certain amount of specimen preparations. They are difficult, if conditions permit, to perform in the field. In this study, several simple rock strength index tests were performed to estimate the uniaxial compressive strength and the uniaxial tensile strength. One of the tests was the point load strength test. The point load test was first introduced to predict uniaxial compressive strength of rocks and later was used for rock strength classification. The point load strength test is simple and inexpensive to carry out in the laboratory and the field. It can be performed on unprepared core specimens, or even on lumped rock specimens. It is reliable when properly conducted (Brook, 1985). In this study, procedures of the point load test were adapted from the ISRM suggested method (ISRM: Point Load Test, 1985) using a portable T-1000 Terrametrics point load testing device. The following equation is suggested by ISRM (1985) to correlate the point load strength with the uniaxial compressive strength:

$$\sigma_c = (14 + 0.175D) I_s \qquad (5.2)$$

where:

D is core diameter in millimeters, and

I_s is the point load strength.

5.3.4 Fracture Toughness

Fracture toughness is the basic material parameter in fracture mechanics. The fracture toughness test differs from ordinary material strength tests by requiring specimens with well-defined cracks.

The International Society for Rock Mechanics (ISRM) Commission on Testing Methods suggests two methods to measure the mode I plane strain fracture toughness on rock (ISRM: Fracture Toughness of Rock, 1988). Both methods require the use of core specimens. Method I (Chevron Bend) uses a bend specimen with a notch cut perpendicular to the core axis, while the method II (Short Rod) uses a specimen, called the short rod, which has a notch cut parallel to the core axis. In the Chevron Bend test, the specimen rests on two support rollers and a compressive load is applied at the center to press apart the notch sides. The Chevron Bend method was employed in this study and Figure 5.1 shows the schematic of the test set-up and specimen geometry. The specimen was failed by crack growth in the unnotched part of the specimen when load was added to it.

Contrary to the Chevron Bend test, a tensile load is applied to the specimen to pull apart the notch sides in the Short Rod test. In this case, a lengthwise splitting of the specimen is caused by crack growth in the uncut part of the specimen. Because in both methods, the ligament of the notched section has the form of a "V" or chevron, this shape generates a relatively long period of stable crack growth under increasing load before fracture.

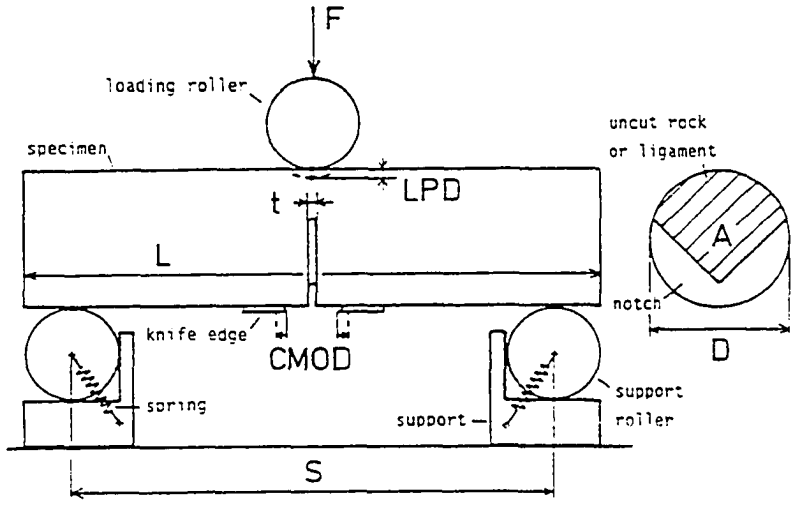

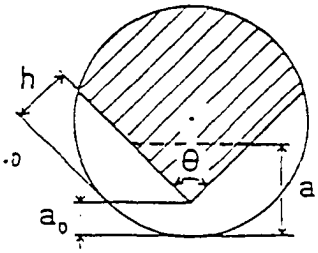

Basic notation:

D = diameter of chevron bend specimen
S = distance between support points, 3.33·D
θ = chevron angle, 90°
a_0 = chevron tip distance from specimen surface, 0.15·D.
a = crack length
t = notch width
h = depth of cut in notch flank
L = specimen length
A = projected ligament area
F = load on specimen
LPD = deflection of load point relative to support points
CMOD = relative opening of knife edges

Figure 5.1: Schematic of the Chevron Bend method and specimen geometry for fracture toughness test (from ISRM, 1988)

5.4 HARDNESS

Hardness is an indication of material behavior under an impact of force rather than a fundamental material property. As such, the quantitative measure of hardness depends on the type of test employed. Three types of tests can be used to measure the hardness of rocks. The first type of hardness test is the scratch test, which is widely used to determine mineral hardness. One of the earliest and most famous scratch tests was proposed by Mohs in 1822. The Mohs Scale, however, can only approximate hardness of minerals for comparison purpose. Latter efforts have been made by Talmage and Bierbaum (ISRM: Hardness and Abrasive of Rocks, 1977) to provide a more quantitative measure of hardness. The scratch hardness test was not employed in this study.

The second type of hardness test is the indentation test, which was originally developed from metallic materials. Hardness measured from an indentation test is a measure of the resistance of a material to permanent deformation. It is commonly measured by placing an indenter in contact with the material being tested. Usually the indenter material is much harder than the specimen, with tungsten carbide or diamond being commonly used. After the indentation has been made, the indenter is removed. The hardness is thus determined from the applied load and the geometry of the indentation.

Several indentation tests have been developed. The Brinell method of determining hardness is by the indentation effect of a hard ball. For the Rockwell method, the indenter can be either a steel ball or a diamond cone, with the geometry of the indenter and the magnitude of load specified. These two tests are widely used in metal but are not generally applicable to rock. The Knoop and the Vickers tests use a diamond pyramid as

the indenter. Both tests determine the microhardness of individual rock minerals. The Vickers test is well-known in hardness determination for both metallic and non-metallic materials, especially for materials with higher hardness.

The third type of hardness test is a dynamic or rebound test. In a dynamic or rebound hardness test, an indenter is employed to strike the test specimen. Any plastic or yielding material behavior produced by the impact will reduce the elastic energy available to rebound the indenter. The height of rebound is taken as a measure of the hardness of the material. The two tests suggested by the International Society of Rock Mechanics are the Schmidt hammer rebound hardness test and the Shore scleroscope hardness test.

5.4.1 Schmidt Hardness

The Schmidt rebound hardness test was originally developed to estimate the compressive strength of concrete. It is now being used for rock hardness determinations as well (ISRM: Hardness and Abrasiveness Determinations, 1977). It consists of a spring-loaded piston and a metal anvil, which is in contact with the rock surface. The piston is rebounded when it is pushed to the full length of the metal anvil. The height of piston rebound is taken as a measure of rock hardness.

The Schmidt hardness test is a simple and quick technique. The advantage of the Schmidt hardness test is that it can be applied directly to unprepared rock samples. It is a good alternative to the uniaxial compressive strength test for medium hard rocks (Cargill and Shakoor, 1990). In this study, the Schmidt hammer hardness test was performed on both bulk and core samples by a Type L Concrete test hammer.

The relationships between the Schmidt rebound hardness and the uniaxial compressive strength for a Type L Schmidt hammer can be found in Hoek & Bray, 1981.

5.4.2 Shore Scleroscope Hardness

Another dynamic hardness test performed in this study was the Shore scleroscope hardness test. The Shore scleroscope is a laboratory test device that measures hardness by dropping a small diamond-tipped indenter on the surface of specimen. As the case in the Schmidt hardness test, the height of the rebound is taken as the measure of hardness. Because of the small size of the diamond indenter tip, rock hardness measured in this test is the hardness of individual mineral grains. It is, therefore, necessary to conduct a large number of rebound tests to obtain an average hardness for a rock. The test is usually repeated in random and the measurements were averaged. In this study, the device used was a Model D Shore scleroscope. The test was conducted on the surface of core specimens which were later used in the uniaxial compressive strength test. The testing procedures were adapted from the International Society for Rock Mechanics suggested method (ISRM: Hardness and Abrasiveness, 1977).

Brady (1971) compiled data of the Vickers hardness (VH, g/mm^2) and the Shore scleroscope hardness (SS, a dimensionless number). His data were plotted in Figure 5.2 by the author of this thesis. An exponential equation was found to best present these data. The equation is:

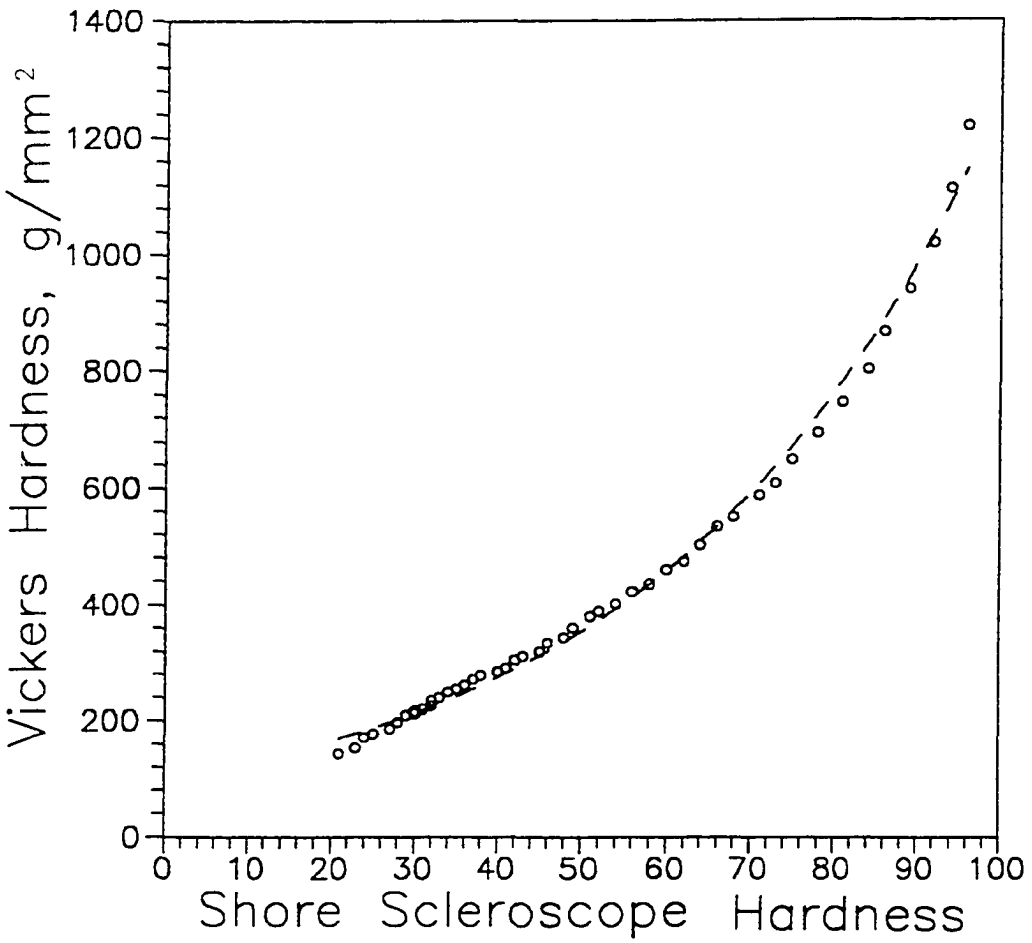

Figure 5.2: Vickers hardness vs. Shore sclerosocpe hardness (data from Bradley, 1977)

$$VH=99.3222e^{0.0255SS} \qquad (5.3)$$

The Vickers hardness was used in some of the drilling models in this study.

5.5 RESULTS AND COMPARISONS

The results of the rock physical property tests are summarized in Table 5.1. It was noted that four (rocks A, B, C, and F) of the six rocks had a uniaxial compressive strength larger than 100 Ma. The uniaxial compressive strengths of schist (D) and limestone (E) were less than 100 MPa.

The splitting tensile strengths were about one order of magnitude less than the uniaxial compressive strengths. It was also noted that the numerical values of the point load strength were very close to that of the splitting tensile strength for the six rocks tested in this study. The diorite (B) had the highest splitting tensile strength (14.36 MPa) and the limestone (E) had the lowest (4.77 MPa) among the six rocks.

The results also indicated that rock C had the highest fracture toughness (2.14 $MN/m^{1.5}$) while rock A had the lowest K_c (1.12 $MN/m^{1.5}$). The largest Shore scleroscope hardness was found in rock B (= 79.5) and the lowest was rock E (= 41.28).

The two types of Schmidt hardness showed a certain deviation in numerical values. For all of the six rocks tested, the Schmidt hardness of bulk specimens was higher on than that of core specimens.

Measurements of the Characteristic Dimension (L_D) varied largely for the six

Table 5.1: Rock physical properties

Rock sample	A	B	C	D	E	F
Rock type	Sandstone	Diorite	Granite	Schist	Limestone	Granodiorite
Shore scleroscope hardness	58.45	79.75	68.86	59.25	41.28	65.49
Schmidt hardness (bulk)	51.65	62.24	54.65	47.34	43.45	56.48
Schmidt hardness (core)	38.15	42.02	41.24	37.59	31.60	38.50
Point load strength (MPa)	9.41	14.88	10.96	8.97	6.28	11.72
Uniaxial compressive strength (MPa)	102.94	163.41	129.98	73.11	83.68	153.16
Splitting tensile strength (MPa)	11.74	14.36	8.30	6.18	4.77	12.10
Fracture toughness ($MN/m^{1.5}$)	1.12	1.63	2.14	1.17	1.52	1.60
Young's Modulus (GPa)	48.70	27.50	38.45	9.75	15.25	36.20
Density (g/cm^3)	2.71	2.72	2.60	2.70	2.73	2.61
Characteristic dimension (mm)	0.28	1.68	3.08	1.96	7.30	2.80

rocks. It was found that rock A had the smallest L_D (i.e., 0.28 mm) and rock E had the largest L_D (i.e., 7.30 mm) among the six rocks. The L_D of rock E was about 26 times as large as the L_D of rock A.

In a rock drillability study, an important task is to find an appropriate rock property so that the drillability of a drill in the rock can be quantified. In this study, the relationships among rock properties were investigated statistically. The properties included in a linear correlation analysis were: 1). Shore scleroscope hardness, 2) Schmidt hardness of bulk specimen, 3) Schmidt hardness of core specimen, 4) point load strength, 5) uniaxial compressive strength, 6) splitting tensile strength, 7) fracture toughness, and 8) Characteristic Dimension.

Table 5.2 lists the coefficients of determination, R^2, of the correlation analyses for the eight rock physical properties. Usually high correlation was found between strength properties and hardness indices. The Characteristic Dimension, however, was found to have weak correlation with the other properties except with the Schmidt hardness (core). The fracture toughness seemed to be uncorrelated with the other properties.

5.5.1 Relationships among Hardness Indices

Three hardness tests were performed in this study, i.e., Schmidt hardness test on bulk specimen (SB), Schmidt hardness test on core specimen (SC), and Shore scleroscope hardness (SS). From Table 5.1 it was noted that the values of Schmidt hardness on bulk specimens was 1.26 to 1.48 times larger than it was on core specimens, with an average of 1.39 for the six rocks tested in this study. A regression analysis was conducted to

Table 5.2: Coefficients of determinations among rock physical properties in the preliminary rock coring test

Rock sample	Schmidt hardness (bulk)	Schmidt hardness (core)	Point load strength	Uniaxial compressive strength	Splitting tensile strength	Fracture toughness	Characteristic dimension dimension
Shore scleroscope hardness	0.89	0.93	0.94	0.64	0.60	0.13	0.42
Schmidt hardness (bulk)		0.76	0.97	0.88	0.81	0.12	0.31
Schmidt hardness (core)			0.78	0.48	0.50	0.16	0.54
Point load strength				0.79	0.73	0.09	0.32
Uniaxial compressive strengt					0.69	0.22	0.08
Splitting tensile strength						0.00	0.45
Fracture toughness							0.07

correlate the two Schmidt hardness values. It was found that a linear equation can best describe the relationship:

$$SC=0.4806SB+12.8895 \qquad (5.4)$$

Where both indices are dimensionless. This relationship is also graphically presented in Figure 5.3.

Figure 5.4 shows the relationships between two measurements of Schmidt hardness indices and the Shore scleroscope hardness. It was noted that the two Schmidt hardness indices had the similar linear relationship with the Shore scleroscope hardness. Linear regression was performed and two linear relationships were found. They are:

$$SB=0.4931SS+21.9749 \qquad (5.5a)$$

and

$$SC=0.2772SS+20.9446 \qquad (5.5b)$$

The Shore scleroscope hardness is also dimensionless.

5.5.2 Relationships among Strengths

Figure 5.5 plots the point load strength and the splitting tensile strength against the uniaxial compressive strength. Two linear relationships are:

$$I_s=0.0695\sigma_c+2.1862 \qquad (5.6a)$$

and

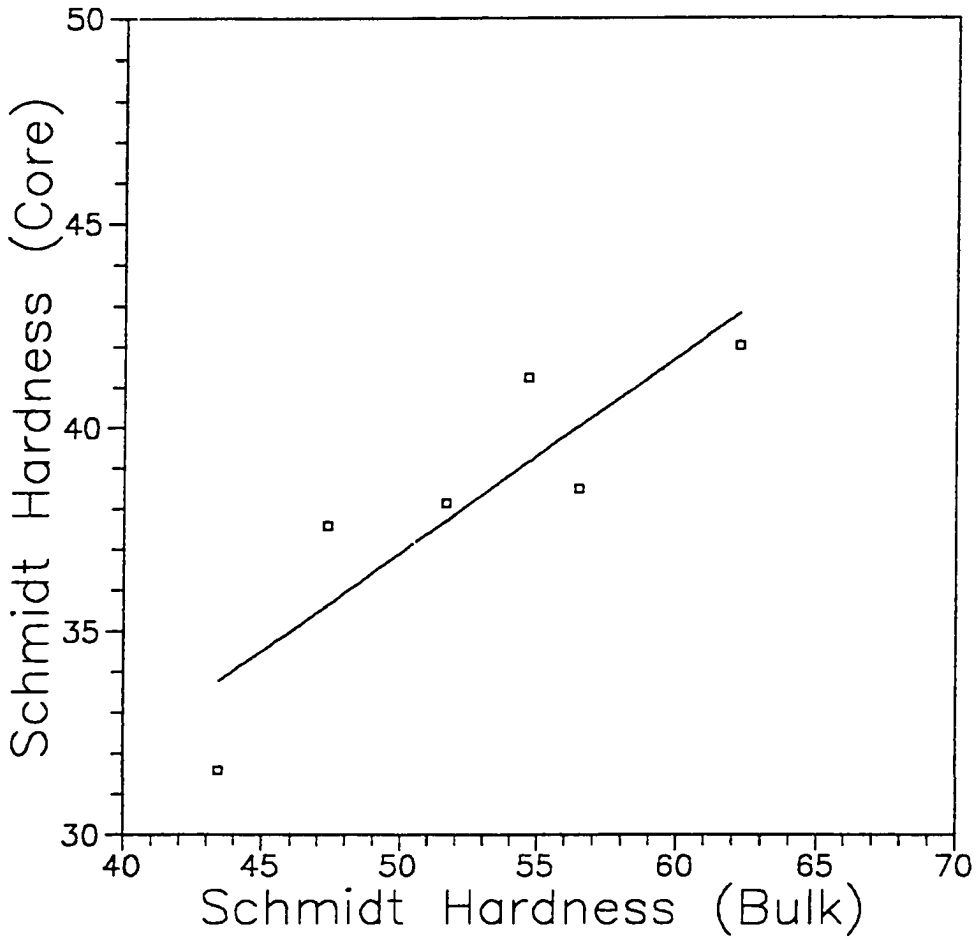

Figure 5.3: Schmidt hardness of core specimens vs. Schmidt hardness of bulk specimens

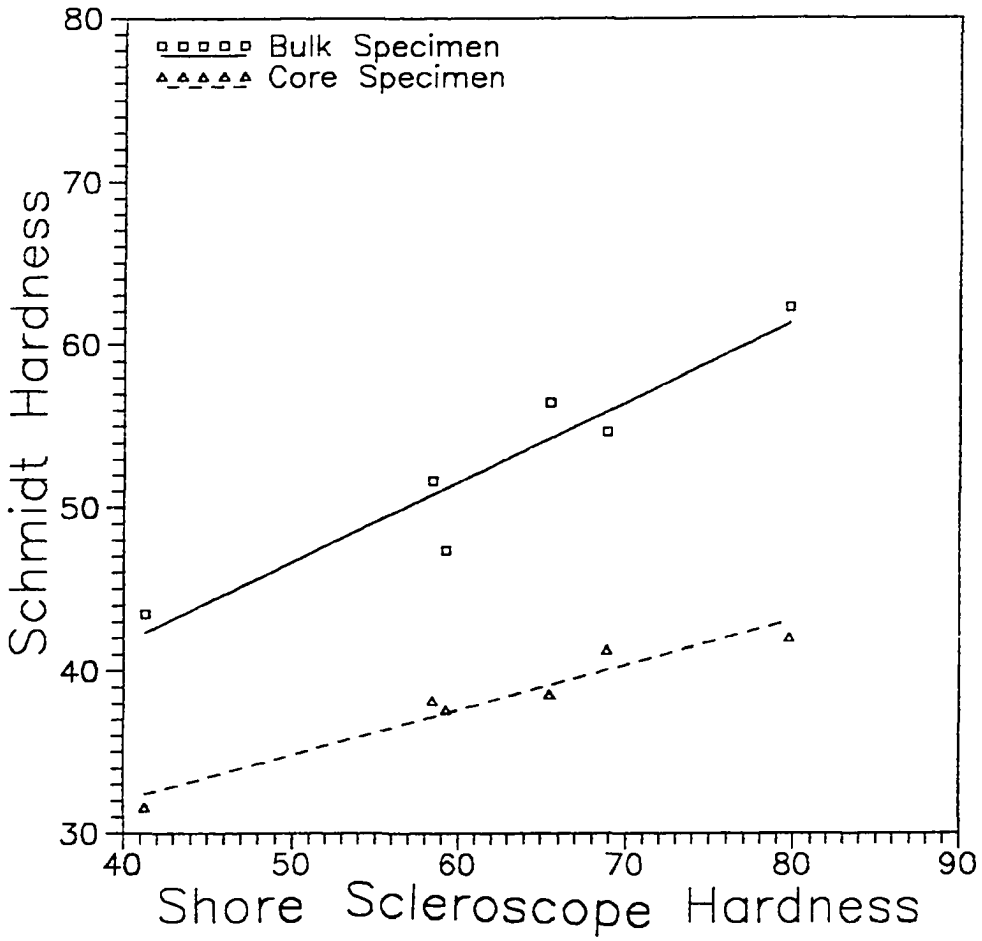

Figure 5.4: Schmidt hardness vs. Shore scleroscope hardness

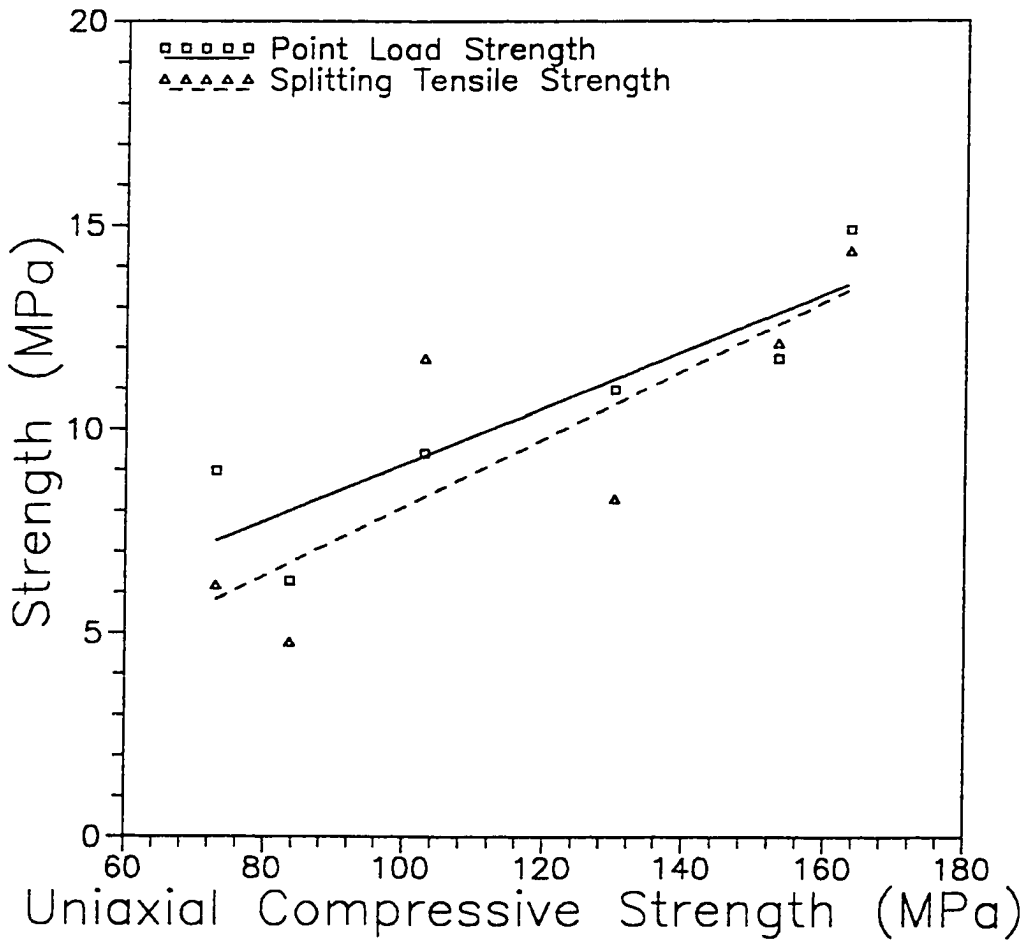

Figure 5.5: Point load strength and splitting tensile strength vs. uniaxial compressive strength

$$\sigma_t = 0.0839\sigma_c - 0.2986 \qquad (5.6b)$$

Where I_s, σ_c, and σ_t are in MPa.

5.5.3 Strengths vs. Shore Scleroscope Hardness

Three strength properties (i.e., point load strength, uniaxial compressive strength, and splitting tensile strength) are plotted against the Shore scleroscope hardness in Figure 5.6. Linear regression was performed. Equations 5.7 expresses these relationships:

$$I_s = 0.2195SS - 3.2812 \qquad (5.7a)$$

and

$$\sigma_c = 2.3061SS - 25.6774 \qquad (5.7b)$$

and

$$\sigma_t = 0.2261SS - 4.4836 \qquad (5.7c)$$

5.5.4 Strengths vs. Schmidt Hardness

As with the hore scleroscope hardness, three strength properties are plotted against the Schmidt hardness of bulk specimens in Figure 5.7. Linear regression was also performed. Equations 5.8 presents the three relationships:

$$I_s = 0.260SB - 12.0521 \qquad (5.8a)$$

and

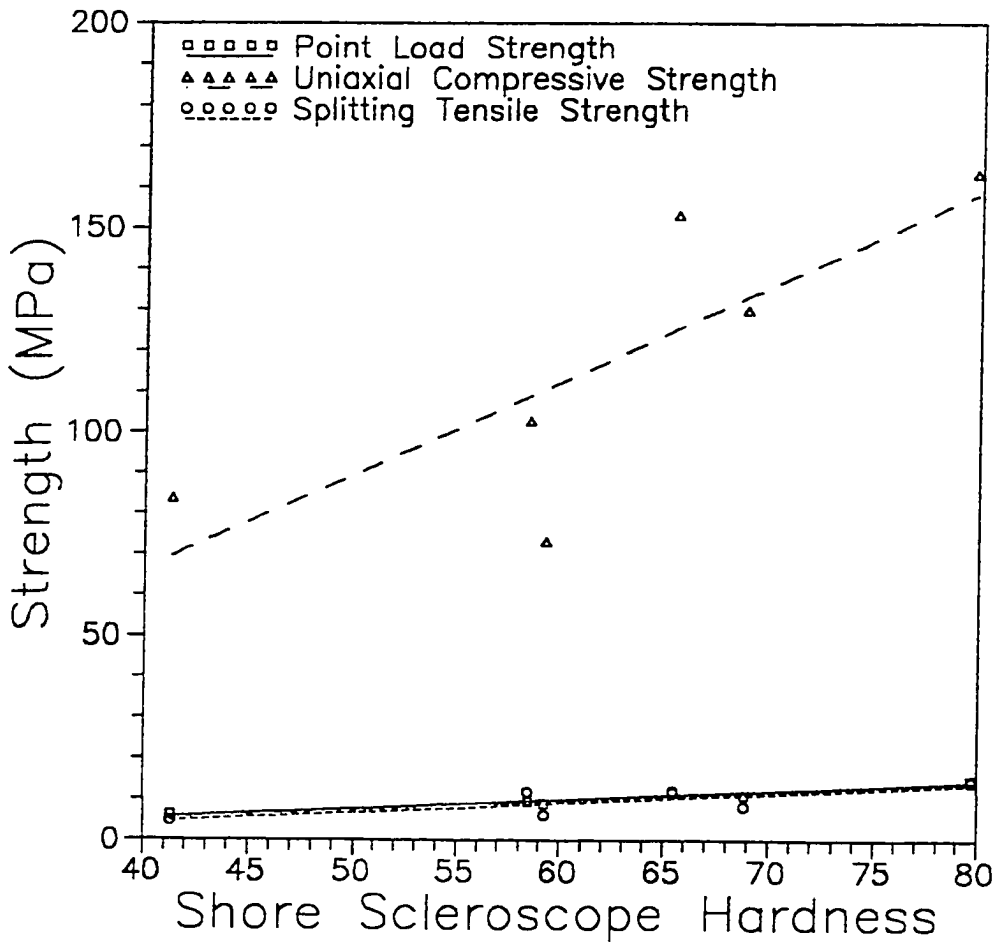

Figure 5.6: Strengths vs. Shore sclerosocpe hardness

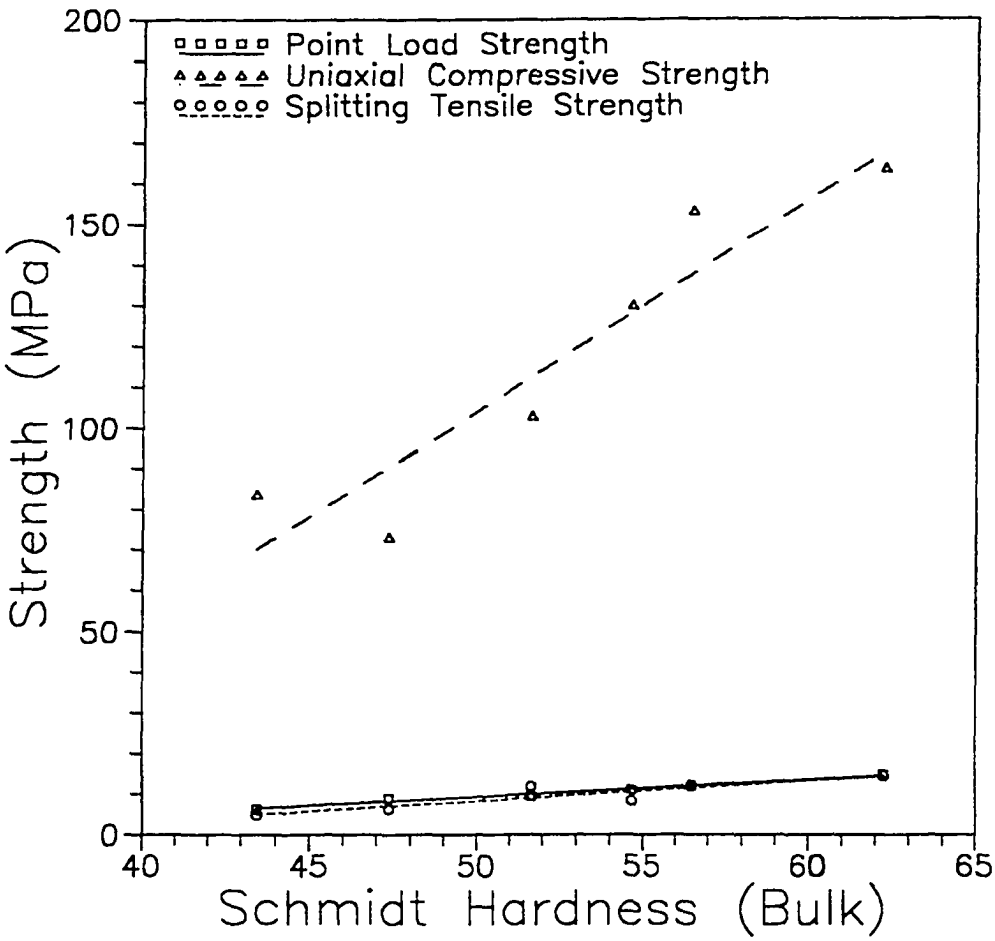

Figure 5.7: Strengths vs. Schmidt hardness of bulk specimens

$$\sigma_c = 5.1822SB - 155.050 \qquad (5.8b)$$

and

$$\sigma_t = 0.5037SB - 16.9398 \qquad (5.8c)$$

CHAPTER 6

RESULTS AND DISCUSSIONS - PART I

6.1 INTRODUCTION

A comprehensive laboratory drilling and coring test program was performed in this research at the University of Alaska Fairbanks. Some of the results from this study were used in the project *"Rock Drilling under the Greenland Ice Sheet"* by the Polar Ice Coring Office of the National Science Foundation in summer 1993. Chapter 4 describes the drilling and coring equipment, measuring devices, and data acquisition system. In each drilling test, a constant load and rotational speed were kept according to the experimental design. The data collected in a drilling test included testing time and measurements from the four transducer amplifiers (i.e., instantaneous weight-on-bit, actual rotational speed of bit, applied torque at drill spindle, and penetration depth of bit). The test results were collected every two seconds. The data could be printed out directly by a printer or sent to a computer. The Procomm program, a communication software, was used to receive data from the data logger. An example of a data sheet from the 6-488B data acquisition system is shown in Appendix 3. A Basic program was developed to extract data for computation. This program is included in Appendix 4. The four transducer measurements mentioned above were plotted against time for each test. Figures 6.1 to 6.6 present examples of those plots. It was noted that of the four measurements, the rotational speed was most stable throughout the test. The actual weight-on-bit, applied torque, and

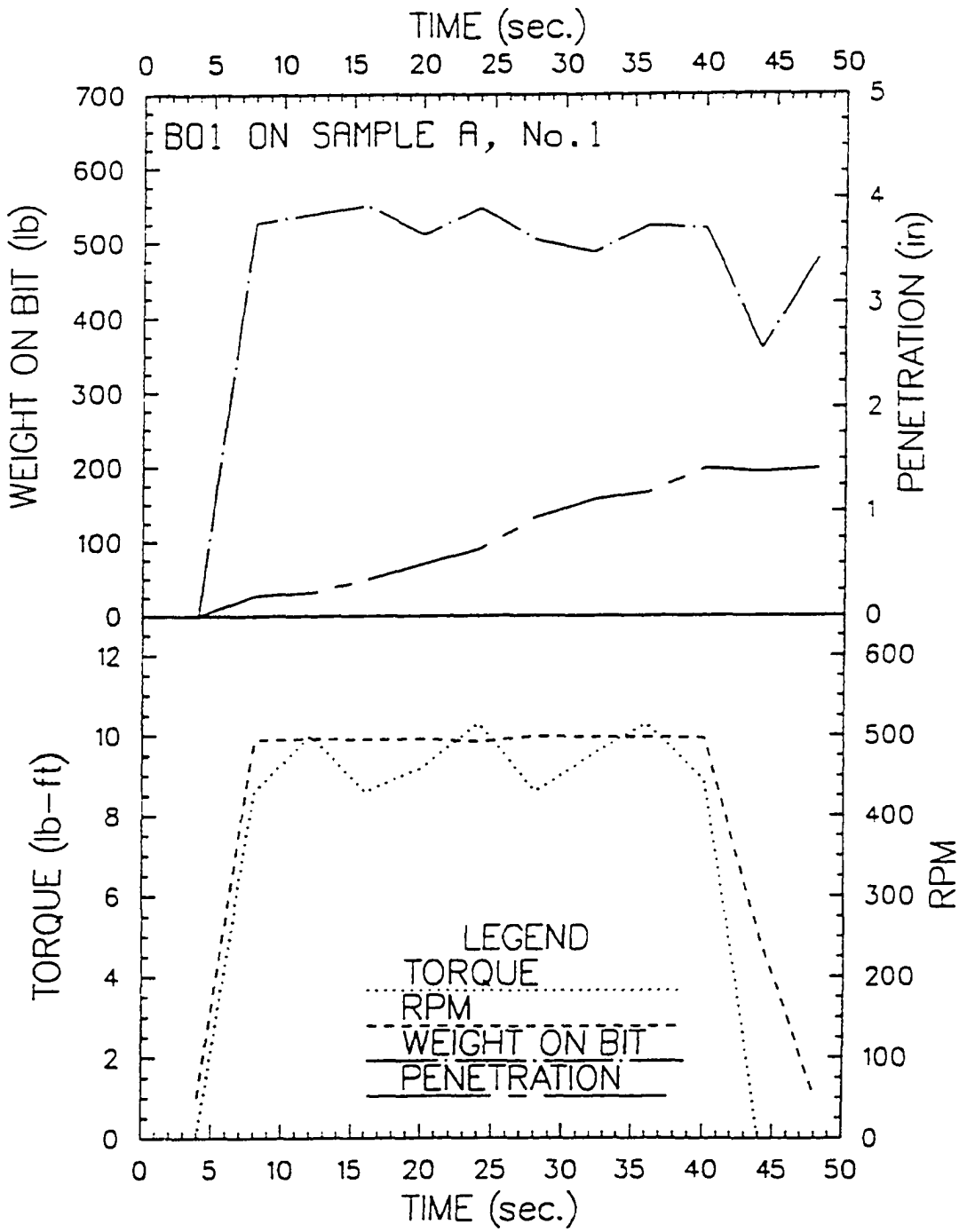

Figure 6.1: Drilling test of BQ1 bit on rock A, Trial No. 1

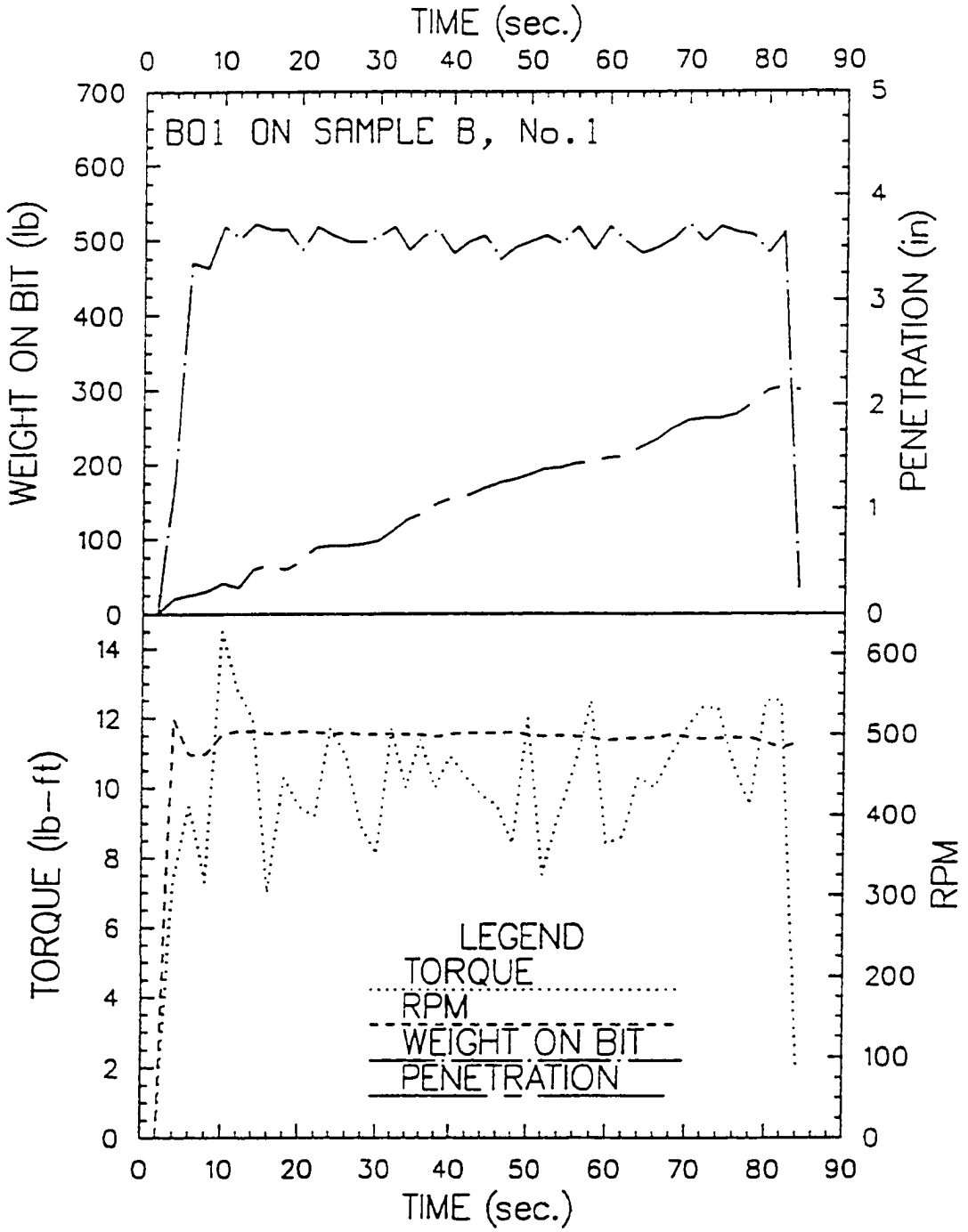

Figure 6.2: Drilling test of BQ1 bit on rock B, Trial No. 1

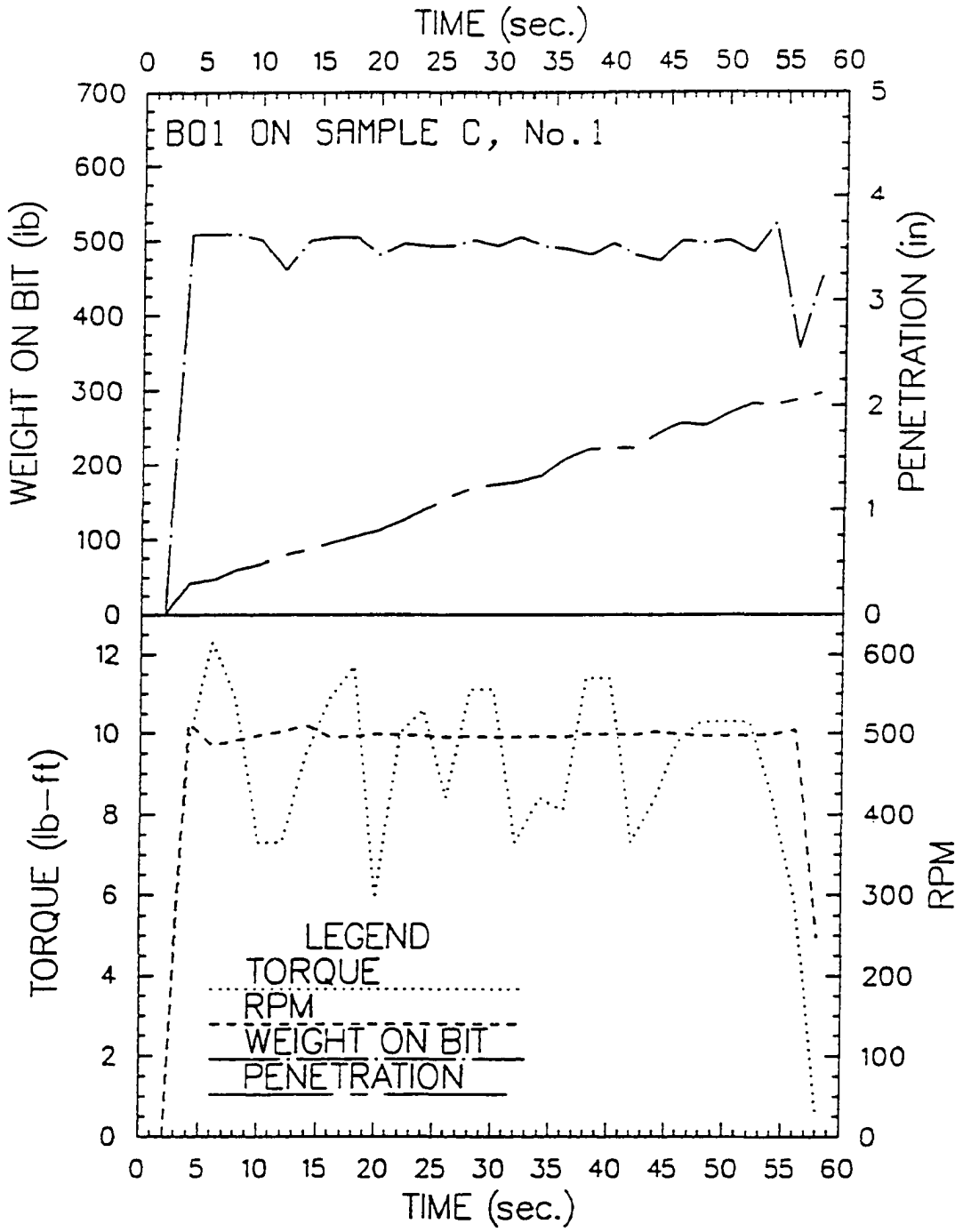

Figure 6.3: Drilling test of BQ1 bit on rock C, Trial No. 1

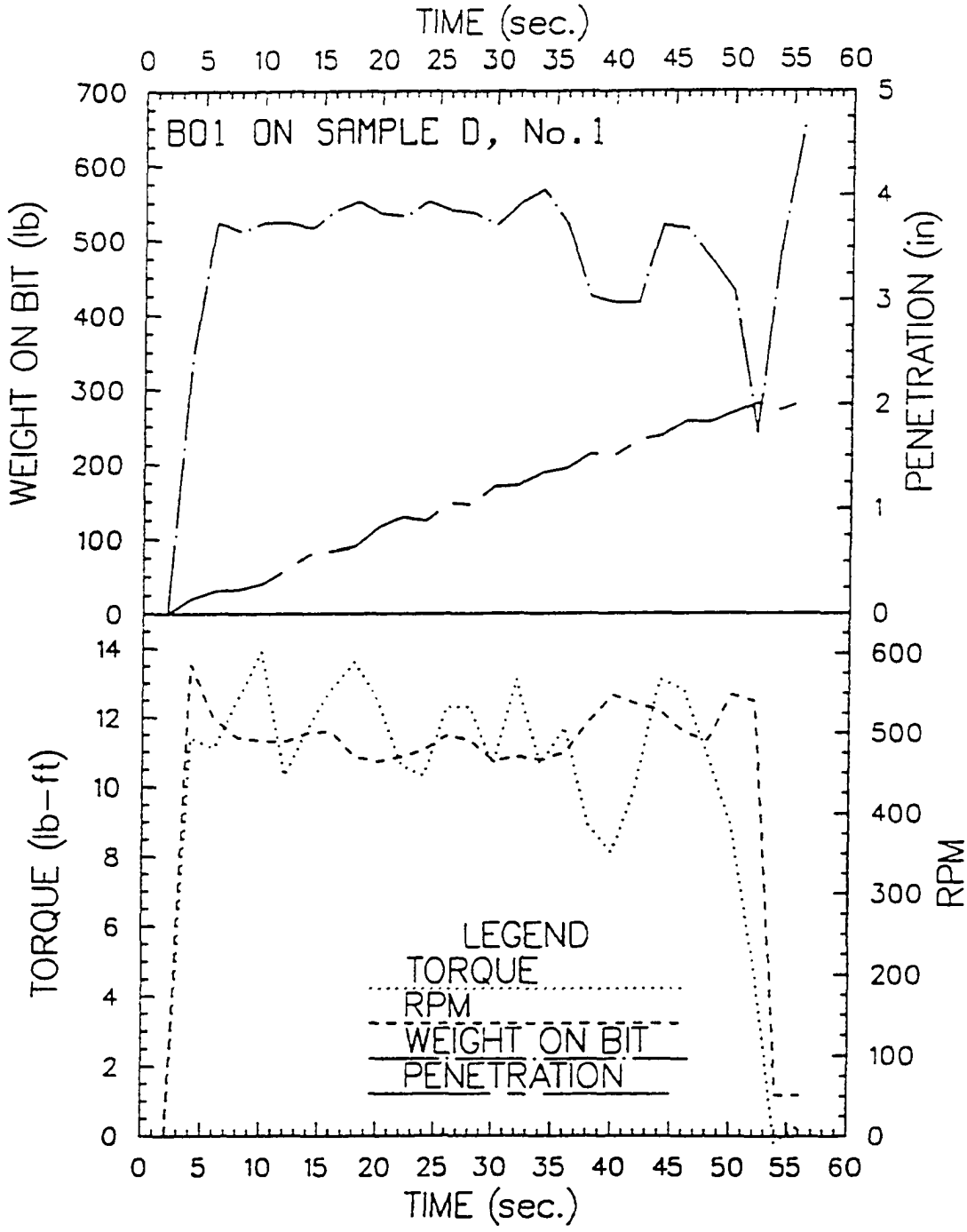

Figure 6.4: Drilling test of BQ1 bit on rock D, Trial No. 1

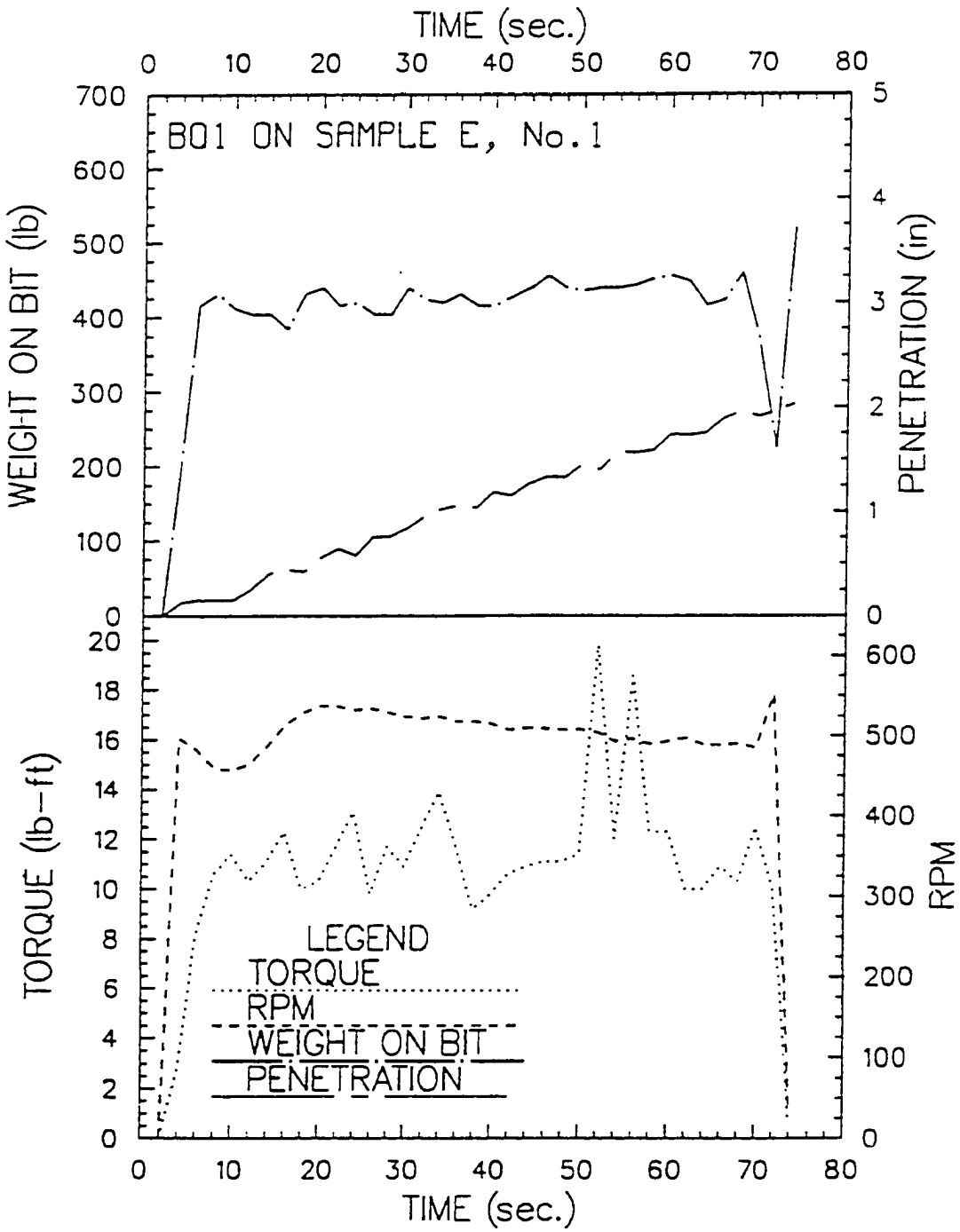

Figure 6.5: Drilling test of BQ1 bit on rock E, Trial No. 1

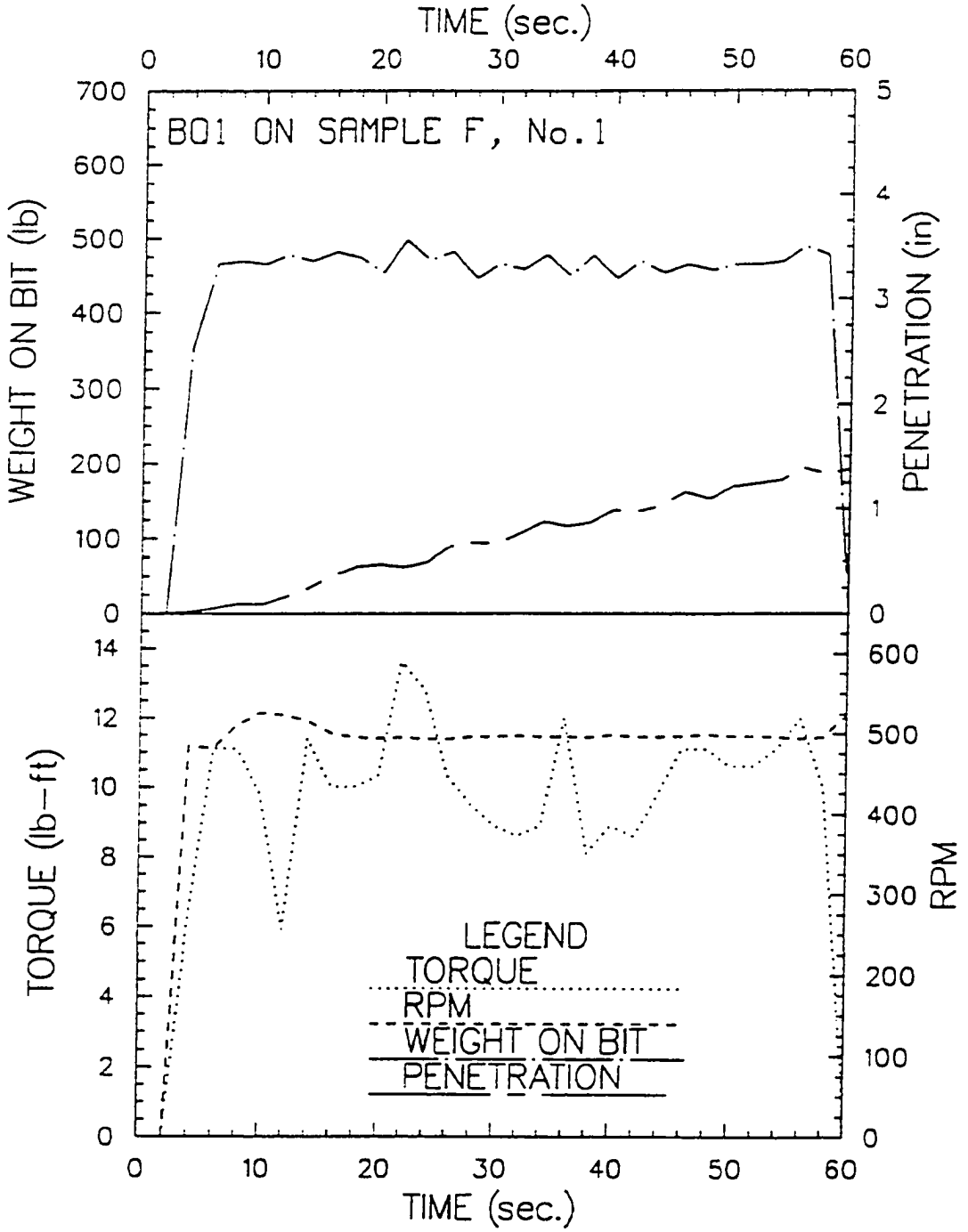

Figure 6.6: Drilling test of BQ1 bit on rock F, Trial No. 1

penetration depth, however, fluctuated with time. The fluctuations could have been caused by vibration of the drill, vertical acceleration of the bit, inhomogeneity of the mineral compositions in rock specimens, and oscillation of the electronic devices. In this study, the weight-on-bit was referred to as the static bit load. The applied torque was obtained by averaging all of the torque measurements at a 2-second interval in the test. Linear regression procedure was conducted on the penetration depth with time, and the slope of the linear regression line was taken as the penetration rate of the test. Usually, the coefficients of determination, R^2, of these linear equations were high, ranging from 0.96 to 1.0, indicating a uniform drilling action.

Results of the preliminary rock coring test are discussed in the following sections of this chapter. The preliminary rock coring test was the first series of rock drilling tests performed in this study. Four Longyear core bits, namely AQ1, AQ2, BQ1, and BQ2, were tested on six rocks (i.e., A-sandstone, B-diorite, C-granite, D-schist, E-limestone, and F-granodiorite). Each bit was tested twice on each rock sample and thus there were 48 tests in total. The testing conditions of those 48 tests were identical at a 2,402 N (540 lb) weight-on-bit, 500 rpm rotational speed, and 5.68 *l/min* (1.5 gpm) flow rate. Purpose of this test was to compare the drilling performance and efficiency of the four bits. Results of this test are summarized in Appendix 5.

6.2 SURFACE-SET BITS

Two surface-set diamond bits were used in this test. One was AQ1 bit and the other was BQ1 bit. The specifications of the AQ1 and BQ1 bits are presented in Table 4.2. There were three major design differences between these two surface-set bits. First, the carat weight of diamonds on the BQ1 bit was 12, versus 10 on the AQ1 bit. Secondly, both the inner and outer diameters of the AQ1 and BQ1 bits were different. As a result, the cross-section areas of the two bits were different. The cross-section area of the BQ1 bit was 42.45% larger than that of the AQ1 bit. Lastly, there were six waterways on the AQ1 bit. These waterways divided the bit matrix into six sections, with each section containing 30 diamond particles. The BQ1 bit, however, had eight waterways and, therefore, eight matrix sections with each section containing 28 diamond particles. If the same load is exerted upon the AQ1 and BQ1 bits, the pressure under each diamond on the BQ1 bit will be only about 80% of the pressure on each diamond of the AQ1 bit.

For each of the four bits tested, there were two duplicate tests performed on each of the six rocks. There were total 48 tests conducted in the preliminary rock coring test with 12 tests for each bit. In those 12 tests for a given bit, because the weight-on-bit, rotational speed, and flow rate were all identical, the bit performance was only a function of the rock properties. The influential rock properties include Shore scleroscope hardness (SS), Schmidt hardness on bulk rock specimens (SB), Schmidt hardness on rock core specimens (SC), point load strength (I_s), uniaxial compressive strength (σ_c), splitting tensile strength (σ_t), fracture toughness (K_c), and Characteristic Dimension (L_D).

The performance of a bit was assessed based on the penetration rate, applied

torque, and specific energy. To relate the bit performance with rock properties, the General Linear Model (GLM) regression analysis was conducted. The GLM regression analysis was performed, including linear, quadratic, and cubic models. Results of these analyses are discussed in the following sections.

6.2.1 Penetration Rate

6.2.1.1 AQ1 Bit

As was explained earlier, the penetration rate of a test was obtained from a linear regression of the penetration depth versus testing time in a test. The GLM linear, quadratic, and cubic procedures were conducted on penetration rate with rock properties. Table 6.1 shows the *coefficients of determination*, R^2, and F-values of these analyses for the AQ1 bit. The critical F-value depends on the *degrees of freedom for regression model* (df_r) and the *degrees of freedom for error* (df_e). In the preliminary rock coring test, there were 6 tests for each bit and thus the *degrees of freedom for total* (df_t) was 5. For the linear GLM model, df_r is 1 and df_e is 4. For the quadratic model, df_r is 2 and df_e is 3. For the cubic model, df_r is 3 and df_e is 2. The critical F-values for the linear, quadratic, and cubic models are 7.71, 9.55, and 19.16 at α=0.05, respectively.

From Table 6.1 it was noted that among all eight linear GLM regression models, only the uniaxial compressive strength showed a significant correlation with the penetration rate (R^2=0.70 and F=9.13 for the linear model). Its corresponding quadratic model also indicated a significant correlation (R^2=0.87 and F=10.32).

Figure 6.7 plots the penetration rate versus the properties for AQ1 bit. It was noted

Table 6.1: Regression analysis of penetration rate for AQ1 bit in the preliminary rock coring test

Rock property	1st Degree GLM		2nd Degree GLM		3rd Degree GLM	
	R-squared	F-value	R-squared	F-value	R-squared	F-value
Shore Scleroscope Hardness	0.18	0.89	0.24	0.47	0.40	0.45
Schmidt Hardness (bulk)	0.46	3.35	0.46	1.26	0.82	3.04
Schmidt Hardness (core)	0.14	0.66	0.25	0.51	0.54	0.77
Point Load Strength	0.29	1.66	0.30	0.64	0.64	1.16
Uniaxial Compressive Strength	0.70	9.13	0.87	10.32	0.94	11.23
Splitting Tensile Strength	0.49	3.78	0.49	1.43	0.58	0.92
Fracture Toughness	0.21	1.03	0.36	0.83	0.78	2.32
Charateristic Dimension	0.01	0.02	0.01	0.02	0.23	0.34

Critical F-values at 0.05 confidence level:		
	Linear (1st) GLM:	7.71
	Quadratic (2nd) GLM:	9.55
	Cubic (3rd) GLM:	19.16

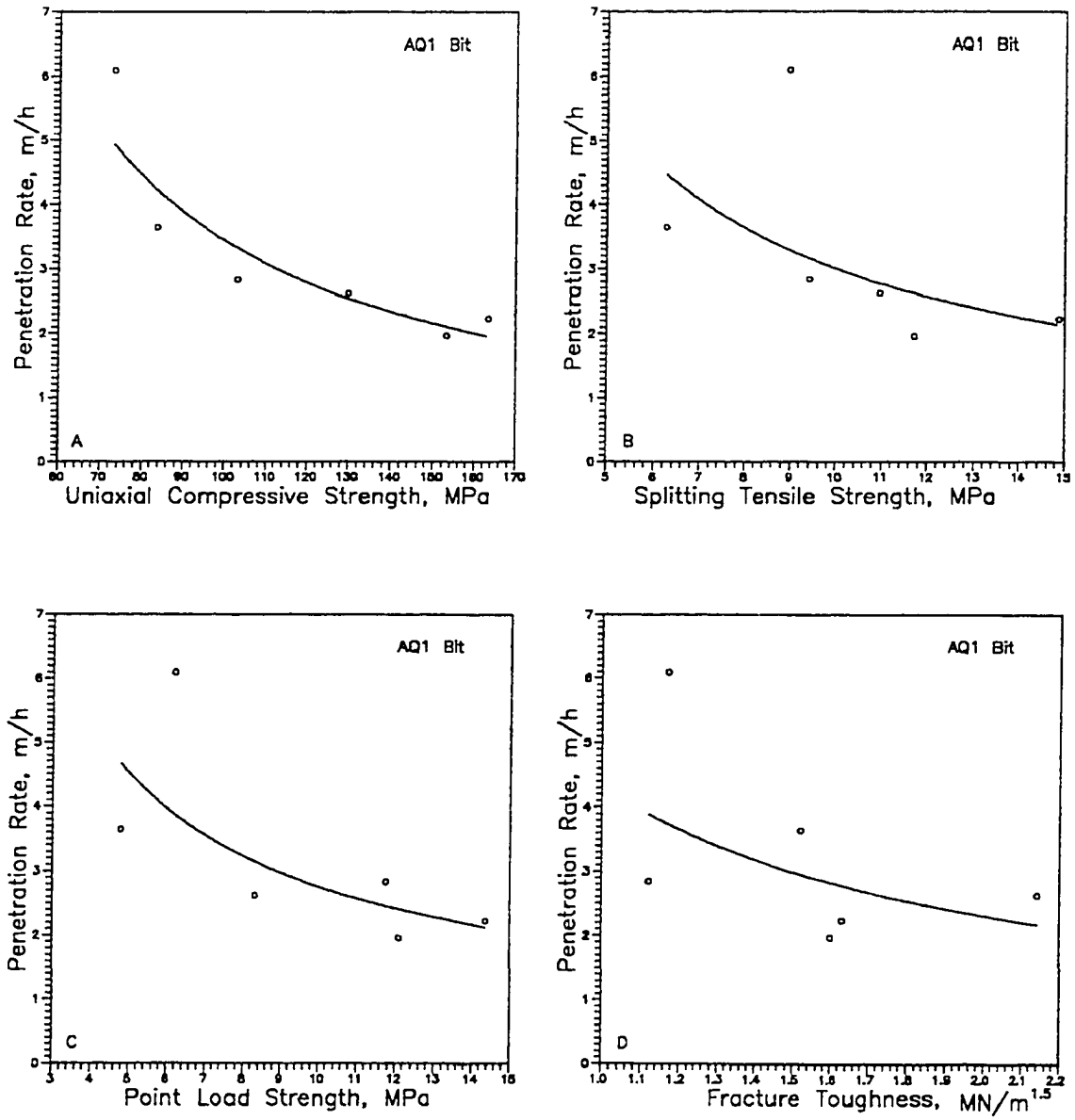

Figure 6.7: Penetration rate vs. rock properties for AQ1 bit in the preliminary rock coring test: (a) uniaxial compressive strength, (b) splitting tensile strength, (c) point load strength, (d) fracture toughness

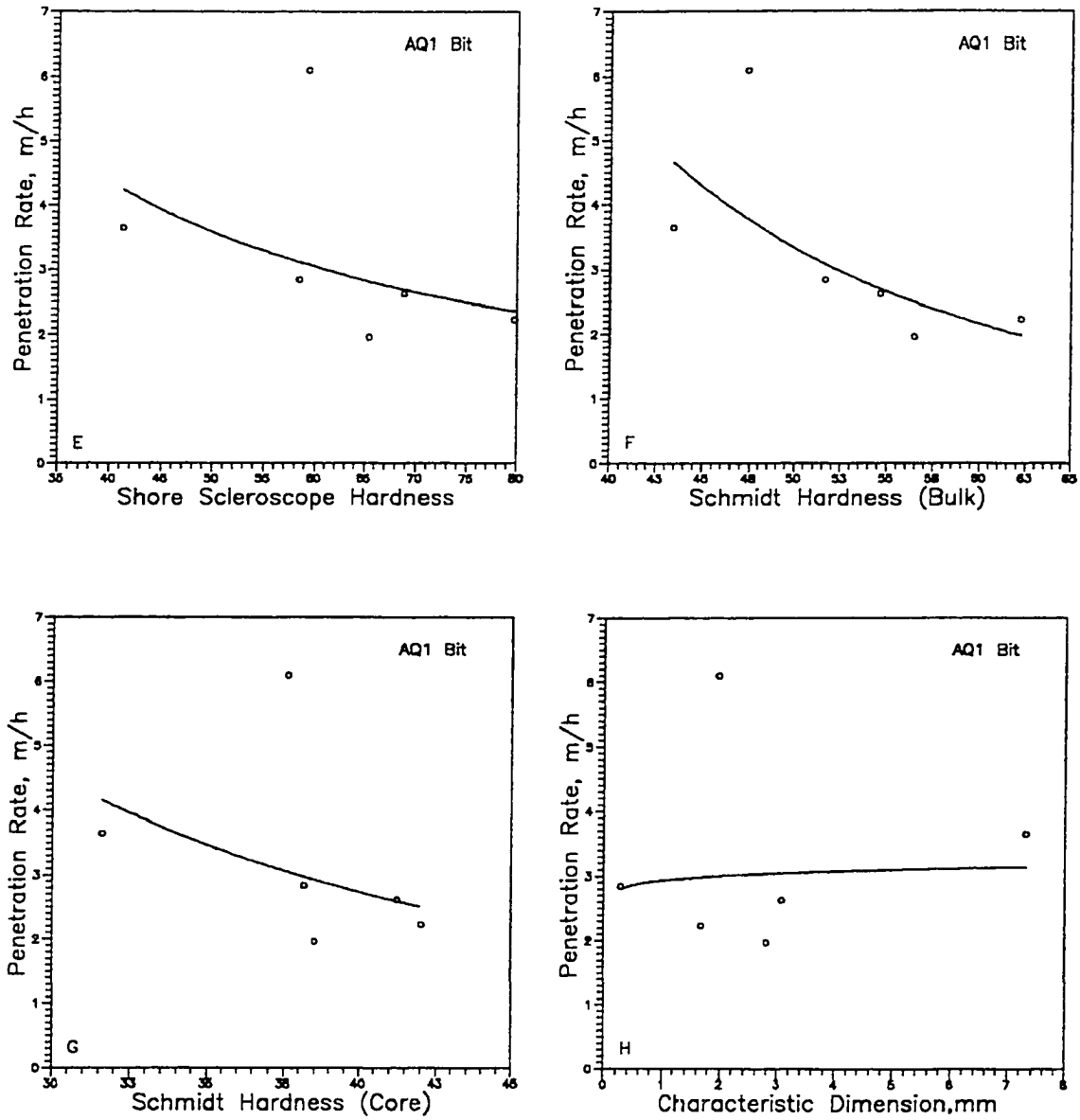

Figure 6.7 (cont'd): (e) Shore scleroscope hardness, (f) Schmidt hardness on bulk specimen, (g) Schmidt hardness on core specimen, and (h) characteristic dimension

that for the four strength properties (i.e., uniaxial compressive strength, splitting tensile strength, point load strength, and fracture toughness) and the three hardness indices (i.e., Shore scleroscope hardness, Schmidt hardness of bulk specimen, and Schmidt hardness of core specimen), a similar trend was obtained; the penetration rate decreased with the increase of strength or hardness of rock. Generally, the penetration rate was an inverse power function of the strength or hardness of rock except for the Characteristic Dimension. As shown in Figure 6.7(h), the data indicate a slightly increasing trend. This phenomenon could have been attributed to the larger limestone grains with low hardness.

6.2.1.2 BQ1 Bit

The similar regression procedures were performed on BQ1 bit and the result is summarized in Table 6.2. For the linear and cubic models, no rock properties were found to be significantly correlated with the penetration rate. For the quadratic model, only the fracture toughness had an F-value exceeding that of the corresponding critical value (12.62).

The penetration rate vs. the rock properties for BQ1 bit is presented in Figure 6.8. The penetration rate decreased with an increase in rock strength or hardness. The decreasing rate of those curves, however, was smaller than it was for the AQ1 bit.

The penetration rate vs. the Characteristic Dimension is presented in Figure 6.8(h). It was noted that the penetration rate decreased with the Characteristic Dimension for the BQ1 bit. Because the Characteristic Dimension indicated the average particle size in a rock, this implied that the larger the rock particles, the faster the rock was drilled by the

Table 6.2: Regression analysis of penetration rate for BQ1 bit in the preliminary rock coring test

Rock property	1st Degree GLM		2nd Degree GLM		3rd Degree GLM	
	R-squared	F-value	R-squared	F-value	R-squared	F-value
Shore Scleroscope Hardness	0.04	0.15	0.40	1.00	0.66	1.31
Schmidt Hardness (bulk)	0.08	0.35	0.44	1.17	0.72	1.76
Schmidt Hardness (core)	0.00	0.00	0.33	0.73	0.33	0.32
Point Load Strength	0.10	0.45	0.37	0.87	0.77	2.19
Uniaxial Compressive Strength	0.24	1.27	0.48	1.36	0.51	0.69
Splitting Tensile Strength	0.00	0.01	0.28	0.57	0.29	0.27
Fracture Toughness	0.19	0.92	0.89	12.62	0.93	9.42
Charateristic Dimension	0.30	1.75	0.64	2.61	0.75	2.00

Critical F-values at 0.05 confidence level:

Linear (1st) GLM:	7.71
Quadratic (2nd) GLM:	9.55
Cubic (3rd) GLM:	19.16

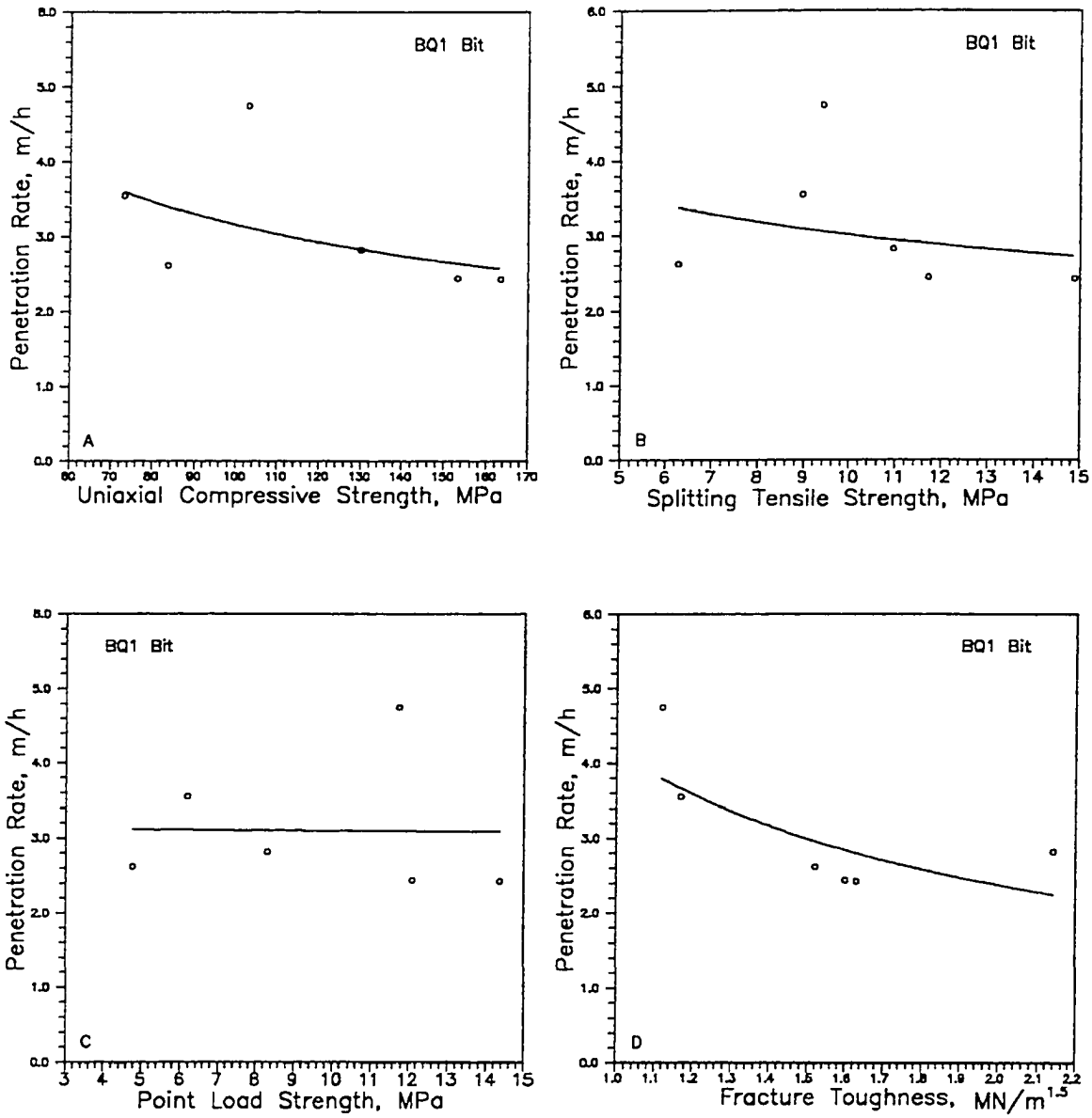

Figure 6.8: Penetration rate vs. rock properties for BQ1 bit in the preliminary rock coring test: (a) uniaxial compressive strength, (b) splitting tensile strength, (c) point load strength, (d) fracture toughness

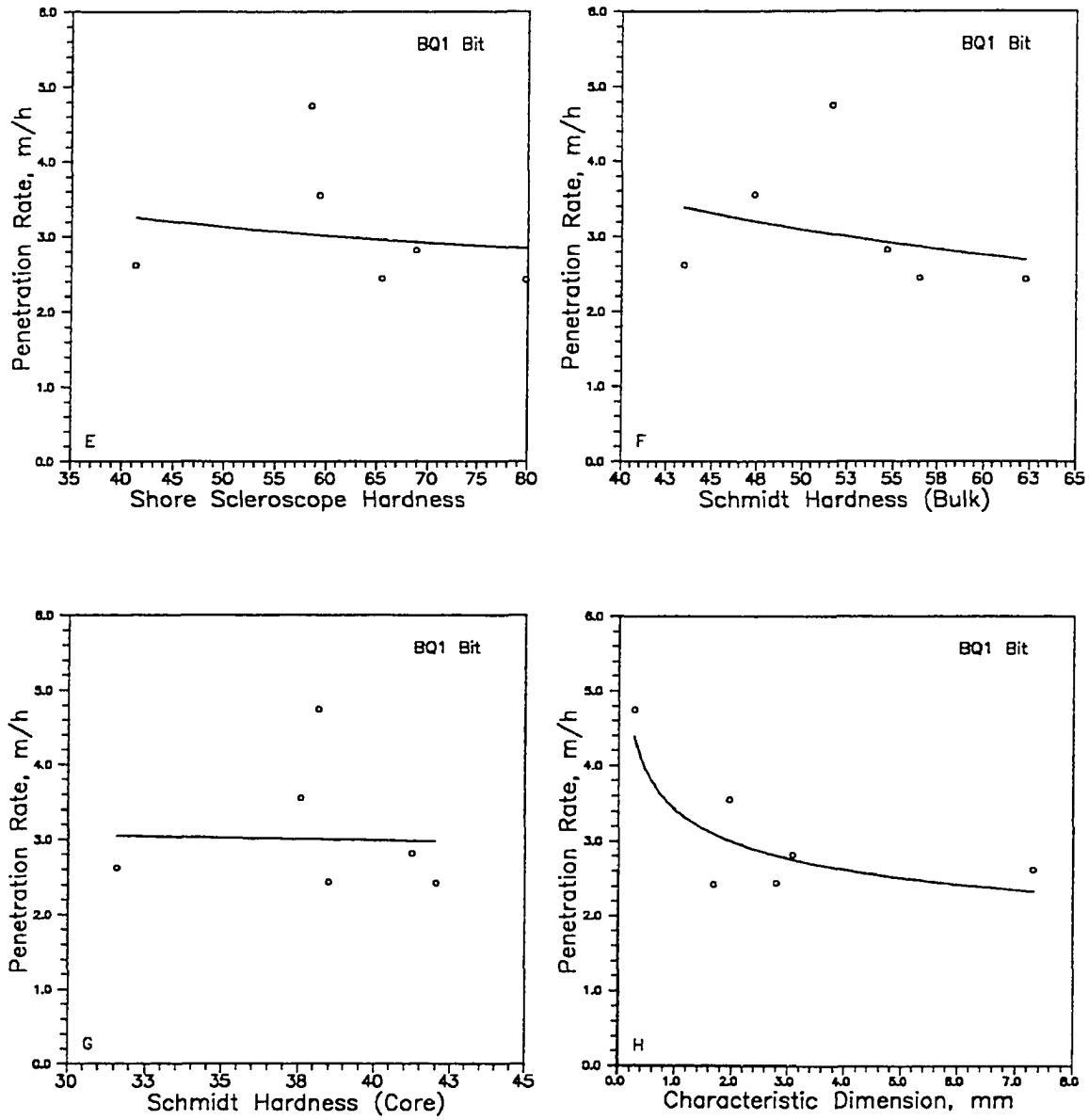

Figure 6.8 (cont'd): (e) Shore scleroscope hardness, (f) Schmidt hardness on bulk specimen, (g) Schmidt hardness on core specimen, and (h) characteristic dimension

BQ1 bit.

6.2.2 Applied Torque

6.2.2.1 AQ1 Bit

The applied torque measured in this experiment was the total torque needed to overcome the resistances of cutting, friction, and fluid. The torque required to overcome the resistance of fluid was minimal in comparison with the force of friction and cutting. Therefore, the measured torque was considered solely as a function of friction and abrasion at the bit-rock interface. The more torque goes to cutting, the more efficient a system is. The applied torque from this experiment was also analyzed by the GLM procedures. Table 6.3 shows the coefficients of determination and F-values of those analyses for the AQ1 bit. Observation of the F-values indicated that of the eight rock properties, only the splitting tensile strength showed a significant correlation with the applied torque in both linear and quadratic models. The Schmidt hardness (bulk), having an F-value of 16.99 for the quadratic model, also indicated a significant correlation with the applied torque.

The applied torque for the AQ1 bit versus the rock properties were presented in diagrams of Figure 6.9. Observation of Figures 6.9(a) to 6.9(g) revealed that a larger torque requirement corresponded to lower strength or hardness value. From Figure 6.9(h) it was noted that the applied torque increased slightly with the Characteristic Dimension. The reason of this, however, was not clear.

Table 6.3: Regression analysis of applied torque for AQ1 bit in the preliminary rock coring test

Rock property	1st Degree GLM		2nd Degree GLM		3rd Degree GLM	
	R-squared	F-value	R-squared	F-value	R-squared	F-value
Shore Scleroscope Hardness	0.44	3.09	0.67	2.99	0.70	1.57
Schmidt Hardness (bulk)	0.55	4.82	0.92	16.99	0.95	11.78
Schmidt Hardness (core)	0.50	4.06	0.64	2.64	0.82	2.98
Point Load Strength	0.43	2.96	0.80	5.82	0.85	3.81
Uniaxial Compressive Strength	0.51	4.25	0.66	2.91	0.71	1.64
Splitting Tensile Strength	0.60	6.11	0.96	31.98	0.96	15.28
Fracture Toughness	0.05	0.22	0.06	0.10	0.70	1.56
Charateristic Dimension	0.44	3.18	0.55	1.83	0.78	2.32

Critical F-values at 0.05 confidence level:

Linear (1st) GLM:	7.71
Quadratic (2nd) GLM:	9.55
Cubic (3rd) GLM:	19.16

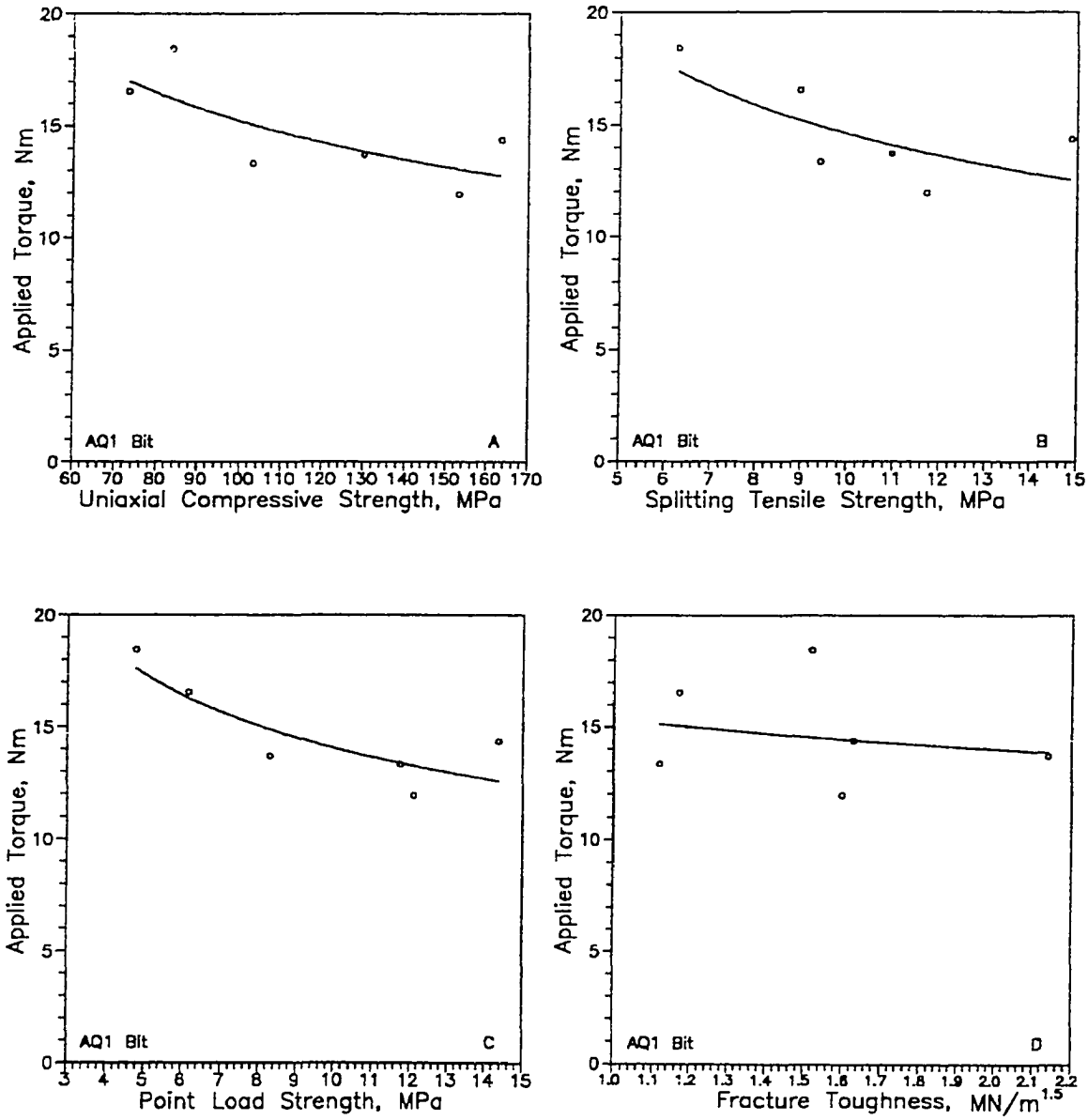

Figure 6.9: Applied torque vs. rock properties for AQ1 bit in the preliminary rock coring test: (a) uniaxial compressive strength, (b) splitting tensile strength, (c) point load strength, (d) fracture toughness

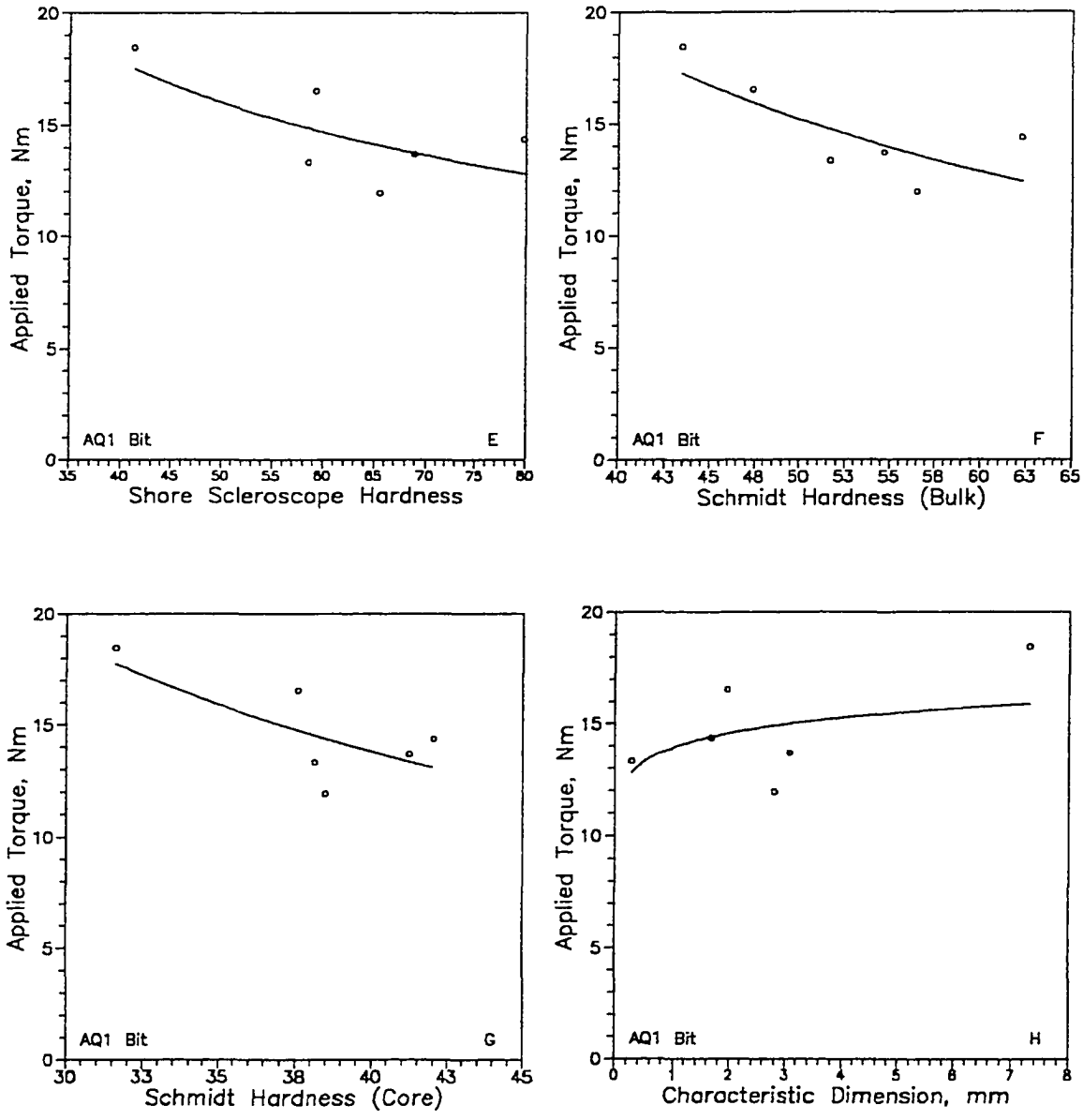

Figure 6.9 (cont'd): (e) Shore scleroscope hardness, (f) Schmidt hardness on bulk specimen, (g) Schmidt hardness on core specimen, and (h) characteristic dimension

6.2.2.2 BQ1 Bit

The R^2 and F-values of the GLM analyses for the BQ1 bit are presented in Table 6.4. For the linear models, a significant correlation was found only for the Shore scleroscope hardness (F-value=9.29). For the quadratic models, four properties showed significant correlations with the applied torque, i.e., the Shore scleroscope hardness (F-value=11.54), the Schmidt hardness of bulk specimen (F-value=72.21), the point load strength (F-value=19.98), and the splitting tensile strength (F-value=10.33). The Schmidt hardness (bulk) and the splitting tensile strength also showed significant correlations with the applied torque in the third degree models (F-values were 42.98 for the Schmidt hardness of bulk specimen and 47.12 for the splitting tensile strength).

The applied torque vs. the rock properties is plotted in Figure 6.10. Similar to the AQ1 bit, a higher torque was found to correspond to a lower strength or hardness value of rock. For the Characteristic Dimension, it was also found that the applied torque increased slightly when rock particles became larger, as was the case for the AQ1 bit.

6.2.3 Specific Energy

By definition (Rabia, 1965), *specific energy* is the energy required to remove a unit volume of material. This specific energy is also referred to as *Volumetric Specific Energy*. When the purpose of drilling is solely to make a hole in rock, the volume of material removed can be considered as the total volume of the borehole. In the case of coring, however, the volume of rock removed includes two parts: the volume of core and the volume of kerf. For the purpose of drilling operation, it is desirable to have a small

Table 6.4: Regression analysis of applied torque for BQ1 bit in the preliminary rock coring test

Rock property	1st Degree GLM		2nd Degree GLM		3rd Degree GLM	
	R-squared	F-value	R-squared	F-value	R-squared	F-value
Shore Scleroscope Hardness	0.70	9.29	0.89	11.54	0.90	6.30
Schmidt Hardness (bulk)	0.65	7.42	0.98	72.21	0.99	42.98
Schmidt Hardness (core)	0.71	4.86	0.74	4.24	0.86	4.09
Point Load Strength	0.58	5.42	0.93	19.98	0.93	8.93
Uniaxial Compressive Strength	0.47	3.55	0.58	2.08	0.66	1.31
Splitting Tensile Strength	0.53	4.52	0.87	10.33	0.99	47.12
Fracture Toughness	0.14	0.66	0.22	0.43	0.87	4.36
Charateristic Dimension	0.59	5.67	0.77	4.96	0.89	5.66

Critical F-values at 0.05 confidence level:

Linear (1st) GLM:	7.71
Quadratic (2nd) GLM:	9.55
Cubic (3rd) GLM:	19.16

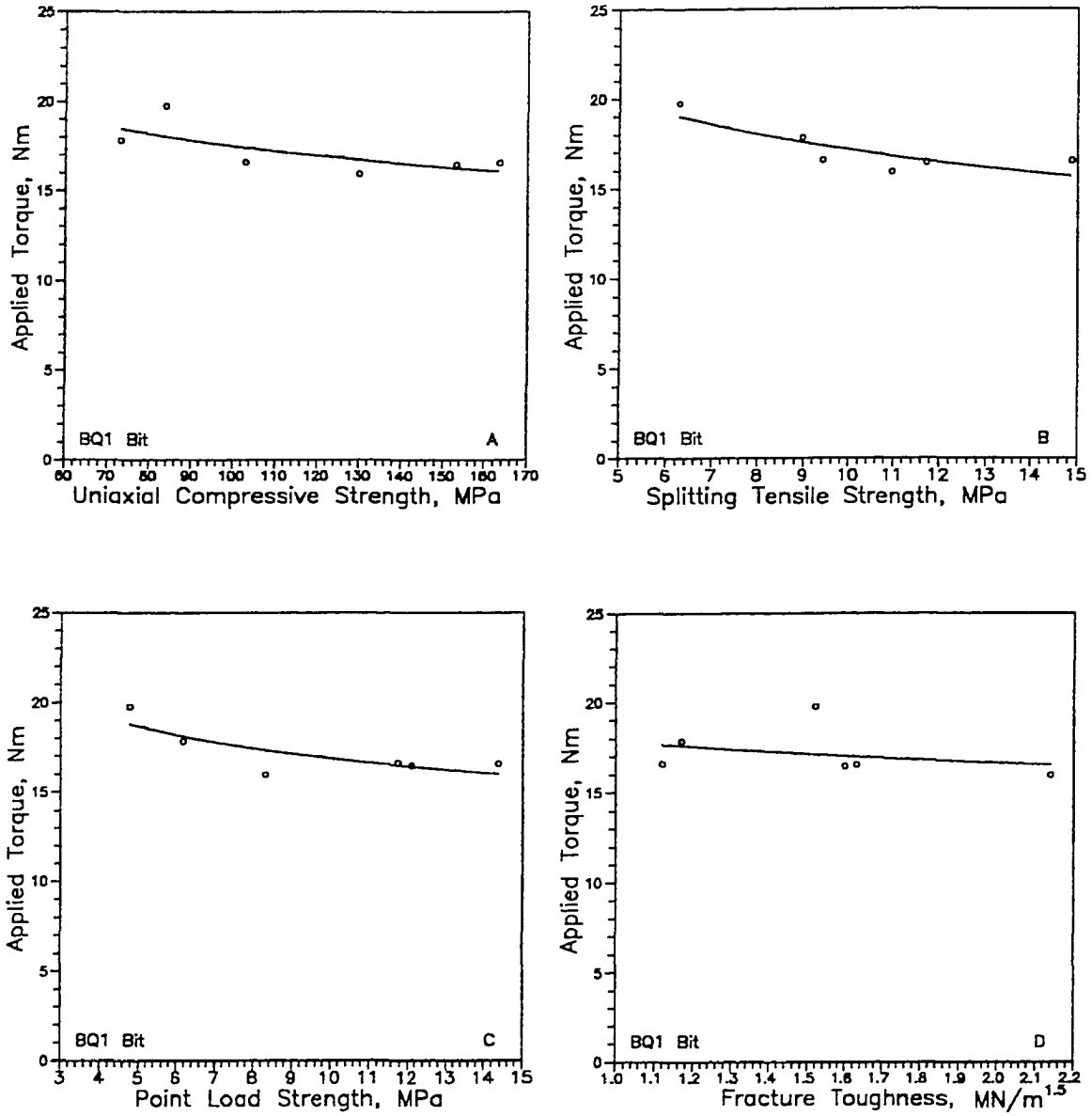

Figure 6.10: Applied torque vs. rock properties for BQ1 bit in the preliminary rock coring test: (a) uniaxial compressive strength, (b) splitting tensile strength, (c) point load strength, (d) fracture toughness

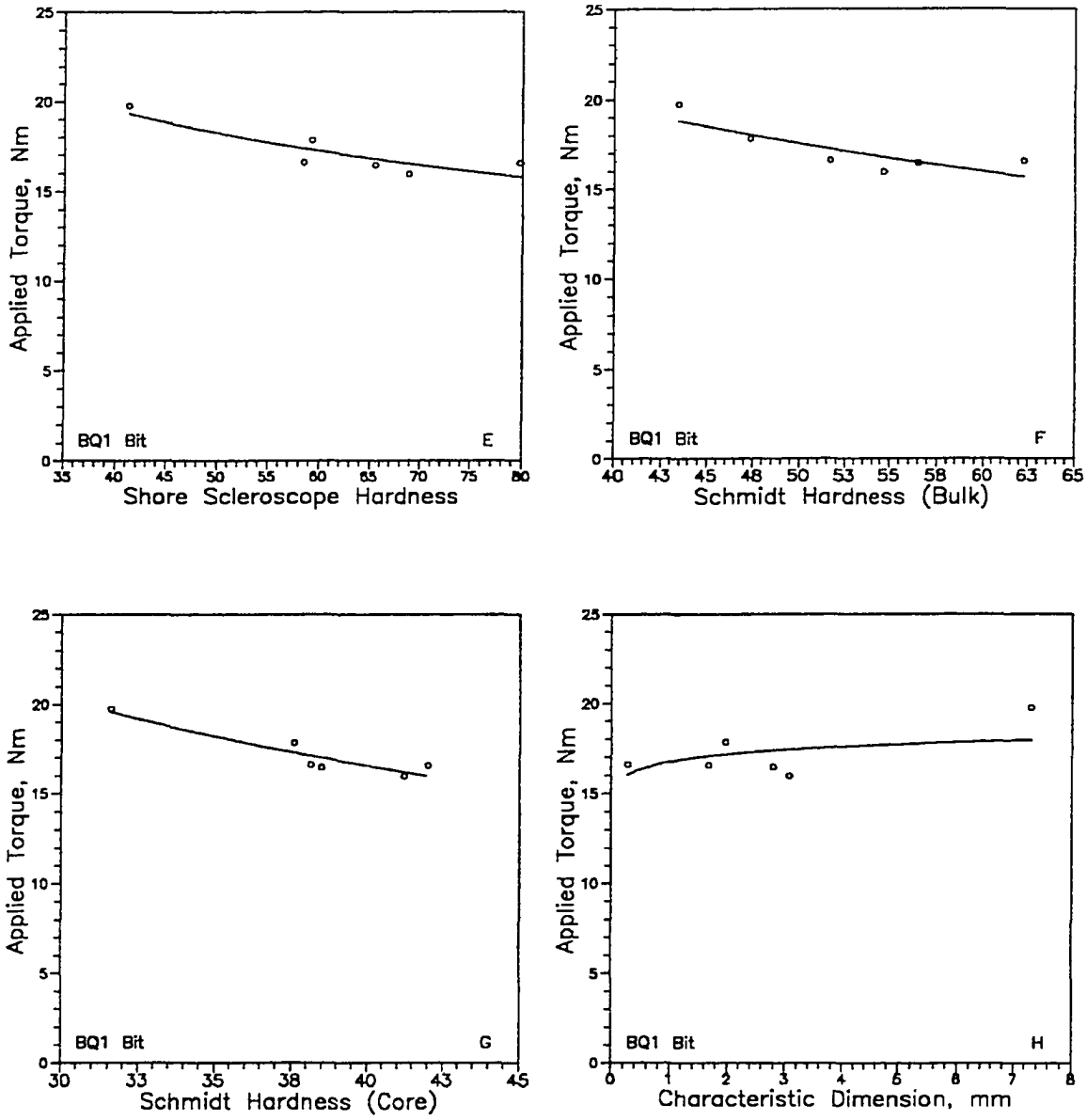

Figure 6.10 (cont'd): (e) Shore scleroscope hardness, (f) Schmidt hardness on bulk specimen, (g) Schmidt hardness on core specimen, and (h) characteristic dimension

kerfing area and a fast penetration rate so as to reduce the energy requirement. The energy required for kerfing was called *Specific Kerfing Energy* (SE_k) or *Effective Specific Energy*. The *volumetric penetration rate*, PR_v, is the product of *penetration rate* (PR) and cross-section area of the kerf:

$$PR_v = \frac{\pi}{4}(D_h^2 - D_c^2)\,PR \qquad (6.1)$$

Hence the Specific Kerfing Energy is

$$SE_k = \frac{8TN}{(D_h^2 - D_c^2)\,PR} \qquad (6.2)$$

where T is the applied torque and N is the rotational speed. D_h and D_c are diameters of the hole and rock core, respectively. The Specific Kerfing Energy is a measurement of cutting efficiency of a bit.

However, in field coring operations one of the important considerations is to retrieve a high percentage of good quality cores. In this case, the Specific Kerfing Energy is no longer a good indication of the efficiency of a coring system. It is thus necessary to use a new term, namely, *Specific Core Recovery Energy* (SE_c), to describe the coring efficiency of a system:

$$SE_c = \frac{8TN}{D_c^2 PR} \qquad (6.3)$$

The relationship between the Specific Core Recovery Energy and Specific Kerfing Energy is:

$$SE_c = [(\frac{D_b}{D_c})^2 - 1] SE_k \qquad (6.4)$$

Both the Specific Kerfing Energy and Specific Core Recovery Energy vary with bit characteristics, drilling and coring procedures, and material properties. In the preliminary rock coring test, the operating procedures and drilling conditions were identical for all tests. The SE_k and SE_c were, thus, affected only by bit and rock type alone. Furthermore, for tests performed by a given bit, the SE_k and SE_c were functions of rock type. Because for each bit the Specific Core Recovery Energy was proportional to the Specific Kerfing Energy, their statistical relations with rock properties would be the same. Therefore, only the Specific Kerfing Energy was used in this statistical analysis and it was simply called *specific energy*.

6.2.3.1 AQ1 Bit

Table 6.5 shows the regression analysis of the specific energy for the AQ1 bit in this test. It was noted that of the eight rock properties investigated, only the uniaxial compressive strength had a significant correlation with the specific energy at linear level (F-value=14.60). The F-values of the remaining models were all less than the corresponding critical F-values.

Figure 6.11 plots the specific energy against the rock properties for the AQ1 bit. It was found that the specific energy was larger as the strength or hardness of rock increased. The specific energy, however, was not affected by the Characteristic Dimension.

Table 6.5: Regression analysis of specific energy for AQ1 bit in the preliminary rock coring test

Rock property	1st Degree GLM		2nd Degree GLM		3rd Degree GLM	
	R-squared	F-value	R-squared	F-value	R-squared	F-value
Shore Scleroscope Hardness	0.23	1.16	0.46	1.28	0.60	0.99
Schmidt Hardness (bulk)	0.52	4.28	0.59	2.18	0.92	7.59
Schmidt Hardness (core)	0.12	0.57	0.40	0.98	0.50	0.67
Point Load Strength	0.39	2.57	0.49	1.47	0.82	3.12
Uniaxial Compressive Strength	0.78	14.60	0.80	6.15	0.90	5.98
Splitting Tensile Strength	0.47	3.57	0.52	1.65	0.56	0.85
Fracture Toughness	0.20	0.99	0.59	2.14	0.91	7.16
Charateristic Dimension	0.00	0.01	0.02	0.04	0.05	0.04

Critical F-values at 0.05 confidence level:	Linear (1st) GLM:	7.71
	Quadratic (2nd) GLM:	9.55
	Cubic (3rd) GLM:	19.16

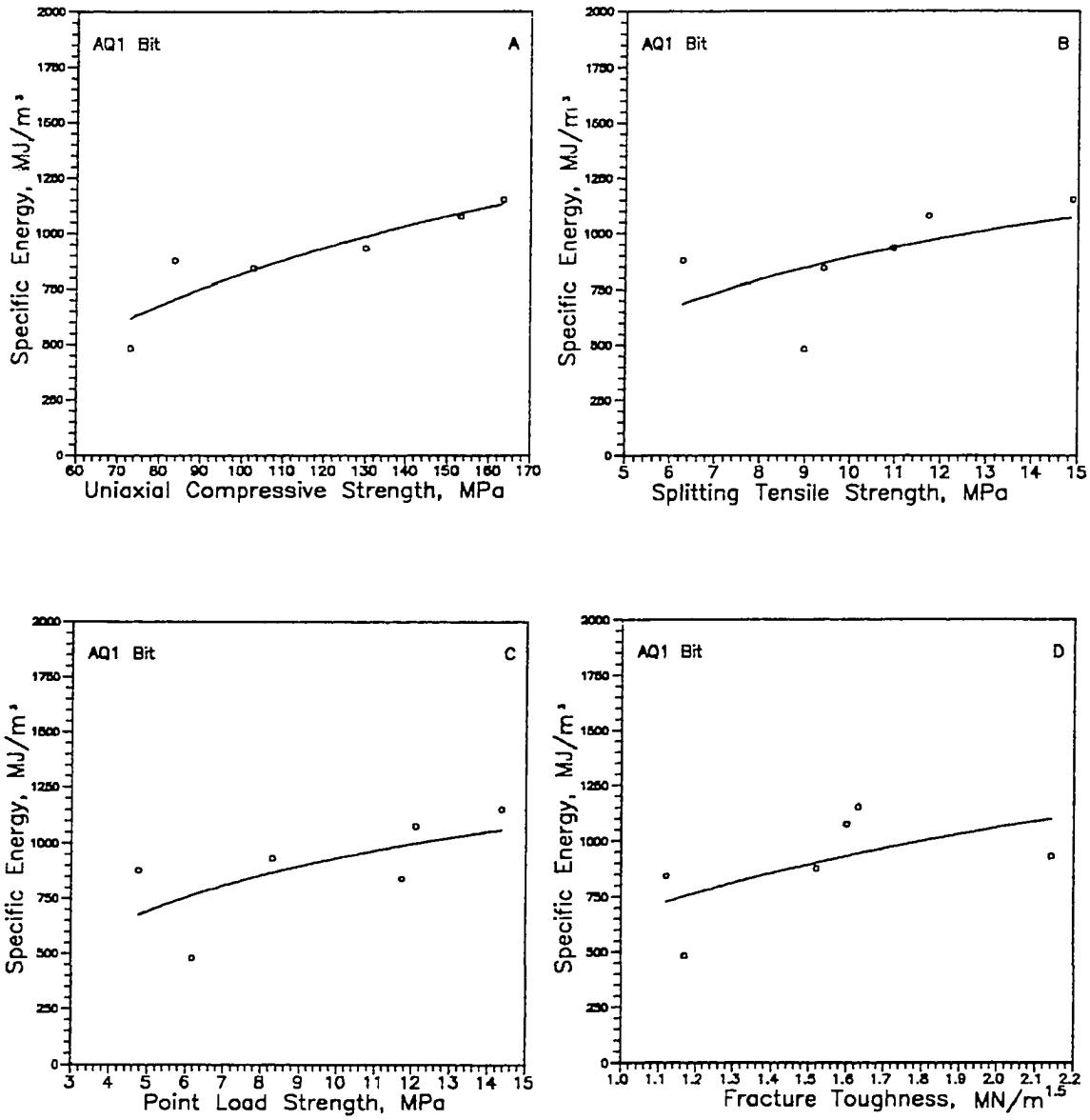

Figure 6.11: Specific energy (kerfing) vs. rock properties for AQ1 bit in the preliminary rock coring test: (a) uniaxial compressive strength, (b) splitting tensile strength, (c) point load strength, (d) fracture toughness

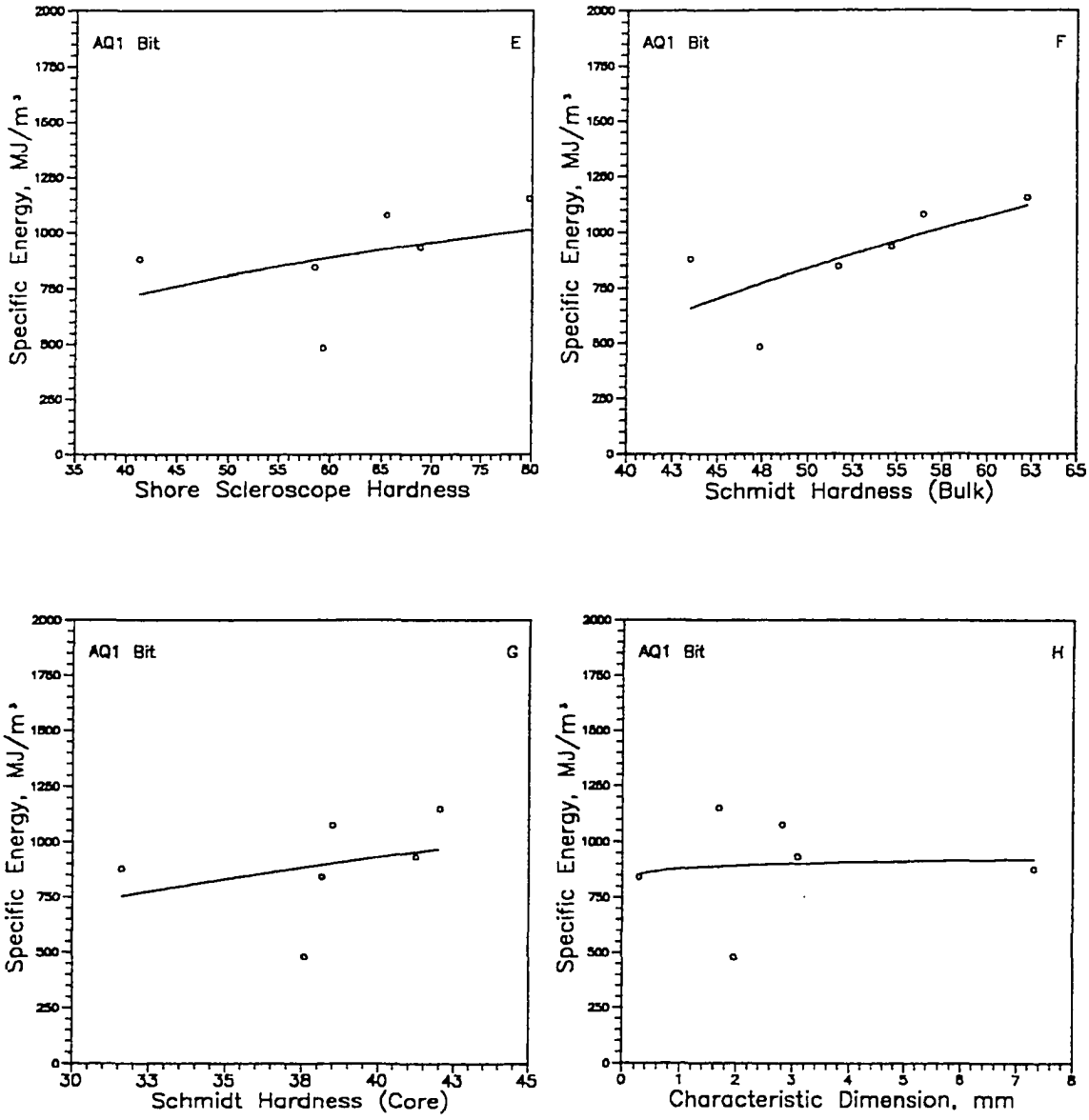

Figure 6.11 (cont'd): (e) Shore scleroscope hardness, (f) Schmidt hardness on bulk specimen, (g) Schmidt hardness on core specimen, and (h) characteristic dimension

6.2.3.2 BQ1 Bit

Table 6.6 shows the regression analysis of the specific energy for the BQ1 bit. It was found that for all the models, only the fracture toughness showed a significant correlation with the specific energy in the quadratic model (F-value=11.40) and the cubic model (F-value=122.58).

The relationship between specific energy and rock properties is presented in Figure 6.12 for the BQ1 bit. It was noted that in most cases (i.e., the uniaxial compressive strength, splitting tensile strength, fracture toughness, and Schmidt hardness of bulk specimen), the specific energy increased with an increase in the strength or hardness. For the point load strength, Shore scleroscope hardness, and Schmidt hardness of core specimen, the specific energy decreased as the property measurements increase. However, a higher specific energy was found when the Characteristic Dimension was larger (Figure 6.12(h)).

6.3 IMPREGNATED BITS

The other two bits used in the preliminary rock coring test were two impregnated bits, i.e., AQ2 and BQ2 bits. The specifications of those two bits are also presented in Table 4.2. The difference between the impregnated diamond bits and the surface-set diamond bits is that the diamonds in the impregnated bits are very fine diamond particles. These diamond particles are uniformly distributed in the bit matrix. When an impregnated bit is used to bore rocks, a certain degree of hardness and abrasiveness of rock is necessary because the bit matrix has to be worn out so new diamond particles can be exposed. The

Table 6.6: Regression analysis of specific energy for BQ1 bit in the preliminary rock coring test

Rock property	1st Degree GLM		2nd Degree GLM		3rd Degree GLM	
	R-squared	F-value	R-squared	F-value	R-squared	F-value
Shore Scleroscope Hardness	0.01	0.04	0.54	1.75	0.68	1.43
Schmidt Hardness (bulk)	0.00	0.01	0.56	1.93	0.87	4.32
Schmidt Hardness (core)	0.10	0.45	0.47	1.30	0.47	0.58
Point Load Strength	0.01	0.02	0.50	1.50	0.85	3.70
Uniaxial Compressive Strength	0.09	0.38	0.33	0.74	0.33	0.34
Splitting Tensile Strength	0.01	0.03	0.49	1.45	0.51	0.69
Fracture Toughness	0.05	0.21	0.88	11.40	0.99	122.58
Charateristic Dimension	0.52	4.29	0.59	2.19	0.74	1.88

Critical F-values at 0.05 confidence level:	Linear (1st) GLM:	7.71
	Quadratic (2nd) GLM:	9.55
	Cubic (3rd) GLM:	19.16

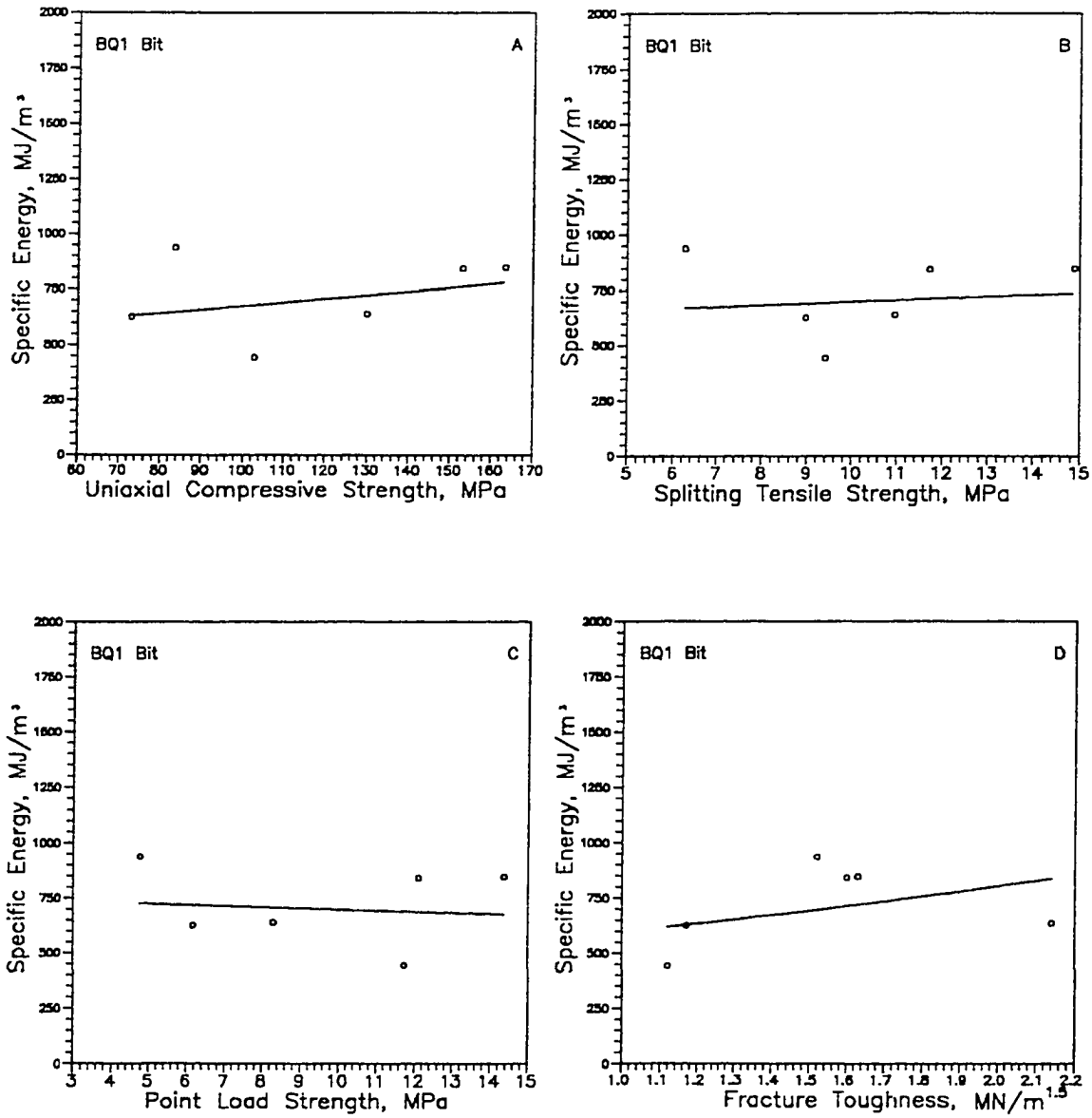

Figure 6.12: Specific energy (kerfing) vs. rock properties for BQ1 bit in the preliminary rock coring test: (a) uniaxial compressive strength, (b) splitting tensile strength, (c) point load strength, (d) fracture toughness

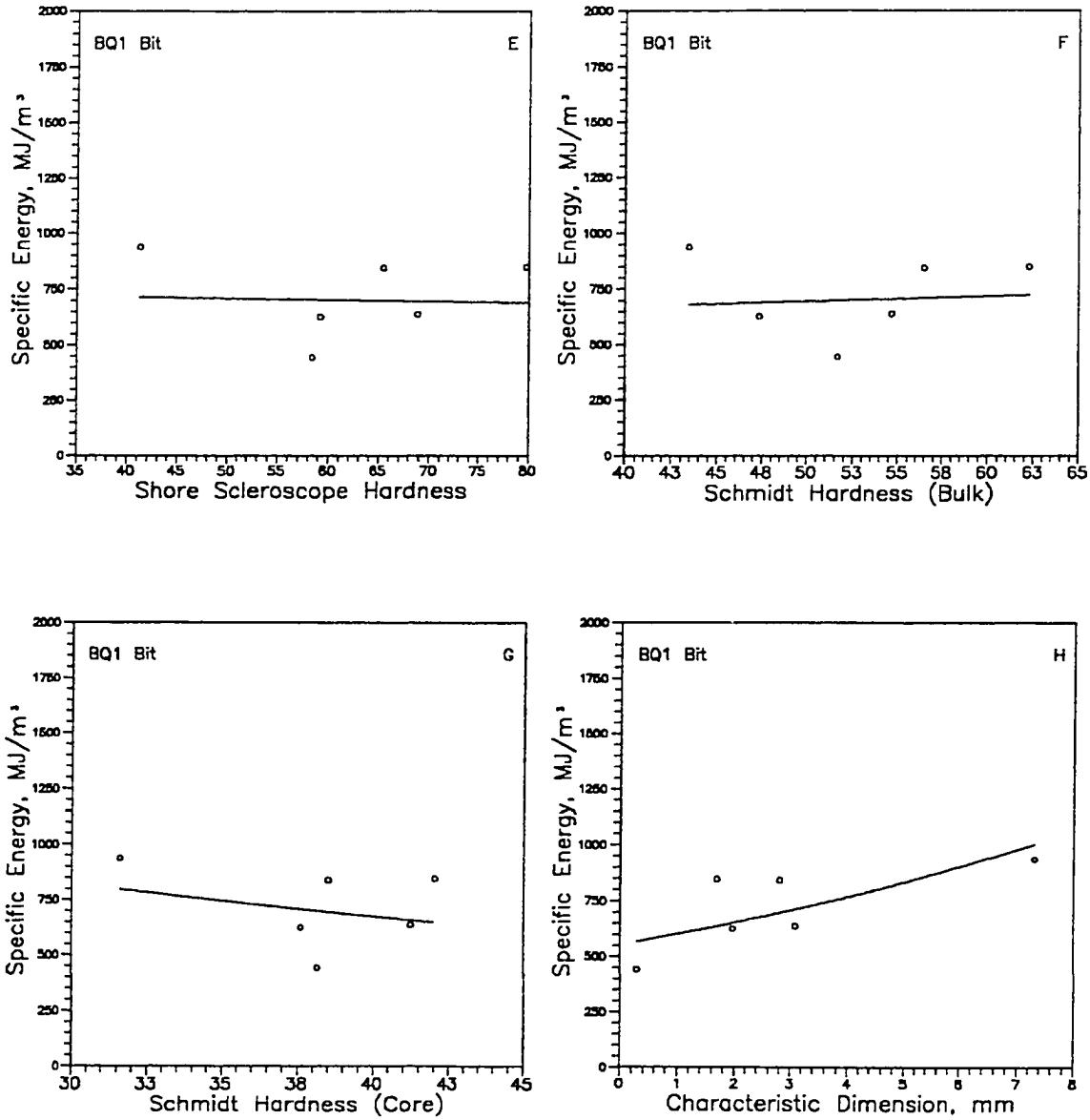

Figure 6.12 (cont'd): (e) Shore scleroscope hardness, (f) Schmidt hardness on bulk specimen, (g) Schmidt hardness on core specimen, and (h) characteristic dimension

new cutting points are gradually exposed to the rock surface during impregnated diamond bit drilling. Therefore, a relatively stable drilling rate can be obtained and the bit life can be also extended.

The design of the two impregnated bits used in this research were very similar. Both the AQ2 and the BQ2 bits contained the same kind of diamonds. There were two waterways on the bit matrix and a "V" shaped notch design on the bit surface. This "V" notch design improved the stability at the beginning of drilling. The major difference between the two impregnated bits was that the cross-section area of the BQ2 bit was about 42.45% larger than that of the AQ2 bit. The similar statistical procedures were employed to analyze data. The experimental design and laboratory testing for the impregnated bits were the same as those used for the surface-set bits. Therefore, the critical F-values for the GLM models were the same as those for the surface-set bits. The results and statistical analyses are presented in this section.

6.3.1 Penetration Rate

6.3.1.1 AQ2 Bit

Table 6.7 shows the regression analysis of the penetration rate for the AQ2 bit. The critical F-values for the GLM linear, quadratic, and cubic models were 7.71, 9.55, and 19.16 at α=0.05, respectively. From Table 6.7 it was found that of the eight rock properties, four of them had significant correlations with the penetration rate at linear level, i.e., the Shore scleroscope hardness (F-value=7.92), the Schmidt hardness of bulk specimen (F-value=17.59), the point load strength (F-value=9.86), and the uniaxial

Table 6.7: Regression analysis of penetration rate for AQ2 bit in the preliminary rock coring test

Rock property	1st Degree GLM		2nd Degree GLM		3rd Degree GLM	
	R-squared	F-value	R-squared	F-value	R-squared	F-value
Shore Scleroscope Hardness	0.67	7.92	0.69	3.27	0.91	6.35
Schmidt Hardness (bulk)	0.81	17.59	0.82	6.81	0.95	12.79
Schmidt Hardness (core)	0.60	5.94	0.72	3.80	0.86	4.16
Point Load Strength	0.71	9.86	0.72	3.82	0.92	7.33
Uniaxial Compressive Strength	0.91	38.61	0.94	24.19	0.96	15.74
Splitting Tensile Strength	0.51	4.14	0.53	1.68	0.60	1.01
Fracture Toughness	0.47	3.53	0.54	1.75	0.98	32.00
Charateristic Dimension	0.07	0.32	0.37	0.89	0.43	0.50

Critical F-values at 0.05 confidence level:	Linear (1st) GLM:	7.71
	Quadratic (2nd) GLM:	9.55
	Cubic (3rd) GLM:	19.16

compressive strength (F-value=38.61). The uniaxial compressive strength also showed a significant correlation with the penetration rate in the quadratic model (F-value=24.19). For the cubic models, the rock property which showed a significant correlation with the penetration rate was the fracture toughness (F-value=32.00).

Figure 6.13 presents the penetration rate of the AQ2 bit versus the rock properties. It was noticed that the penetration rate decreased rapidly with the strength properties or hardness indices of rock. The data for the Characteristic Dimension were scattered.

6.3.1.2 BQ2 Bit

Table 6.8 presents the coefficients of determination and F-values of the GLM models of the penetration rate for the BQ2 bit. Significant correlations were found only for the uniaxial compressive strength, having the F-values of 15.10, 38.20, and 72.61 for the linear, quadratic, and cubic models, respectively.

Figure 6.14 plots the penetration rate against the rock properties for the BQ2 bit. It was found that the penetration rate decreased rapidly with an increase of strength or hardness of rock. For the Characteristic Dimension, the data were too uncorrelated to draw any reasonable conclusions.

6.3.2 Applied Torque

6.3.2.1 AQ2 Bit

The results of regression analysis of the applied torque for the AQ2 bit are shown in Table 6.9. For the linear models, it was found that five of the eight rock properties had

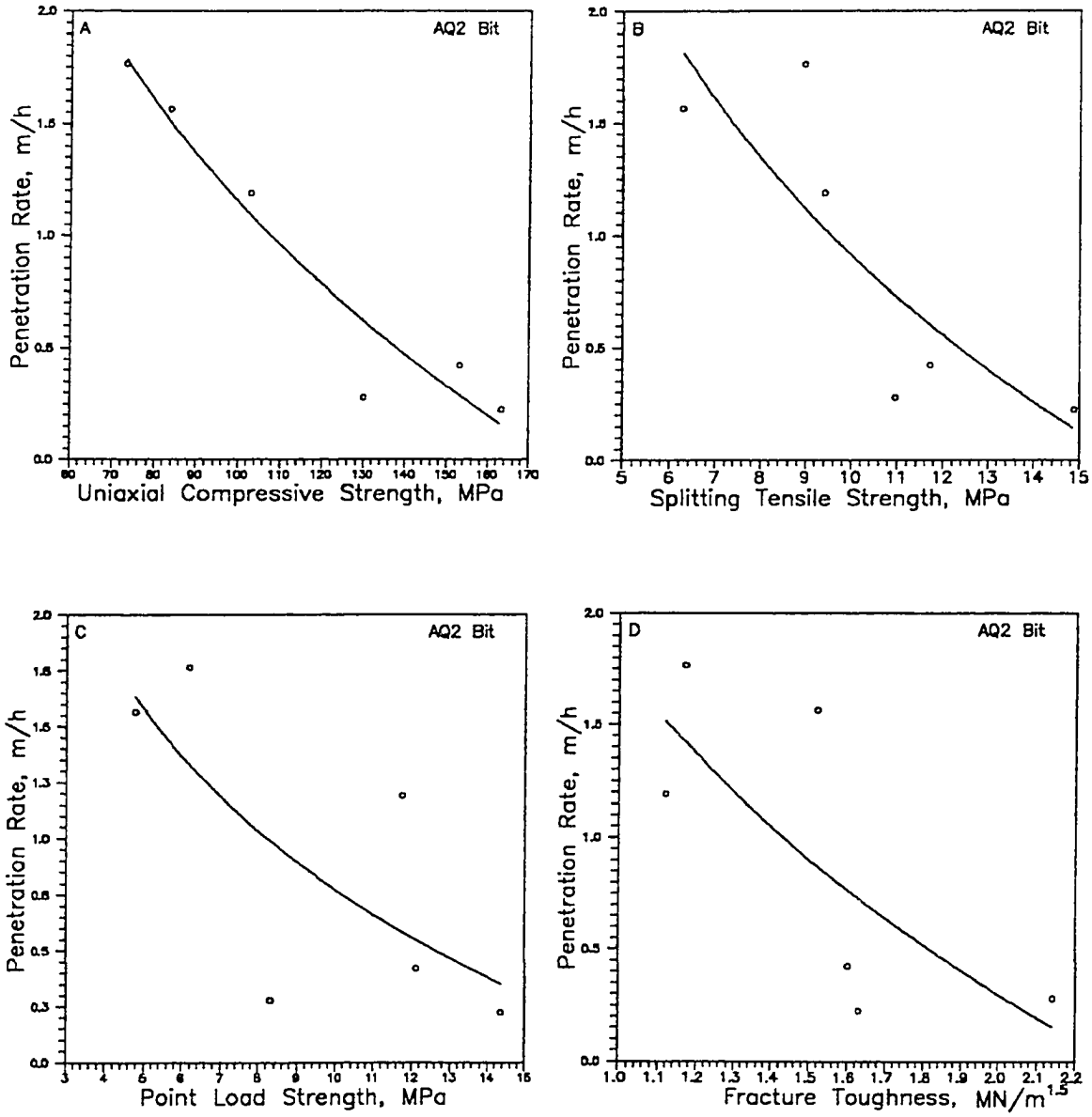

Figure 6.13: Penetration rate vs. rock properties for AQ2 bit in the preliminary rock coring test: (a) uniaxial compressive strength, (b) splitting tensile strength, (c) point load strength, (d) fracture toughness

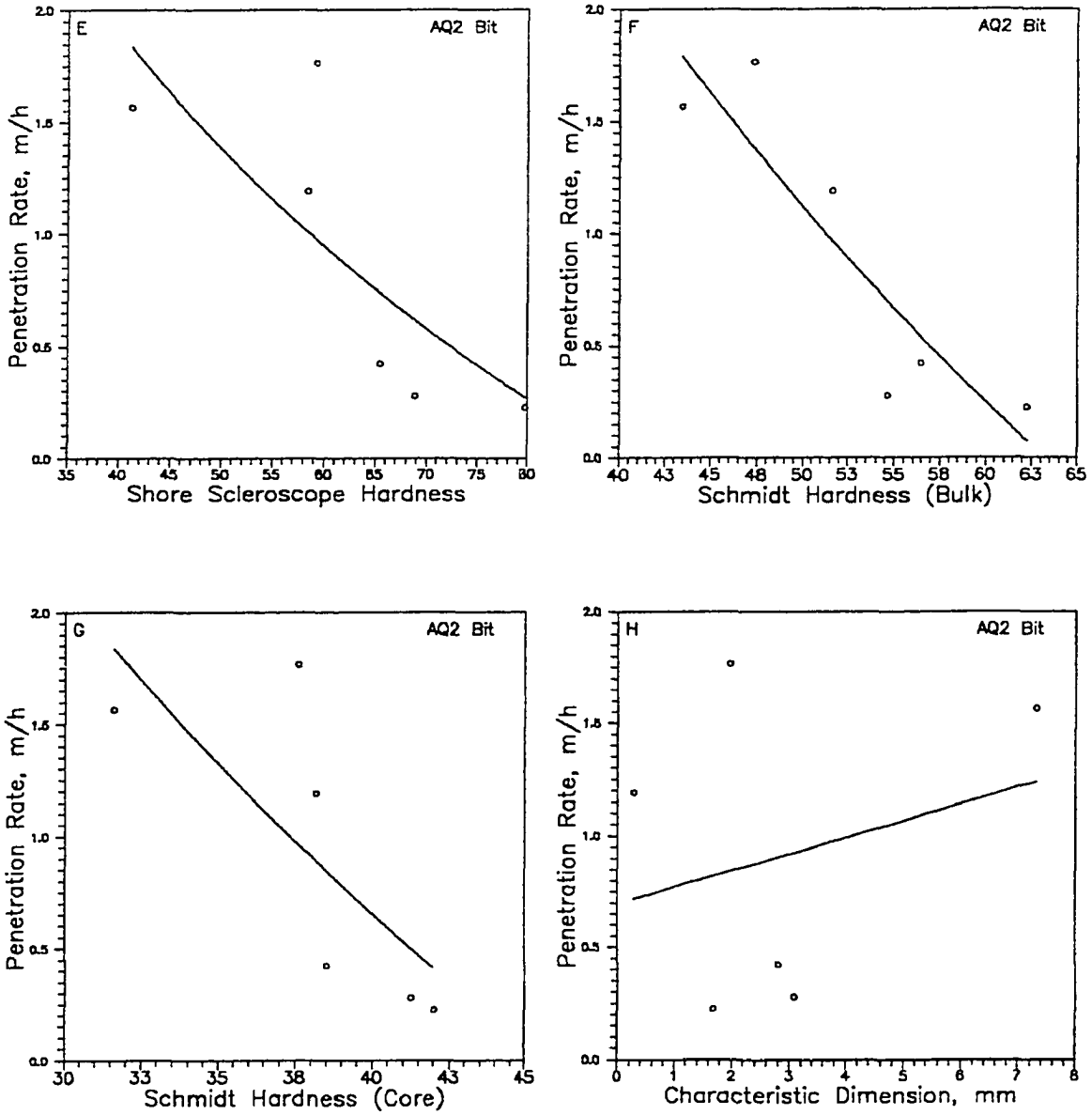

Figure 6.13 (cont'd): (e) Shore scleroscope hardness, (f) Schmidt hardness on bulk specimen, (g) Schmidt hardness on core specimen, and (h) characteristic dimension

Table 6.8: Regression analysis of penetration rate for BQ2 bit in the preliminary rock coring test

Rock property	1st Degree GLM		2nd Degree GLM		3rd Degree GLM	
	R-squared	F-value	R-squared	F-value	R-squared	F-value
Shore Scleroscope Hardness	0.36	2.26	0.41	1.02	0.58	0.91
Schmidt Hardness (bulk)	0.62	6.57	0.63	2.50	0.86	4.19
Schmidt Hardness (core)	0.33	1.96	0.47	1.32	0.72	1.68
Point Load Strength	0.45	3.32	0.45	1.24	0.69	1.51
Uniaxial Compressive Strength	0.79	15.10	0.96	38.20	0.99	72.61
Splitting Tensile Strength	0.54	4.67	0.55	1.85	0.57	0.84
Fracture Toughness	0.33	1.96	0.40	1.02	0.91	6.84
Charateristic Dimension	0.04	0.16	0.08	0.13	0.25	0.23

Critical F-values at 0.05 confidence level:

Linear (1st) GLM:	7.71
Quadratic (2nd) GLM:	9.55
Cubic (3rd) GLM:	19.16

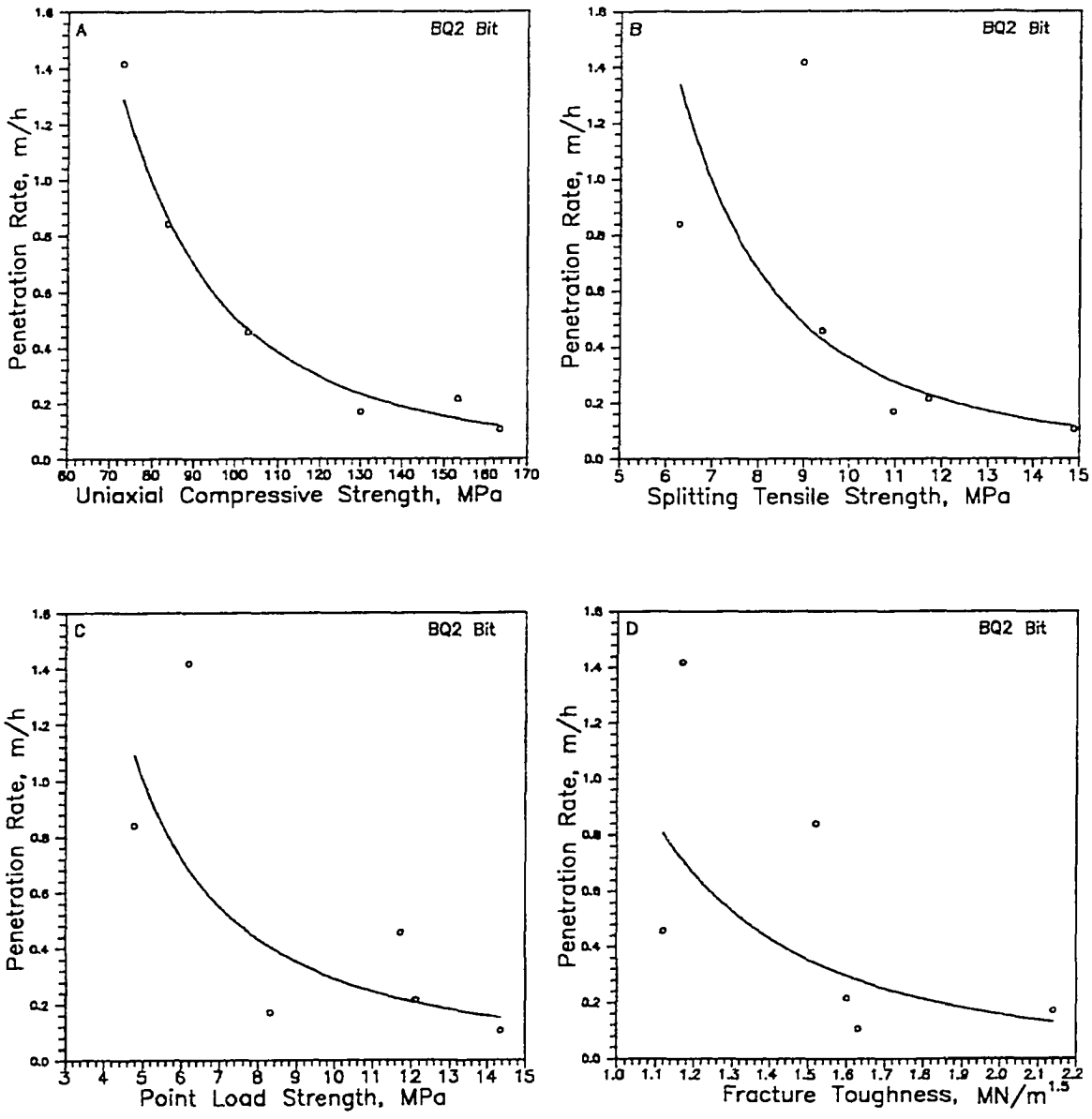

Figure 6.14: Penetration rate vs. rock properties for BQ2 bit in the preliminary rock coring test: (a) uniaxial compressive strength, (b) splitting tensile strength, (c) point load strength, (d) fracture toughness

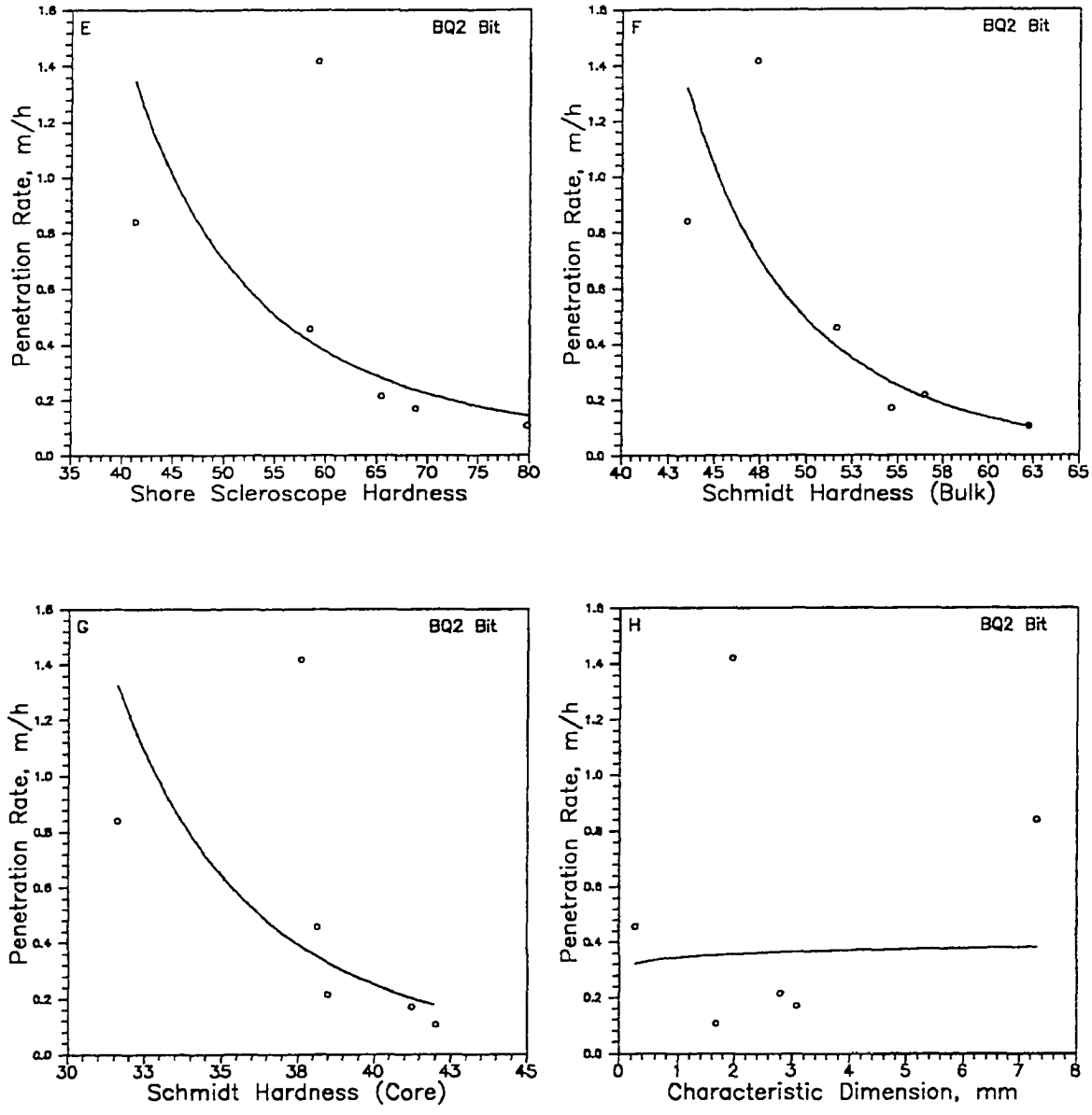

Figure 6.14 (cont'd): (e) Shore scleroscope hardness, (f) Schmidt hardness on bulk specimen, (g) Schmidt hardness on core specimen, and (h) characteristic dimension

Table 6.9: Regression analysis of applied torque for AQ2 bit in the preliminary rock coring test

Rock property	1st Degree GLM		2nd Degree GLM		3rd Degree GLM	
	R-squared	F-value	R-squared	F-value	R-squared	F-value
Shore Scleroscope Hardness	0.76	12.67	0.78	5.27	0.86	4.18
Schmidt Hardness (bulk)	0.85	22.78	0.96	32.91	0.98	36.70
Schmidt Hardness (core)	0.78	14.41	0.79	5.50	0.90	6.30
Point Load Strength	0.74	11.39	0.85	8.77	0.91	7.12
Uniaxial Compressive Strength	0.79	15.13	0.87	9.66	0.89	5.62
Splitting Tensile Strength	0.65	7.54	0.78	5.45	0.86	3.96
Fracture Toughness	0.27	1.48	0.27	0.56	0.94	10.06
Charateristic Dimension	0.32	1.86	0.54	1.75	0.63	1.15

Critical F-values at 0.05 confidence level:	Linear (1st) GLM:	7.71
	Quadratic (2nd) GLM:	9.55
	Cubic (3rd) GLM:	19.16

significant correlations with the applied torque, i.e., the Shore scleroscope hardness (F-value=12.67), the Schmidt hardness of bulk specimen (F-value=22.78), the Schmidt hardness of core specimen (F-value=14.41), the point load strength (F-value=11.39), and the uniaxial compressive strength (F-value=15.13). For the quadratic models, the two rock properties showing significant correlations with the applied torque were the Schmidt hardness of bulk specimen (F-value=32.91) and the uniaxial compressive strength (F-value=for the cubic model, i.e., the Schmidt hardness of bulk specimen (F-value=36.70).

Figure 6.15 plots the applied torque against the rock properties for the AQ2 bit. It was found that the applied torque decreased with an increasing strength or hardness of rock. There was a slight increase of the applied torque with an increase in the Characteristic Dimension, as it was shown in Figure 6.15(h). The data in Figure 6.15(h), however, were scattered.

6.3.2.2 BQ2 Bit

Table 6.10 presents the coefficients of determination and F-values of the GLM models of rock properties with the applied torque for the BQ2 bit. It was noted that of all the eight rock properties tested, three of them showed significant correlations with the applied torque, i.e., the Schmidt hardness of bulk specimens (F-value=9.84), the Schmidt hardness of core specimens (F-value=9.86), and the splitting tensile strength (F-value=9.04). The Schmidt hardness of bulk specimens and the splitting tensile strength also showed significant correlations with the applied torque in the quadratic and cubic models.

Figure 6.16 plots the applied torque against the rock properties for the BQ2 bit.

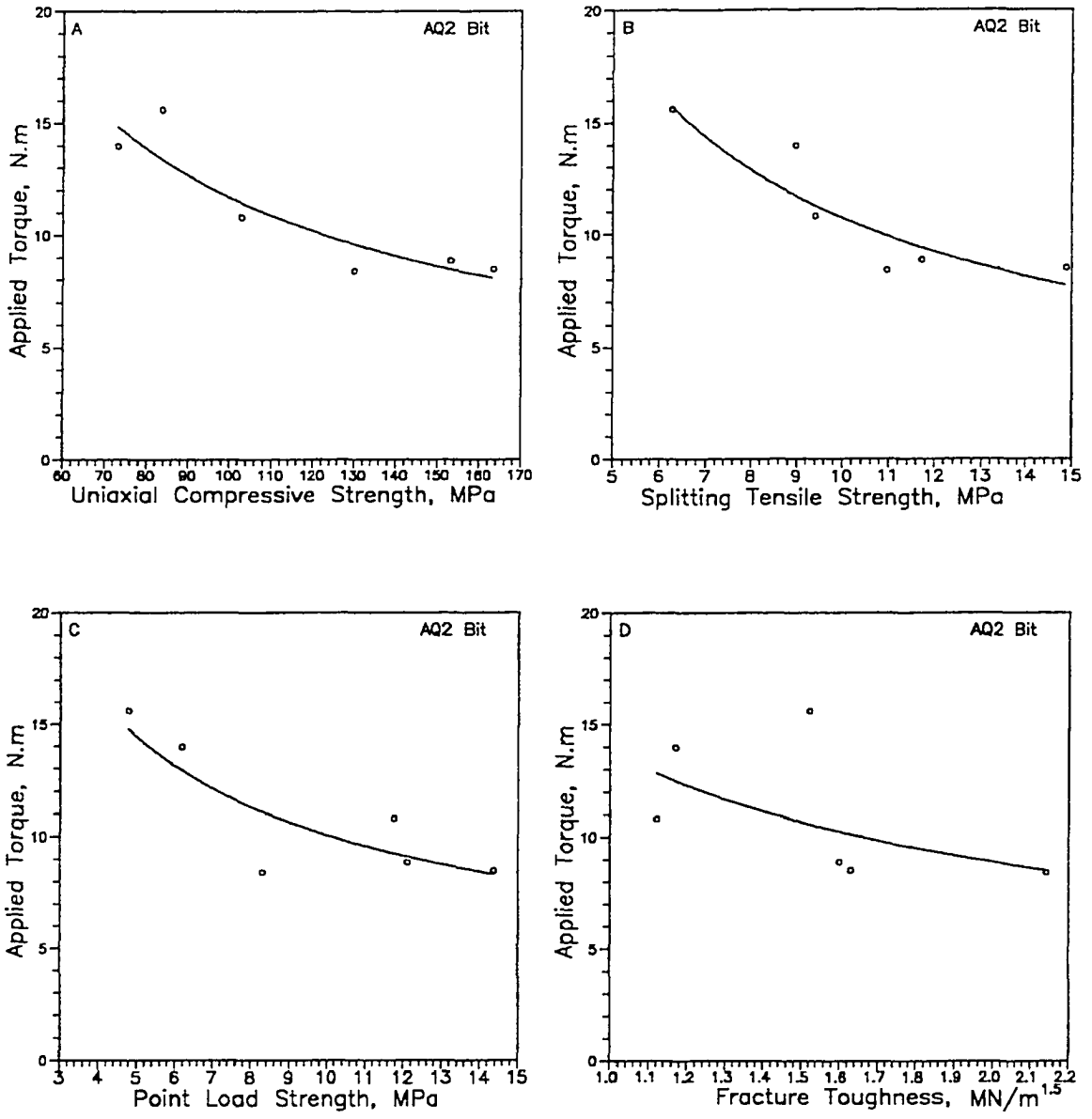

Figure 6.15: Applied torque vs. rock properties for AQ2 bit in the preliminary rock coring test: (a) uniaxial compressive strength, (b) splitting tensile strength, (c) point load strength, (d) fracture toughness

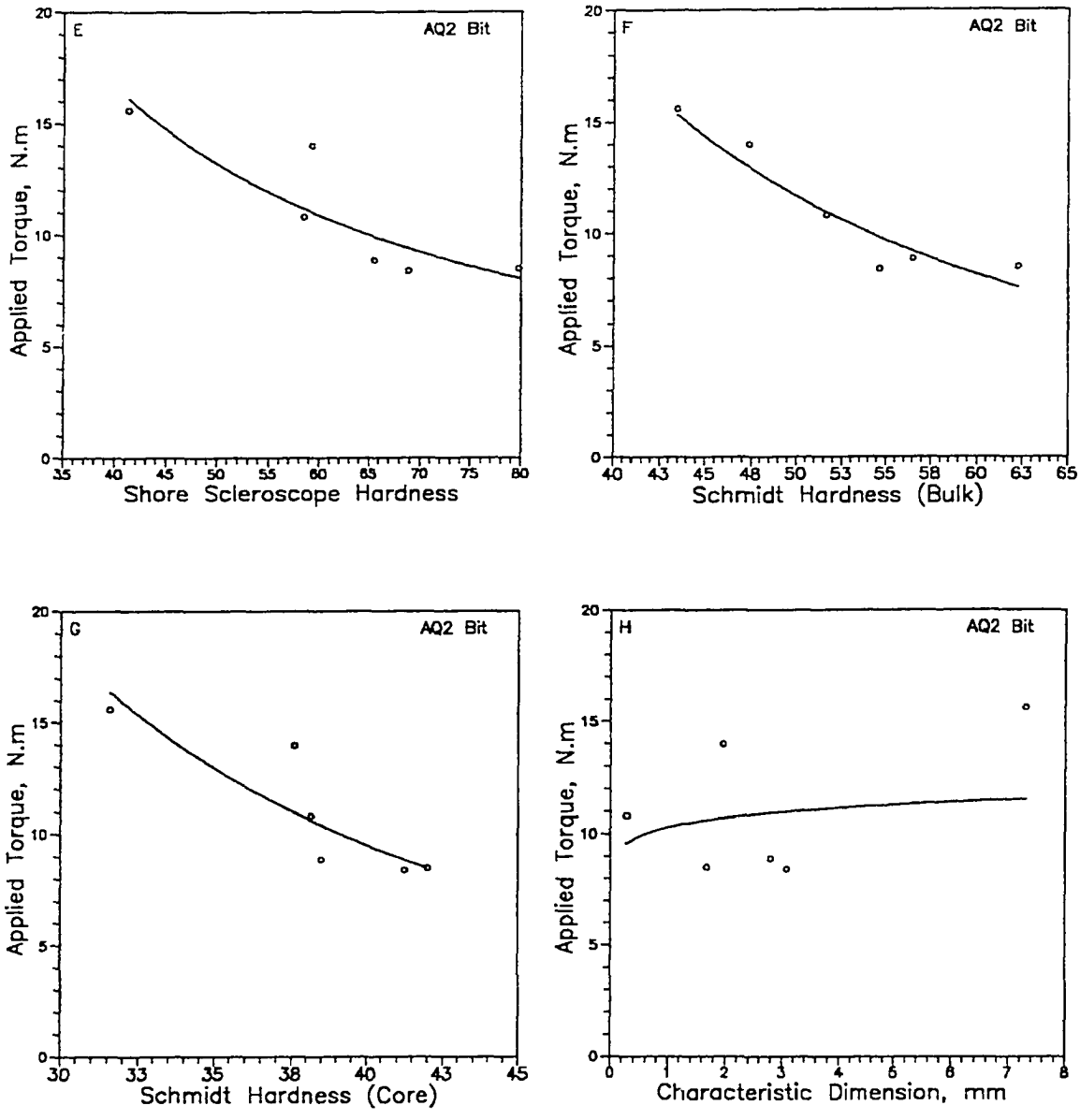

Figure 6.15 (cont'd): (e) Shore scleroscope hardness, (f) Schmidt hardness on bulk specimen, (g) Schmidt hardness on core specimen, and (h) characteristic dimension

Table 6.10: Regression analysis of applied torque for BQ2 bit in the preliminary rock coring test

Rock property	1st Degree GLM		2nd Degree GLM		3rd Degree GLM	
	R-squared	F-value	R-squared	F-value	R-squared	F-value
Shore Scleroscope Hardness	0.62	6.59	0.73	4.02	0.75	1.99
Schmidt Hardness (bulk)	0.71	9.84	0.96	36.68	0.97	18.20
Schmidt Hardness (core)	0.71	9.86	0.74	4.24	0.86	4.09
Point Load Strength	0.58	5.62	0.82	7.00	0.84	3.46
Uniaxial Compressive Strength	0.60	6.03	0.75	4.53	0.76	2.15
Splitting Tensile Strength	0.69	9.04	0.95	25.86	0.96	17.13
Fracture Toughness	0.11	0.51	0.13	0.23	0.92	7.21
Charateristic Dimension	0.50	4.06	0.59	2.17	0.76	2.11

Critical F-values at 0.05 confidence level:	Linear (1st) GLM:	7.71
	Quadratic (2nd) GLM:	9.55
	Cubic (3rd) GLM:	19.16

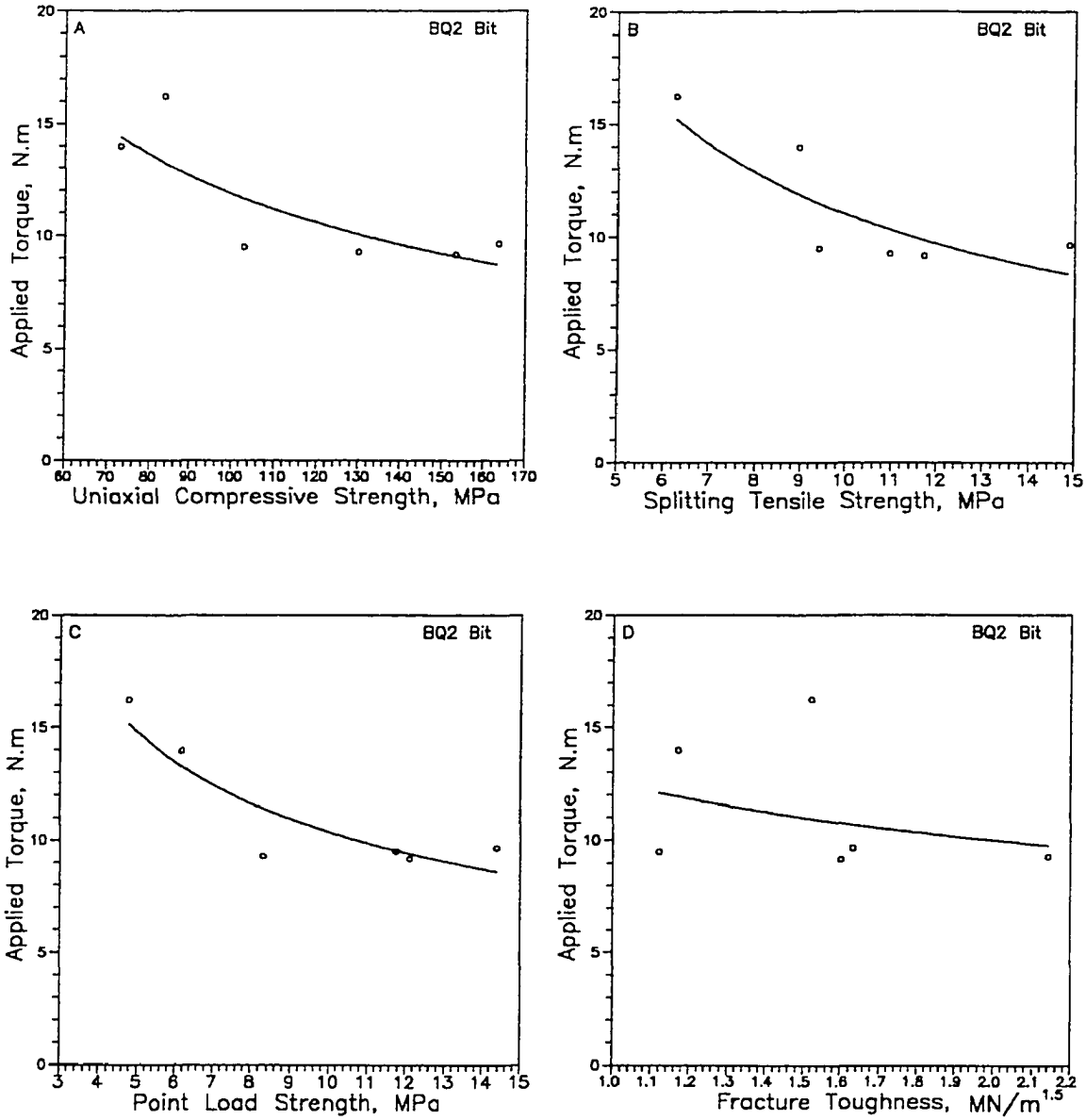

Figure 6.16: Applied torque vs. rock properties for BQ2 bit in the preliminary rock coring test: (a) uniaxial compressive strength, (b) splitting tensile strength, (c) point load strength, (d) fracture toughness

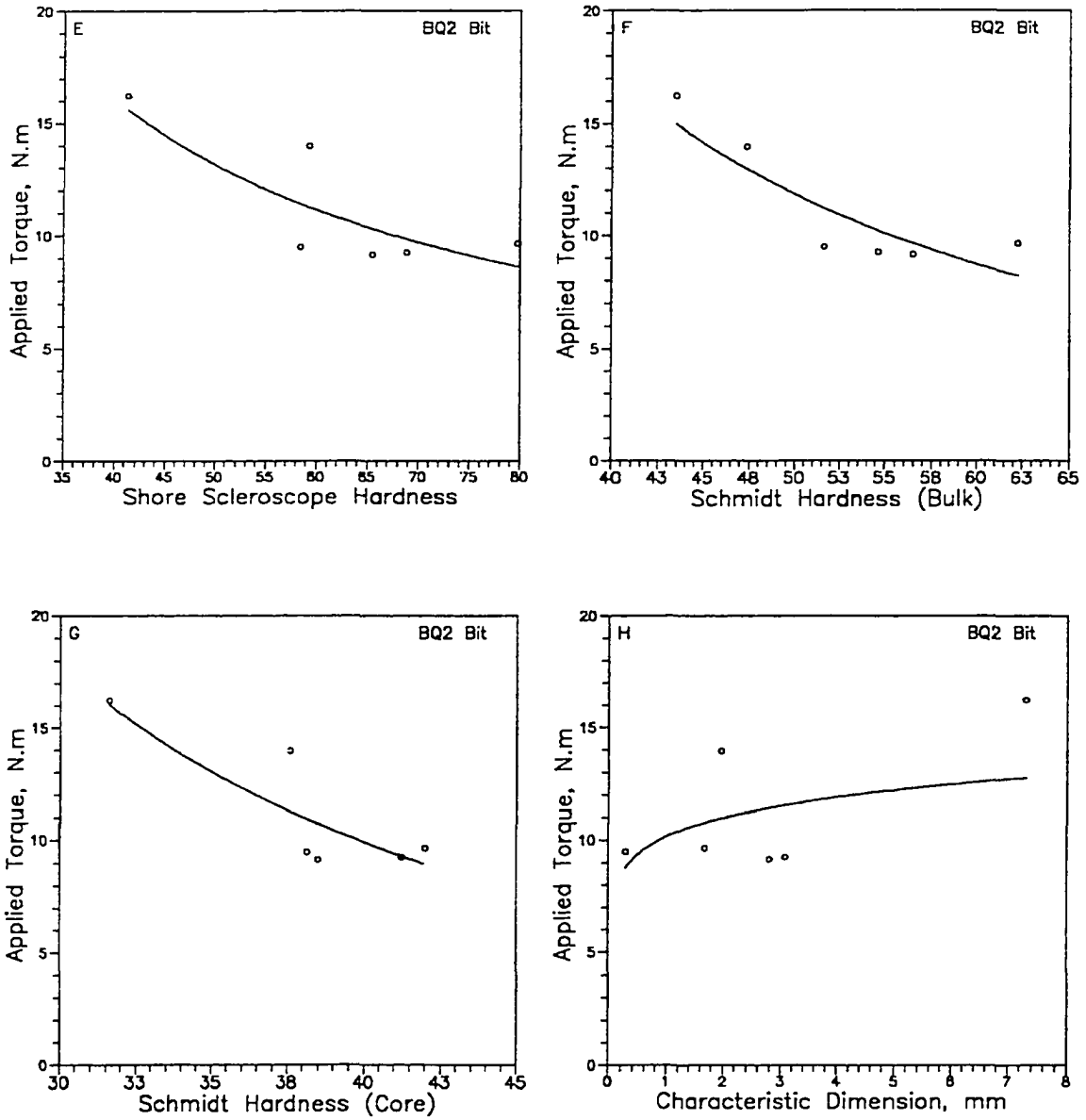

Figure 6.16 (cont'd): (e) Shore scleroscope hardness, (f) Schmidt hardness on bulk specimen, (g) Schmidt hardness on core specimen, and (h) characteristic dimension

It was noted that the applied torque decreased inversely with the strength properties and hardness indices of rock. Figure 6.16(h) shows that the applied torque increased with an increase of the Characteristic Dimension.

6.3.3 Specific Energy

The specific energy of the impregnated bits was calculated and analyzed. As in the case of the surface-set bits, the specific energy term in this analysis was the Specific Kerfing Energy. The statistical relationship would be the same for the Specific Core Recovery Energy because the analysis for any given bit was independent of the type of bit used.

6.3.3.1 AQ2 Bit

Table 6.11 presents the *coefficients of determination*, R^2, and F-values of GLM models for the AQ2 bit with the specific energy. The F-values of the linear models indicated that among the eight rock properties, four of them had significant correlations with the specific energy, i.e., the Shore scleroscope hardness (F-value=9.56), the Schmidt hardness of bulk specimen (F-value=12.67), the point load strength (F-value=12.93), and the uniaxial compressive strength (F-value=12.15). For the quadratic models, it was noted that the Shore scleroscope hardness and the Schmidt hardness had significant correlations with the specific energy. For the cubic models, only the Shore scleroscope hardness was found to have a significant correlation with the specific energy.

For the AQ2 bit the specific energy also was plotted against the rock properties in Figure 6.17. It was found that the specific energy increased rapidly with an increase

Table 6.11: Regression analysis of specific energy for AQ2 bit in the preliminary rock coring test

Rock property	1st Degree GLM		2nd Degree GLM		3rd Degree GLM	
	R-squared	F-value	R-squared	F-value	R-squared	F-value
Shore Scleroscope Hardness	0.71	9.56	0.91	15.40	1.00	121.37
Schmidt Hardness (bulk)	0.76	12.67	0.84	8.15	0.86	4.27
Schmidt Hardness (core)	0.56	5.00	0.92	16.72	0.92	7.56
Point Load Strength	0.76	12.93	0.83	7.10	0.88	4.83
Uniaxial Compressive Strength	0.75	12.15	0.77	4.94	0.77	2.19
Splitting Tensile Strength	0.39	2.51	0.43	1.13	0.69	1.52
Fracture Toughness	0.40	2.68	0.54	1.74	0.84	3.45
Charateristic Dimension	0.03	0.13	0.29	0.61	0.31	0.30

Critical F-values at 0.05 confidence level:	Linear (1st) GLM:	7.71
	Quadratic (2nd) GLM:	9.55
	Cubic (3rd) GLM:	19.16

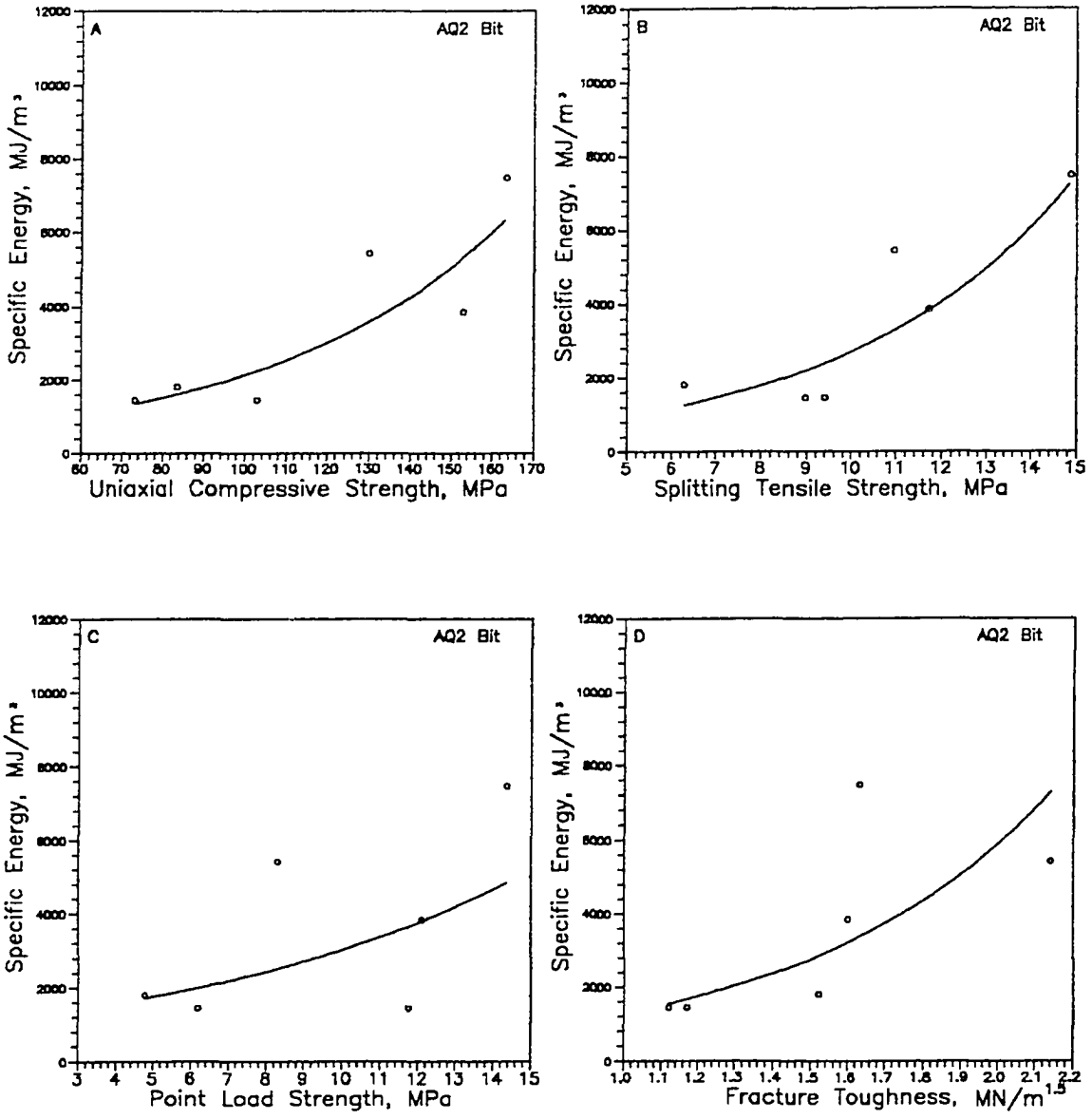

Figure 6.17: Specific energy (kerfing) vs. rock properties for AQ2 bit in the preliminary rock coring test: (a) uniaxial compressive strength, (b) splitting tensile strength, (c) point load strength, (d) fracture toughness

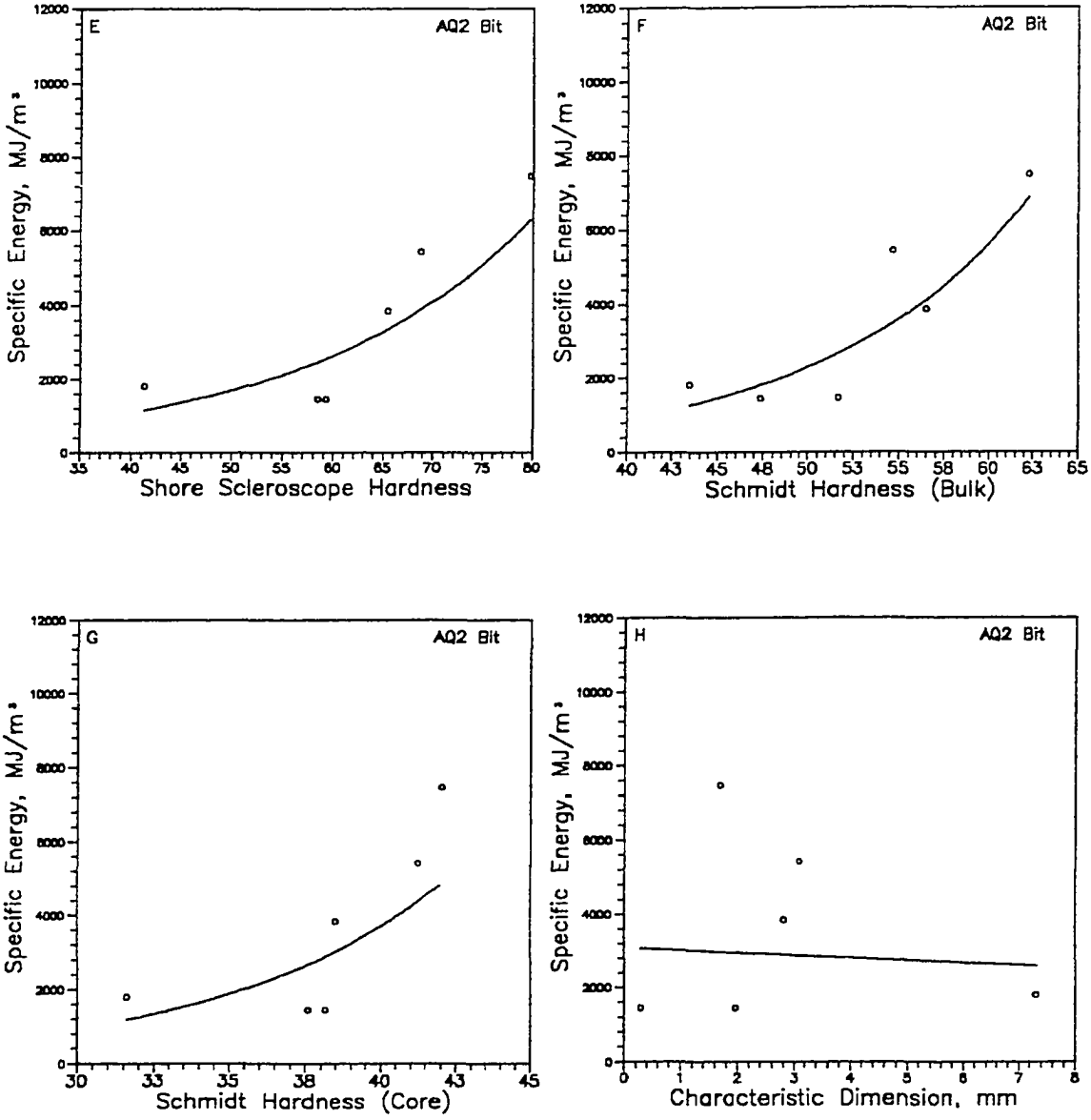

Figure 6.17 (cont'd): (e) Shore scleroscope hardness, (f) Schmidt hardness on bulk specimen, (g) Schmidt hardness on core specimen, and (h) characteristic dimension

of strength or hardness of rock. The increase rate was much higher than it was for AQ1 bit, though. The data for the Characteristic Dimension in Figure 6.17(h) were, however, scattered.

6.3.3.2 BQ2 Bit

The coefficients of determination and F-values of the GLM models for BQ2 bit with the specific energy are presented in Table 6.12. It was noted that for the linear models, four of the eight rock properties showed significant correlations with the specific energy, i.e., the Shore scleroscope hardness (F-value=9.21), the Schmidt hardness of bulk specimen (F-value=19.90), the point load strength (F-value=17.03), and the uniaxial compressive strength (F-value=16.71). The Shore scleroscope hardness and the Schmidt hardness of bulk specimen also showed significant correlations with the specific energy for the quadratic models. For the cubic models, no rock properties were found to have significant correlation with the specific energy.

The specific energy versus the eight rock properties is plotted in Figure 6.18. It was found that the specific energy increased with an increase in the strength or hardness of rock. For the Characteristic Dimension, the data were scattered.

Table 6.12: Regression analysis of specific energy for BQ2 bit in the preliminary rock coring test

Rock property	1st Degree GLM		2nd Degree GLM		3rd Degree GLM	
	R-squared	F-value	R-squared	F-value	R-squared	F-value
Shore Scleroscope Hardness	0.70	9.21	0.93	20.18	0.95	13.03
Schmidt Hardness (bulk)	0.83	19.90	0.93	21.35	0.94	11.29
Schmidt Hardness (core)	0.53	4.57	0.86	8.97	0.86	4.01
Point Load Strength	0.81	17.03	0.90	13.44	0.93	8.31
Uniaxial Compressive Strength	0.81	16.71	0.82	6.77	0.86	3.96
Splitting Tensile Strength	0.56	5.18	0.64	2.62	0.78	2.29
Fracture Toughness	0.24	1.26	0.41	1.03	0.87	4.49
Charateristic Dimension	0.07	0.29	0.18	0.32	0.20	0.17

Critical F-values at 0.05 confidence level:	Linear (1st) GLM:	7.71
	Quadratic (2nd) GLM:	9.55
	Cubic (3rd) GLM:	19.16

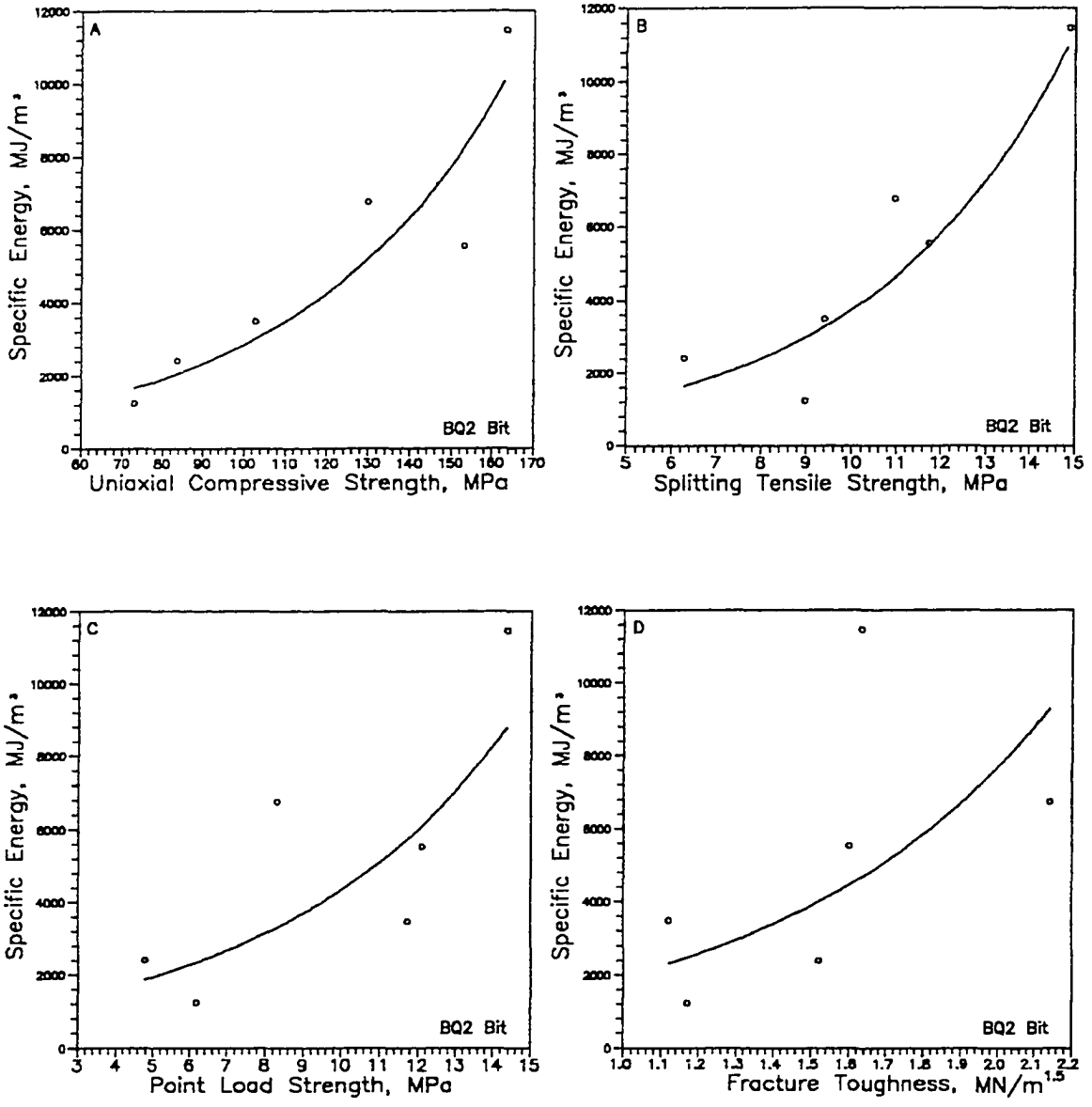

Figure 6.18: Specific energy (kerfing) vs. rock properties for BQ2 bit in the preliminary rock coring test: (a) uniaxial compressive strength, (b) splitting tensile strength, (c) point load strength, (d) fracture toughness

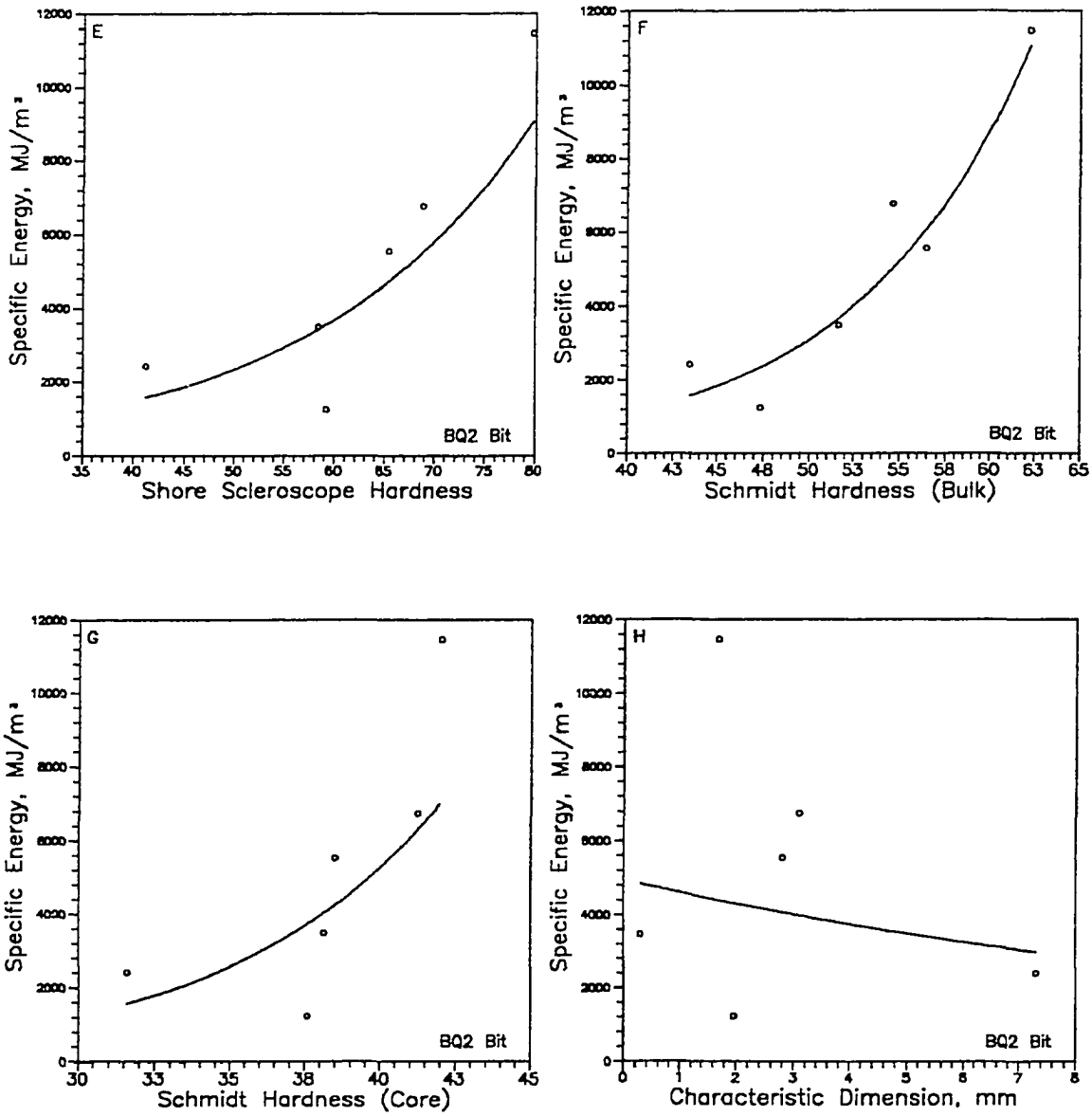

Figure 6.18 (cont'd): (e) Shore scleroscope hardness, (f) Schmidt hardness on bulk specimen, (g) Schmidt hardness on core specimen, and (h) characteristic dimension

6.4 COMPARISON

6.4.1 Penetration Rate

To compare the drilling performance of the four bits, the penetration rate achieved by each bit was averaged for each rock type. The average penetration rate in the six rocks was then plotted against the uniaxial compressive strengths of rock in Figure 6.19. It was noted that the penetration rate achieved by the two surface-set bits (i.e., AQ1 and BQ1) were much higher than that achieved by the two impregnated bits (i.e., AQ2 and BQ2) in all six rocks. The penetration rate of the larger diameter impregnated bit (BQ2) was lower than that of the smaller diameter impregnated bit (AQ2). Generally, the penetration rate of a drill bit decreased when encountering a harder rock.

The two surface-set bits behaved differently. For hard rocks ($\sigma_c \geq 100$ MPa), the penetration rate of BQ1 bit was higher than that of AQ1 bit. This trend was reversed for rocks with uniaxial compressive strength less than about 100 MPa. The reason for this, however, was not clear.

6.4.2 Applied Torque

Similarly, the applied torque for each rock type was averaged and plotted against the uniaxial compressive strength in Figure 6.20. It was found that the applied torque was higher in softer rocks ($\sigma_c < 100$ MPa) than it was in harder rocks ($\sigma_c \geq 100$ MPa). It was also noted that for all four bits tested, the applied torque did not change much among the harder rocks.

It was further noted that the applied torque of the two surface-set bits was larger

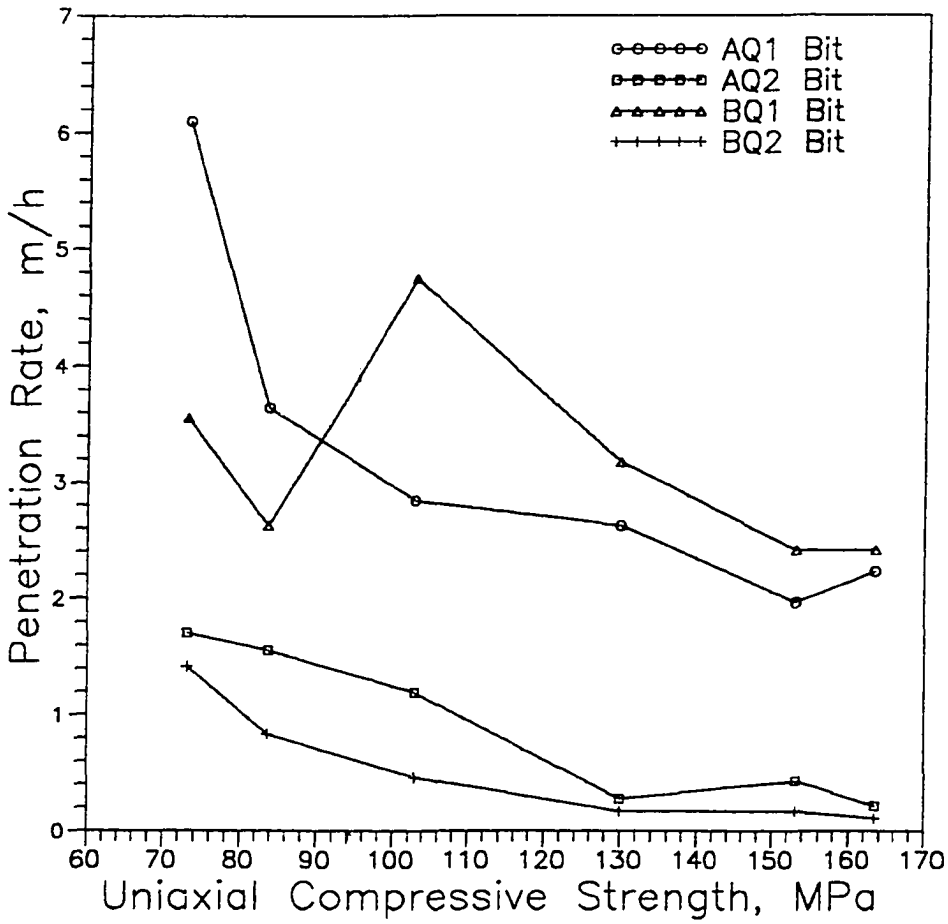

Figure 6.19: Penetration rate vs. uniaxial compressive strength for all the four bits in the preliminary rock coring test

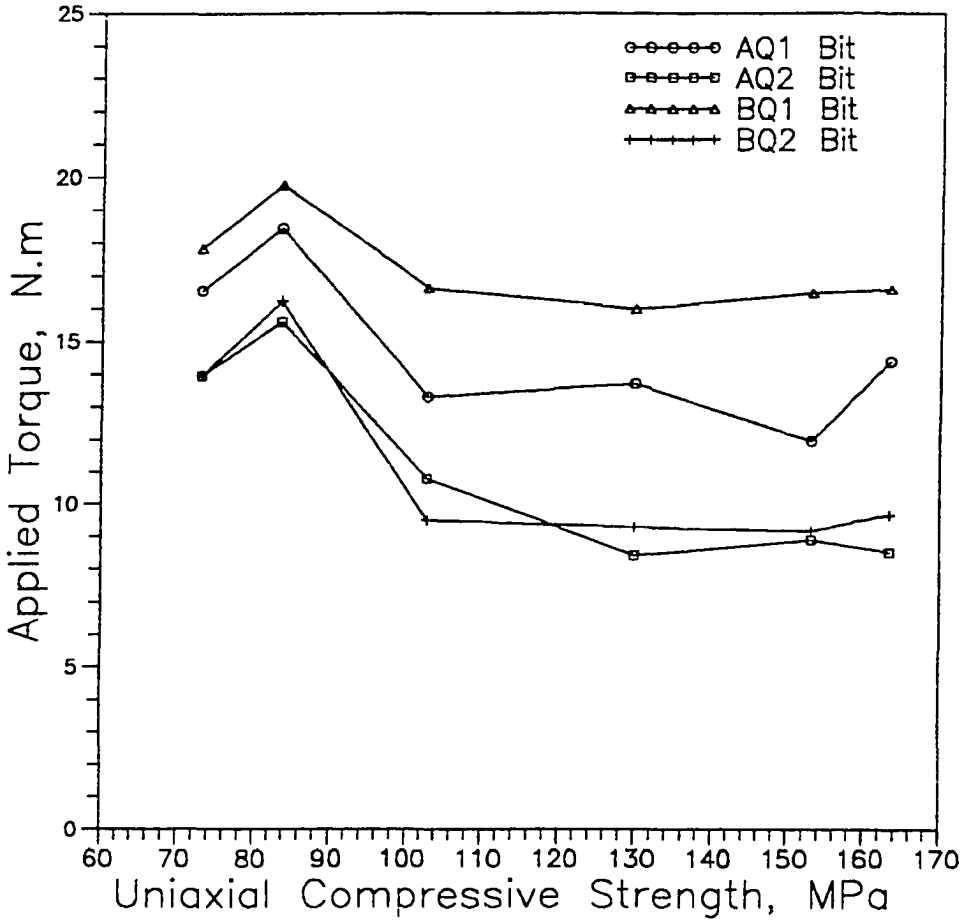

Figure 6.20: Applied torque vs. uniaxial compressive strength for all the four bits in the preliminary rock coring test

than that of the two impregnated bits, and the applied torque of the larger diameter surface-set bit BQ1 was larger than that of the smaller diameter surface-set bit AQ1. The torque difference between the two impregnated bits, however, was small.

6.4.3 Specific Energy

To compare the specific energy of the four bits, the Specific Kerfing Energy and the Specific Core Recovery Energy were calculated separately. Figure 6.21 presents the average Specific Kerfing Energy versus the uniaxial compressive strength of rock for the four bits. As was observed in the previous sections, the Specific Kerfing Energy of the two impregnated bits AQ2 and BQ2 increased rapidly with an increase in the uniaxial compressive strength of rock, but it did not change significantly for the two surface-set bits. Between the two impregnated bits, the Specific Kerfing Energy of the AQ2 bit was less than that of the BQ2 bit.

The average Specific Core Recovery Energy versus the uniaxial compressive strength of rock is shown in Figure 6.22. Comparing with Figure 6.21, it was found that the energy required to recover cores for the AQ2 and BQ2 bits were close in the six rocks. The Specific Kerfing Energy of the AQ2 bit was, however, slightly less than that of the BQ2 bit.

It was further noted that for the two surface-set bits AQ1 and BQ1, the energy for kerfing was close to each other. The Specific Core Recovery Energy of the BQ1 bit was less than that of other bits for all rock types, however. From the standpoint of recovering rock cores, the BQ1 bit was the most effective bit among the four bits tested. Therefore,

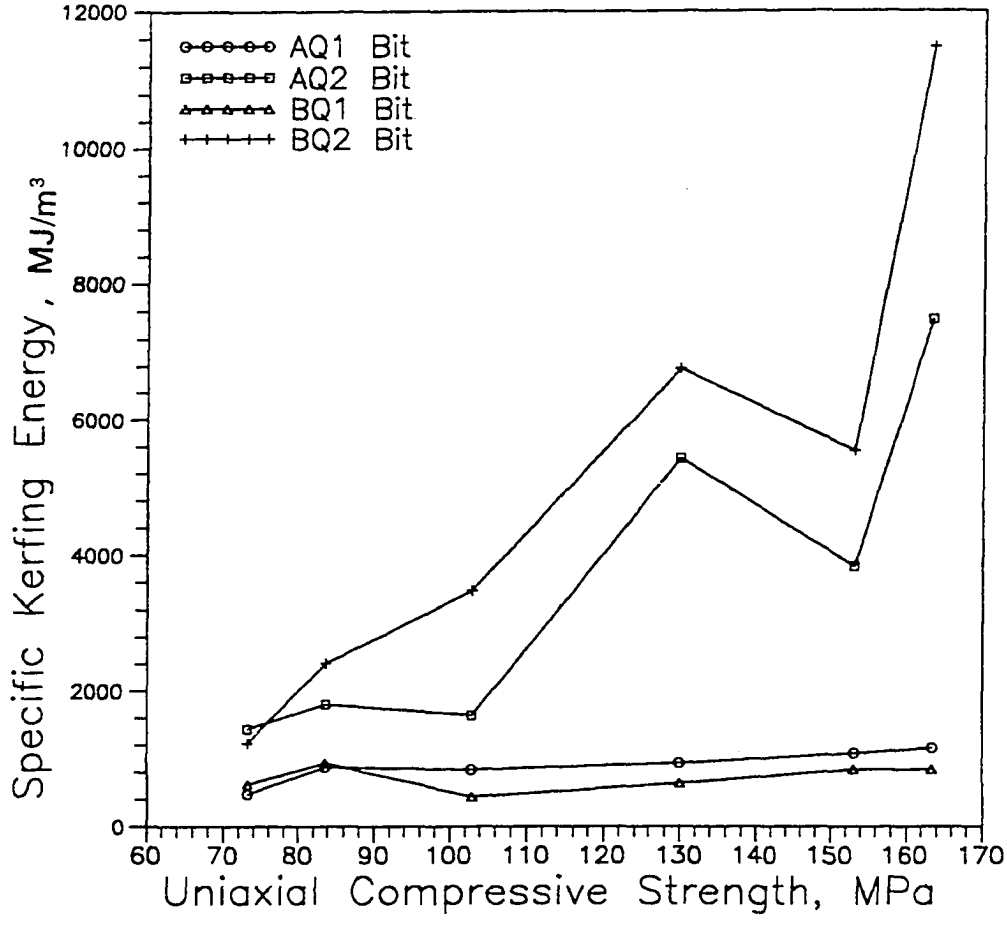

Figure 6.21: Specific energy (kerfing) vs. uniaxial compressive strength for all the four bits in the preliminary rock coring test

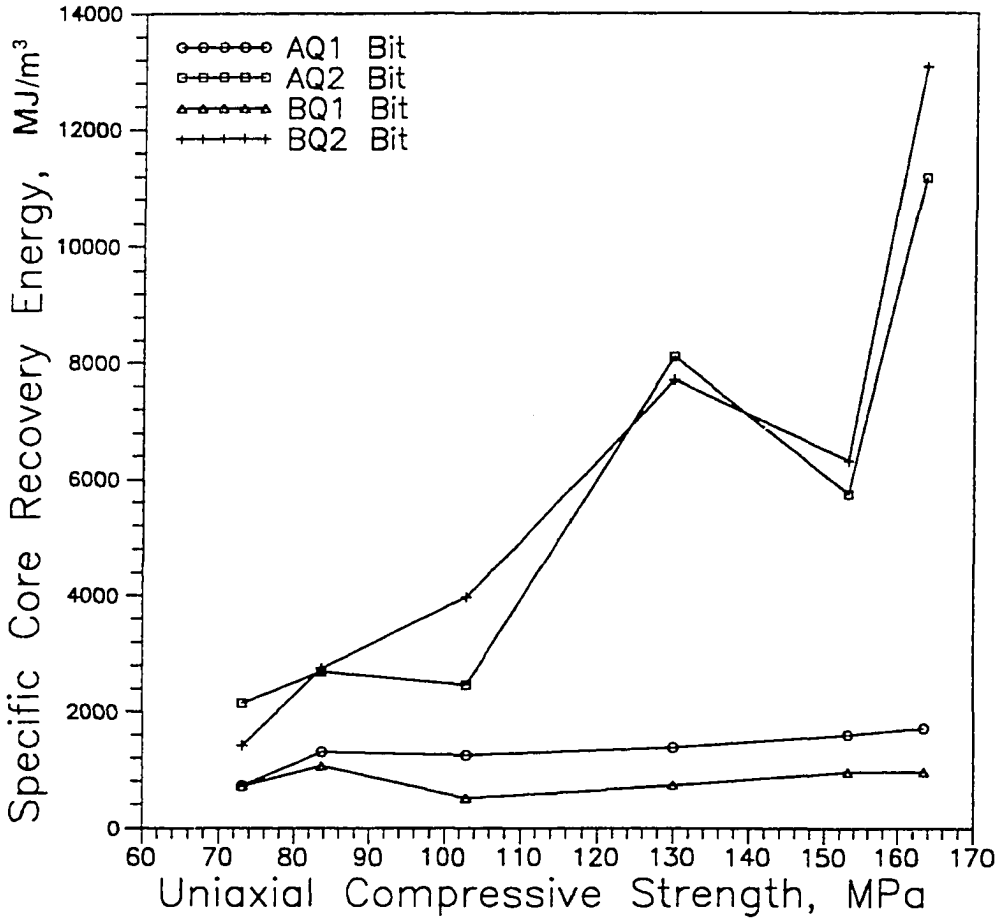

Figure 6.22: Specific energy (core recovery) vs. uniaxial compressive strength for all the four bits in the preliminary rock coring test

it was chosen to do further tests in this study.

6.5 CHAPTER SUMMARY

1. The uniaxial compressive strength was not necessarily the best rock property to describe bit performance under all conditions. In some cases, the splitting tensile strength, Shore scleroscope hardness, Schmidt hardness, fracture toughness, or even particle size were better indications of the bit performance. However, in most cases, the uniaxial compressive strength was a good indication of the bit performance.
2. The penetration rate decreased with strength or hardness of rock. The rate of decrease varied with types of bits. The impregnated bits were more sensitive to strength or hardness of rock, while the surface-set bits seemed to be more sensitive to the fracture toughness and particle size of rock.
3. Larger torque was needed in softer rocks (σ_c<100 MPa). For rocks with σ_c larger than about 100 MPa, the torque requirements did not change much with rock strength or hardness.
4. The energy requirement increased rapidly with the strength or hardness of rock for the impregnated bits, but it only increased slightly for the surface-set bits.
5. Surface-set bits achieved a much higher penetration rate than did the impregnated bits.
6. The larger diameter surface-set bit (BQ1) was more efficient than the smaller

diameter (AQ1) bit in rocks with uniaxial compressive strength higher than 100 MPa.

CHAPTER 7

RESULTS AND DISCUSSIONS - PART II

7.1 INTRODUCTION

Once a bit is selected (i.e., BQ1 bit in this study), it is important to test the bit performance at various bit weights and rotational speeds so optimum parameters for drilling operation can be found. In order to maximize information from a limited number of tests, a 6×6 Latin square was employed. The 6×6 Latin square design is shown in Table 4.1. Factors considered to be influential were weight-on-bit, rotational speed, and rock type. In this experimental design, these three factors were randomly distributed in each row, each column, and each treatment. The Row-factor in this square was six bit weights, ranging from 889.6 to 2,668.8 Newtons (200 to 600 lb). Six rotational speeds ranging from 200 to 600 rpm were used as the Column-factor. The treatment of this test included six rock types, namely, A, B, C, D, E, and F. These rocks were characterized by their physical properties.

To minimize variations caused by repetitive use of the bit during this experiment, the testing sequence was also randomized. This randomization process was to reduce the effect due to wear of the bit. In addition, water was used as the flushing fluid and the flow rate was kept constant at 5.68 l/min (1.5 gpm) throughout the experiment.

During each test, weight-on-bit, rotational speed, applied torque, and penetration depth were continuously recorded by a 6-488B data acquisition system. Data recorded by

the logger were transmitted to a computer at a 2-second interval. Based on the measurements, penetration rate and specific energy were computed. The above two parameters and applied torque were the criteria upon which the evaluation of drilling performance was based. The results of this test sequence are presented in Appendix 5. In the following sections, statistical analyses of the results are discussed.

7.2 PENETRATION RATE

7.2.1 ANOVA Test

The result of the ANOVA test on the penetration rate is presented in Table 7.1. F-values of the three investigated factors were calculated with the penetration rate as the dependent parameter. A critical F-value can be found in a statistical table (Appendix 1). For a 6×6 Latin square design, the critical F-value at α=0.05 is 2.71. Therefore, it was concluded that the penetration rate in this test was affected by all three factors. The weight-on-bit, with a F-value of 12.54, showed the greatest effect on the penetration rate. The next influential factor was the rock type with an F-value of 10.71. The rotational speed, with an F-value of 3.54, showed the least (but still significant) effect on the penetration rate.

7.2.2 Newman-Keuls Test

Since statistically significant influences of the weight-on-bit, rock type, and rotational speed on the penetration rate have been noted, the Newman-Keuls test was conducted to evaluate how each of the factors influenced the penetration rate. To do this, the penetration rates were averaged according to each influential factor regardless the effects

Table 7.1 Result of ANOVA Test for Penetration Rate

Variable	df	SS	MSS	F-value
W	5	4.295	0.859	12.54
N	5	1.213	0.243	3.54
RT	5	3.669	0.734	10.71
Error	20	1.370	0.068	

df: Degree of freedom

SS: Sum of square

MSS: Mean sum of square

W: Weight-on-bit, N

N: Rotational speed, rpm

RT: Rock type

$F_{(\alpha=0.05)}=2.71$

of others. Then the mean values of the penetration rate were arranged in descending order from the highest to the lowest. The mean differences of the penetration rate were arranged according to Table 3.3. The least significant values, R_k, were calculated by Equation 3.10. By comparing the mean differences with the least significant values, the degree of influence of each factor was evaluated.

7.2.2.1 Weight-on-Bit

By averaging the six penetration rates at each weight-on-bit regardless of the influences of the rotational speed and rock type, it was found that the average penetration rate at 2,668.8 Newtons (600 lb) bit weight was the largest and at 889.6 Newtons (200 lb) bit weight it was the lowest. The descending order of the average penetration rate is as following:

$$PR_w(600) > PR_w(500) > PR_w(450) > PR_w(400) > PR_w(300) > PR_w(200)$$

or

$$1.327 > 0.754 > 0.750 > 0.610 > 0.393 > 0.232 \, (m/h)$$

Result of the Newman-Keuls test for the effect of weight-on-bit upon the penetration rate is presented in Table 7.2. The mean differences were compared with the least significant values. It was found that the weight-on-bit could be classified into three groups. The first group of bit weight was at W>2,224 Newtons (500 lb). At this weight-on-bit, the penetration rate was the highest. The second group of bit weight was at 1,334.4 Newtons<W≤2,224 Newtons. At this weight-on-bit an intermediate penetration rate was

Table 7.2 Newman-Keuls Test for Weight-on-bit on Penetration Rate

No. of mean spanned	6	5	4	3	2
Least signifcant value (m/h)	0.353	0.347	0.340	0.331	0.315
Mean differences of the average applied torque (m/h)	1.095	0.934	0.717	0.577	0.573
		0.522	0.361	0.144	0.004
			0.518	0.357	0.140
				0.378	0.217
					0.161

achieved. The third group of bit weight was at W≤1,334.4 Newtons (300 lb). At this weight-on-bit group the penetration rate was the lowest. The differences of penetration rate among three groups were significant; however, they were not differentiable within each group.

7.2.2.2 Rock Type

Similar procedures were also performed on the type of rock. By averaging the six penetration rates according to each rock type, it was found that the average penetration rate on rock D (schist) was the highest and the lowest on rock B (diorite). The descending order of average penetration rate is as following:

$$PR(D) > PR(E) > PR(A) > PR(C) > PR(F) > PR(B)$$

or

$$1.141 > 0.983 > 0.759 > 0.565 > 0.320 > 0.300 (m/h)$$

Table 7.3 lists the results of Newman-Keuls test for rock type on the penetration rate. Three groups of rock were distinguished according to penetration rate. The first group consisted of rocks D (schist) and E (limestone) which corresponded to the highest penetration rate. The second group consisted of rocks F (granodiorite) and B (diorite). Penetration rates in this group of rocks were the lowest. The third group of rocks included rocks A (limestone) and C (granite), which corresponded to the intermediate penetration rate. Statistically, the differences of penetration rate between each group of rocks were significant, but were insignificant within each group.

Table 7.3 Newman-Keuls Test for Rock Type on Penetration Rate

No. of mean spanned	6	5	4	3	2
Least signifcant value (m/h)	0.353	0.347	0.340	0.331	0.315
Mean differences of the average applied torque (m/h)	0.841	0.821 0.683	0.567 0.663 0.459	0.382 0.418 0.439 0.265	0.158 0.224 0.194 0.245 0.020

7.2.2.3 Rotational Speed

The penetration rates were also averaged according to each of the six levels of rotational speed regardless of effects of the bit weight and rock type. It was found that the penetration rate was the highest at 600 rpm and the lowest at 200 rpm. The descending order of the mean penetration rate is:

$$PR_N(600) > PR_N(500) > PR_N(450) > PR_N(400) > PR_N(300) > PR_N(200)$$

or

$$0.943 > 0.823 > 0.718 > 0.654 > 0.553 > 0.375 \ (m/h)$$

The result of the Newman-Keuls test of rotational speed on penetration rate is shown in Table 7.4. The six rotational speeds could be resorted into two groups. One group included the four higher speeds at 400, 450, 500, and 600 rpm. Another group included the two lower speeds at 200 and 300 rpm. The penetration rates at higher rotational speeds were higher, and were lower at the lower speeds. The differences of penetration rates within each speed group were insignificant, but statistically differentiable between the two groups.

7.2.3 Regression Analysis

Because all of the three factors (i.e., weight-on-bit, rotational speed, and rock type) have affected the penetration rate significantly, regression analysis procedures were therefore conducted to formulate relationships between the influential factors and the penetration rate. First, a single variable regression analysis was performed on each of the three

Table 7.4 Newman-Keuls Test for Rotational Speed on Penetration Rate

No. of mean spanned	6	5	4	3	2
Least signifcant value (m/h)	0.353	0.347	0.340	0.331	0.315
Mean differences of the average applied torque (m/h)	0.568	0.390	0.289	0.225	0.120
		0.448	0.270	0.169	0.105
			0.343	0.165	0.064
				0.279	0.101
					0.178

factors, regardless of the effects caused by other factors. Then a multi-variable regression analysis was conducted including all three factors. For all analyses, both GLM and NLIN procedures were conducted, and the best statistical model was chosen, based on its accuracy, simplicity, and consistency with physical conditions.

7.2.3.1 Weight-on-bit

The GLM and NLIN regression techniques were conducted to relate the penetration rate with the weight-on-bit, regardless of the effects of the rotational speed and rock type. The penetration rates at a specific tested weight-on-bit were averaged. An exponential equation was found to best fit the averaged experimental data, with a R^2 of 0.94 and F-value of 45.83. The relationship is also illustrated in Figure 7.1. The mathematical expression of the above relationship is:

$$PR = 0.107 e^{0.001W} \qquad (7.1)$$

where PR is penetration rate in m/h, and W is weight-on-bit in Newton.

7.2.3.2 Rock Type

The effects of various rock properties on the penetration rate were discussed in the previous chapter. Because all of the strength properties and indices of rock were highly correlated, and because the uniaxial compressive strength is the most commonly used rock property in drillability study, only the uniaxial compressive strength was employed in this regression analysis. The best fitting equation was found to be a NLIN equation in the

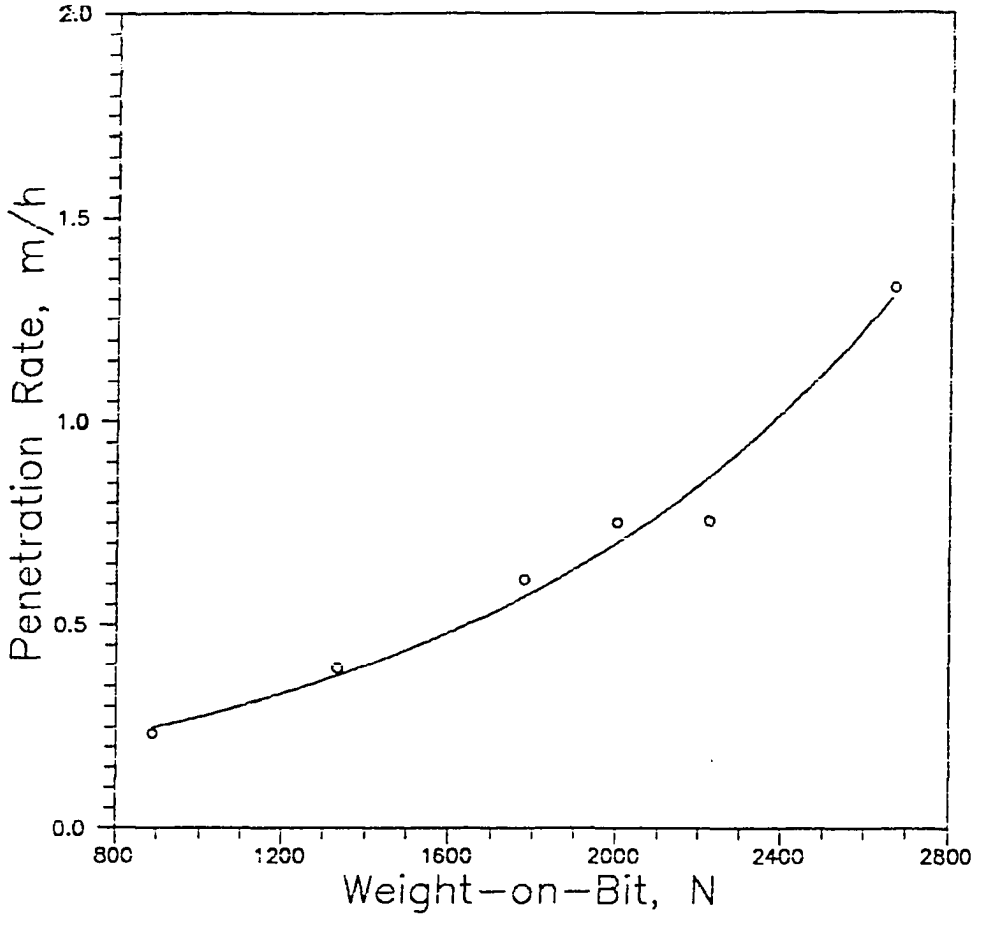

Figure 7.1: Penetration rate vs. weight-on-bit in the Latin square drilling test

following form:

$$PR=1.96e^{-0.01\sigma_c} \qquad (7.2)$$

where σ_c is uniaxial compressive strength in MPa, and PR is penetration rate in m/h. This relationship is also illustrated graphically in Figure 7.2. As has been found in the preliminary rock coring test, a higher penetration rate was obtained when the strength of rock was lower.

7.2.3.3 Rotational Speed

The similar regression procedures were performed for the penetration rate and rotational speed, regardless of the effects of weight-on-bit and rock type. It was found that the penetration rate increased with an increase in the rotational speed, and a strong linear relationship was found. The mathematical expression of this relation is:

$$PR=0.107+1.4\times10^{-3}N \qquad (7.3)$$

where N is the rotational speed in rpm. This equation has a R^2 of 0.99 and an F-value of 493.45. Figure 7.3 graphically presents this relationship.

7.2.3.4 Multi-variable Regression Analysis

A regression equation can seldom accurately predict an observation using any particular variable if the observation is affected by more than one factor. Because all of the three factors investigated in this study were found to be influential upon the penetration rate, it was necessary to include all three parameters in the prediction equation. Considering

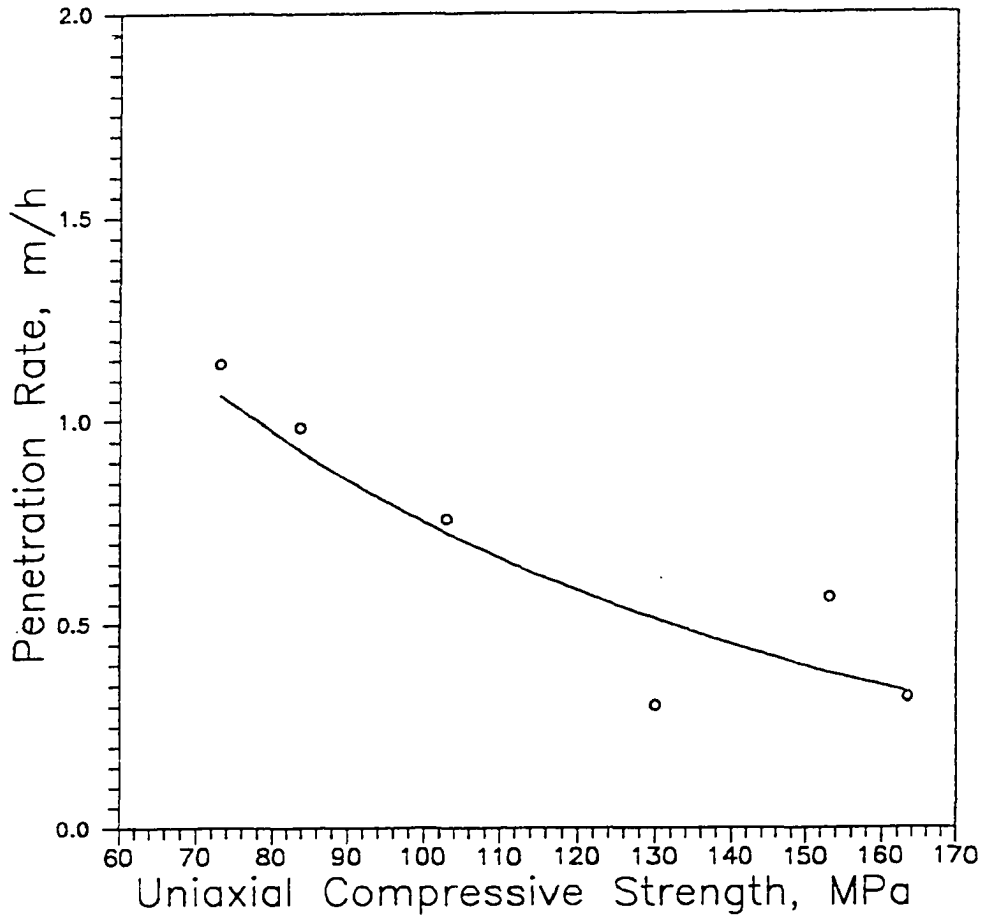

Figure 7.2: Penetration rate vs. uniaxial compressive strength in the Latin square drilling test

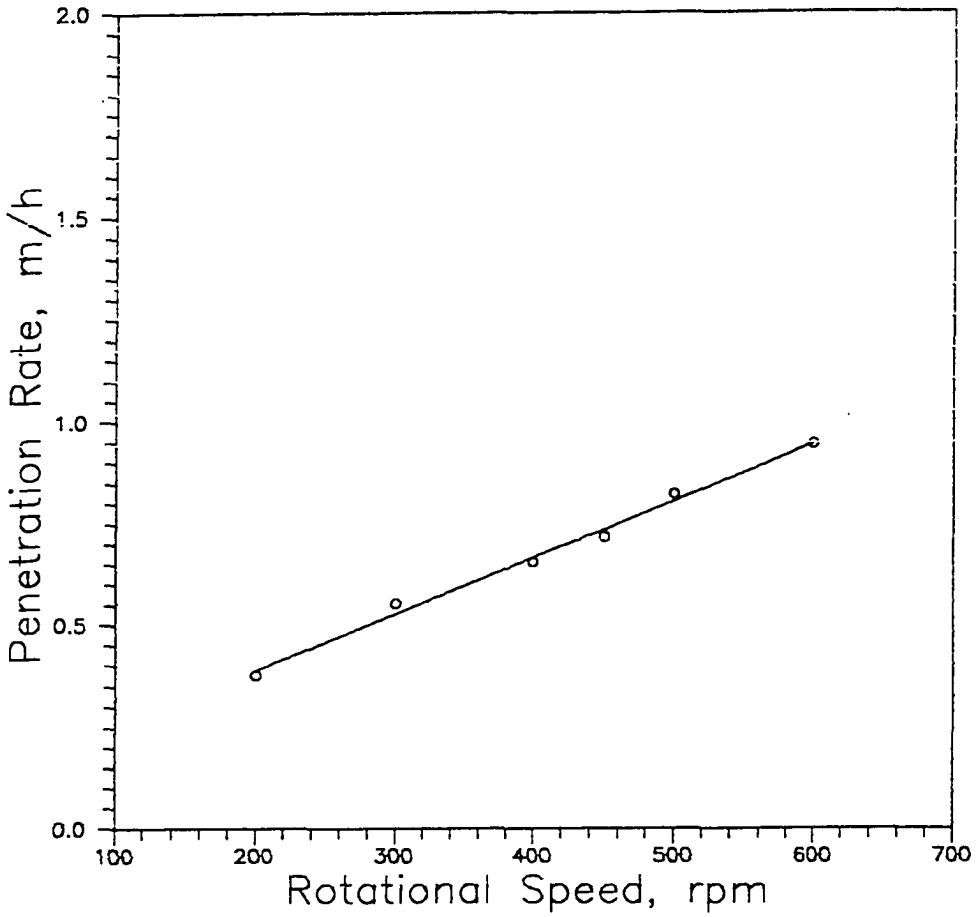

Figure 7.3: Penetration rate vs. rotational speed in the Latin square drilling test

the sample size of this experiment, a quadratic GLM regression technique was employed to conduct the multi-variable regression analysis. The parameters considered in the quadratic model included all three parameters (i.e., weight-on-bit, rotational speed, and uniaxial compressive strength of rock), their second-degree parameters (i.e., squared), and their crossed interactions. Then BACKWARD stepwise regression procedure was conducted on the same set of parameters to select the most significant influential factors among them. The backward elimination method was conducted at a 0.25 significance level. Table 7.5 summarizes the results of these statistical procedures. The quadratic GLM model contained all the ten items and its R^2 and F-value were 0.93 and 32.02, respectively. The backward elimination method generated a polynomial equation of six parameters for the penetration rate. Its R^2 and F-value were 0.92 and 58.80, respectively. The R^2 of the quadratic GLM model was slightly higher than that of the stepwise model. The F-value of the stepwise, however, was much higher than it was for the quadratic GLM model. The simplicity of the stepwise model could offset the slight lose of accuracy. Therefore, the backward stepwise model was chosen to express the best fitting equation for the penetration rate:

$$PR = 1.46667 - 0.00496W - 0.01490\sigma_c + 0.00001W^2 + 0.00006\sigma_c^2 + 0.00001WN \qquad (7.4)$$

where:

PR is the penetration rate in m/h;

W is the weight-on-bit in Newton;

N is the rotational speed in rpm; and

Table 7.5: Summary of regression analysis for penetration rate in Latin square drilling test

	GLM			Stepwise		
Factor	Coefficient	F	Pr>F	Cofficient	F	Pr>F
Intercept	1.29806	n/a	n/a	1.46667	6.92	0.0135
W	-0.00446	130.56	0.0001	-0.00496	11.92	0.0017
N	0.00011	39.36	0.0001			
UCS	-0.01020	116.98	0.0001	-0.01490	2.89	0.1000
W*W	0.00001	7.80	0.0099	0.00001	18.88	0.0002
N*N	0.00000	0.00	0.9493			
UCS*UCS	0.00006	1.05	0.3154	0.00006	2.59	0.1182
W*N	0.00001	5.00	0.0346	0.00001	41.66	0.0001
W*UCS	-0.00001	9.75	0.0045			
N*UCS	-0.00001	9.97	0.0041			
W*N*UCS	-0.00000	0.19	0.6665	-0.00000	20.74	0.0001

W: Weight-on-bit, N
N: Rotational speed, rpm
UCS: Uniaxial compressive strength, MPa

σ_c is the uniaxial compressive strength in MPa.

7.3 APPLIED TORQUE

7.3.1 ANOVA Test

ANOVA test was employed to analyze effects of the investigated factors on applied torque and the results are presented in Table 7.6. The critical F-value at α=0.05 was 2.71 for this test. It was noted that the weight-on-bit, with an F-value of 27.49, had affected the applied torque most significantly, with the rock type being the next influential factor, having an F-value of 22.40. The effect of rotational speed on the applied torque, with an F-value of 1.01, did not significantly affect the result.

7.3.2 Newman-Keuls Test

Because two influential factors, the weight-on-bit and rock type, were found to significantly affect the applied torque, the Newman-Keuls test was performed on the two factors to evaluate how they have affected the applied torque in this test.

7.3.2.1 Weight-on-Bit

The applied torques from this test were averaged according to each bit weight, and then the mean values of applied torque were arranged in a descending order from the highest to the lowest. It was found that the average torque at 2,668.8 Newtons (600 lb) bit weight was the highest and was the lowest at 889.6 Newtons (200 lb) bit weight. The arrangement is as follow:

Table 7.6 Results of ANOVA Test for Applied Torque

Variable	df	SS	MSS	F-value
W	5	144.025	28.805	27.49
N	5	5.315	1.063	1.01
RT	5	117.331	23.466	22.40
Error	20	20.953	1.048	

df: Degree of freedom

SS: Sum of square

MSS: Mean sum of square

W: Weight-on-bit, N

N: Rotational speed, rpm

RT: Rock type

$F_{(\alpha=0.05)}=2.71$

$$T_W(600) > T_W(500) > T_W(450) > T_W(400) > T_W(300) > T_W(200)$$

or

$$14.493 > 13.013 > 11.674 > 11.449 > 9.515 > 8.534\ (N.m)$$

The result of Newman-Keuls test was shown in Table 7.7. By comparing the mean differences of the applied torque with the least significant values, it was found that the six bit weights could be re-sorted into three groups, namely: W≥2,224 Newtons (500 lb), 1,334.4 Newtons (300 lb)<W<2,224 Newtons (500 lb), and W≤1,334.4 Newtons (300 lb). The differences of torque in each group were statistically insignificant, but significant between any two groups.

7.3.2.2 Rock Type

Similar analysis procedures were used to evaluate the effects of the rock type on the applied torque. The mean values of applied torque were arranged according to the six rock types. It was found that the mean torque for rock E was the highest, and mean torque was the lowest for rock F. The descending order of mean torques is as following:

$$T(E) > T(D) > T(B) > T(A) > T(C) > T(F)$$

or

$$14.010 > 13.861 > 10.837 > 10.401 > 9.996 > 9.544\ (N.m)$$

The result of Newman-Keuls test on rock type is tabulated in Table 7.8. By comparing the mean differences of torque with the least significant values, it was found

Table 7.7 Newman-Keuls Test for Weight-on-bit on Applied Torque

No. of mean spanned	6	5	4	3	2
Least signifcant value (N.m)	1.379	1.358	1.329	1.296	1.233
Mean differences of the average applied torque (N.m)	5.959	4.978 4.479	3.044 3.498 3.140	2.819 1.564 2.159 2.915	1.480 1.339 0.225 1.934 0.981

Table 7.8 Newman-Keuls Test for Rock Type on Applied Torque

No. of mean spanned	6	5	4	3	2
Least signifcant value (N.m)	1.379	1.358	1.329	1.296	1.233
Mean differences of the average applied torque (N.m)	4.466	4.014 4.317	3.609 3.865 1.293	3.173 3.460 0.841 0.857	0.149 3.024 0.436 0.405 0.452

that the six rocks can be classified into two groups. One group included rocks E and D, the other group included rocks A, B, C, and F. The torque differences between the two groups were significant, but were insignificant within each group.

7.3.3 Regression Analysis

Because the applied torque was found to be significantly influenced by two of the three investigated factors (i.e. weight-on-bit and rock type), the regression analysis was performed to correlate the applied torque with them, respectively. The regression analysis techniques used to formulate the relationship between the applied torque and the influential factors included both GLM and NLIN procedures for single variable analysis.

7.3.3.1 Weight-on-Bit

The GLM and NLIN regression procedures were used on the applied torque with weight-on-bit, regardless of the effects of rock type. The result indicated that an exponential equation could best express the relationship between the applied torque and weight-on-bit, with a R^2=0.99 and F=255.45. This relationship is also illustrated in Figure 7.4. The equation is:

$$T=6.462e^{0.0003W} \qquad (7.5)$$

where T is applied torque in Newton-meter (Nm), and W is weight-on-bit in Newton.

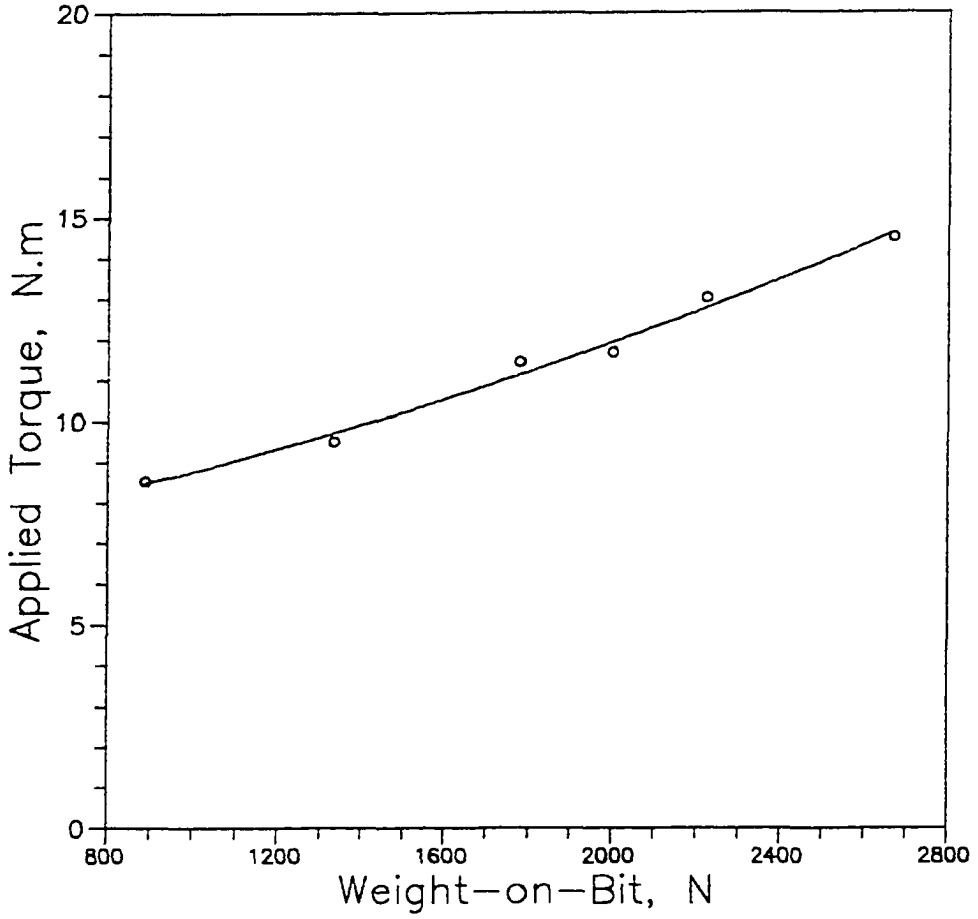

Figure 7.4: Applied torque vs. weight-on-bit in the Latin square drilling test

7.3.3.2 Rock Type

The similar regression procedures were performed on applied torque with the uniaxial compressive strength of rock. The best fitting equation was found to be an inversed power equation in the following form:

$$T=103.26\sigma_c^{-0.468} \qquad (7.6)$$

where σ_c is uniaxial compressive strength in MPa. Figure 7.5 graphically presents this relationship.

7.3.3.3 Multi-variable Regression Analysis

As it was in the case of the penetration rate, the GLM and stepwise backward regression procedures were performed on the applied torque. The number of parameters used in this analysis were kept the same as those used in the previous analysis. Table 7.9 summarizes the results. The R^2 and F-value of the quadratic GLM model were 0.91 and 24.04, respectively. The backward stepwise method generated an equation having seven parameters, with R^2 of 0.90 and F-value of 37.45. The R^2 of the stepwise model was slightly lower than that of the quadratic GLM model. It, however, contained less parameters and had a higher F-value. Therefore, the backward stepwise model was chosen to predict the applied torque:

$$T=15.06063+0.03299W+0.02186N-0.28201\sigma_c -0.00002N^2+0.00117\sigma_c^2-0.00002WN-0.00008W\sigma_c \qquad (7.7)$$

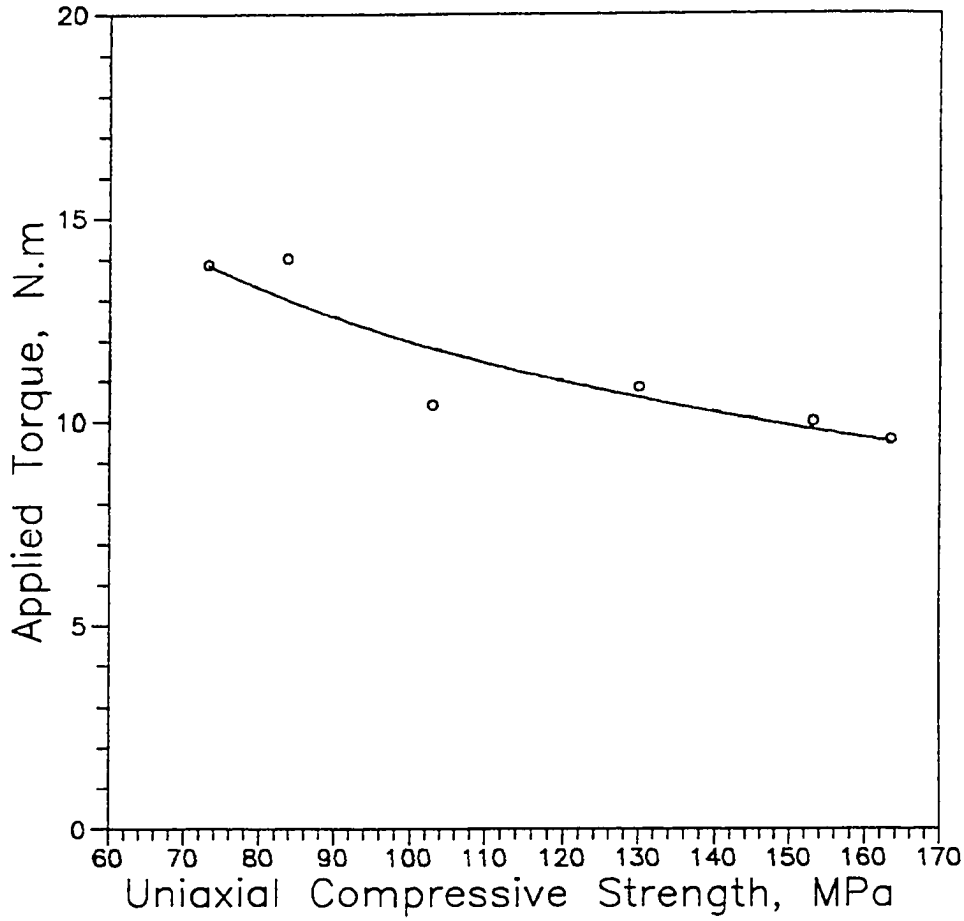

Figure 7.5: Applied torque vs. uniaxial compressive strength in the Latin square drilling test

Table 7.9: Summary of regression analysis for applied torque in Latin square drilling test

	GLM			Stepwise		
Factor	Coefficient	F	Pr>F	Cofficient	F	Pr>F
Intercept	15.15735	n/a	n/a	15.06063	12.88	0.0012
W	0.02853	130.81	0.0001	0.03299	34.71	0.0001
N	0.02417	0.09	0.7634	0.02186	5.63	0.0247
UCS	-0.27256	68.49	0.0001	-0.28201	26.65	0.0001
W*W	0.00001	0.61	0.4433			
N*N	-0.00002	2.81	0.1062	-0.00002	2.82	0.1045
UCS*UCS	0.00116	27.86	0.0001	0.00117	28.19	0.0001
W*N	-0.00002	6.31	0.0188	-0.00002	3.05	0.0918
W*UCS	-0.00010	3.42	0.0761	-0.00008	3.74	0.0632
N*UCS	-0.00002	0.00	0.9775			
W*N*UCS	0.00000	0.01	0.9325			

W: Weight-on-bit, N
N: Rotational speed, rpm
UCS: Uniaxial compressive strength, MPa

where:

T is the applied torque in Nm;

W is the weight-on-bit in Newton;

N is the rotational speed in rpm; and

σ_c is the uniaxial compressive strength in MPa.

7.4 SPECIFIC ENERGY

It was discussed in Chapter 6 that for a single type of bit the Specific Core Recovery Energy is a direct function of the Specific Kerfing Energy. In the 6×6 Latin square rock drilling experiment, all the tests were conducted by the BQ1 bit. Therefore, only the Specific Kerfing Energy was used in this discussion and it was simply called *specific energy*. The statistical relationships, however, would be exactly the same for the Specific Core Recovery Energy.

7.4.1 ANOVA Test

The ANOVA test was performed to evaluate the effects of the three investigated factors on the specific energy and the results are presented in Table 7.10. It was found that for the specific energy, both weight-on-bit and rock type have shown significant influences. The F-value of weight-on-bit was 5.07 and showed the greatest effect. The F-value of rock type was 3.87 and thus its effect was also statistically significant. The rotational speed, with an F-value of 1.61, did not show a significant effect on the specific energy.

It was discussed in Chapter 2 that the cutting efficiency of a diamond drill may

Table 7.10 Result of ANOVA Test of Specific Energy

Variable	df	SS	MSS	F-value
W	5	8.10×10^{8}	1.62×10^{8}	5.07
N	5	2.56×10^{8}	5.13×10^{7}	1.61
RT	5	6.18×10^{8}	1.24×10^{8}	3.87
Error	20	6.38×10^{8}	3.19×10^{7}	

df: Degree of freedom

SS: Sum of square

MSS: Mean sum of square

W: Weight-on-bit, N

N: Rotational speed, rpm

RT: Rock type

$F_{(\alpha=0.05)}=2.71$

be affected by the rotational speed in some cases. This hypothesis could be verified by checking the significance of the rotational speed on the specific energy. The insignificant effect of the rotational speed on the specific energy, found in the ANOVA test, indicated that the specific energy was not a function of the rotational speed. It was thus concluded that in the ranges of bit weight and speed used in this test the cutting efficiency of a diamond bit did not depend on the rotational speed. However, the conclusion may not be valid should the weight and speed fall beyond the ranges studied in this work.

7.4.2 Newman-Keuls Test

7.4.2.1 Weight-on-bit

The Newman-Keuls test was performed for the weight-on-bit as related to the specific energy. First all the specific energy measurements in this test were averaged according to each weight-on-bit regardless of the influences of rock type. The smallest average specific energy was found at a weight-on-bit of 2,668.8 Newtons (600 lb), and the largest average specific energy was at 889.6 Newtons (200 lb) weight-on-bit. The means of the specific energy were arranged in descending order:

$$SE_W(200) > SE_W(300) > SE_W(400) > SE_W(450) > SE_W(500) > SE_W(600)$$

or

$$15375 > 4855 > 3839 > 3302 > 2155 > 1122\ (MJ/m^3)$$

Results of the Newman-Keuls test are presented in Table 7.11. By comparing the mean differences with the least significant values, it was found that the six bit weights

Table 7.11 Newman-Keuls Test for Weight-on-Bit on Specific Energy

No. of mean spanned	6	5	4	3	2
Least signifcant value (MJ/m^3)	7,609	7,494	7,332	7,148	6,802
Mean differences of the average specific energy (MJ/m^3)	14,253	13,220 3,733	12,073 2,700 2,717	11,536 1,553 1,684 2,180	10,520 1,016 537 1,147 1,033

could be categorized into two groups. The first group had weight-on-bit less than 300 lb, at which the specific energy was higher. The second group was at weight-on-bit larger than 300 lb. In this group of weight-on-bit values, the specific energy was substantially smaller than it was in the first group. The specific energy differences among each group were statistically insignificant, and were significant between two groups.

Observation of six means of the specific energy revealed that at an 889.6 Newtons (200 lb) weight-on-bit, the specific energy was at a magnitude of 10^4 MJ/m^3, as compared to the magnitude of 10^3 MJ/m^3 at the weight-on-bit from 1,334.4 to 2,668.8 Newtons (300 to 600 lb). It was obviously that at the 889.6 Newtons (200 lb) weight-on-bit, the cutting was not efficient.

It has long been recognized by drill operators and practicing engineers that the weight-on-bit is the most important factor in a drilling operation. Statistical analyses in this study also revealed that it was the most influential among the three factors tested in this drilling experiment. This is because the imbedding of diamonds into the rock surface is the prerequisite for effective diamond drilling. When the weigh-on-bit was less than 1,334.4 Newtons (300 lb), the penetration rate was very small. For example, at the 889.6 Newtons (200 lb) weight-on-bit, the average penetration rate was only 17.48% of the average penetration rate at the 2,668.8 Newtons (600 lb) weight-on-bit. Meanwhile, the average applied torque at the 889.6 Newtons (200 lb) weight-on-bit was 8.534 Nm, compared to 14.493 Nm at the 2,668.8 Newtons (600 lb) weight-on-bit. The energy consumed as friction became substantially high at a low weight-on-bit, and this required a significant increase of the specific energy. In this drilling test, the average specific

energy at 889.6 Newtons (200 lb) bit weight was 13.7 times as much as it was at 2,668.8 Newtons (600 lb) bit weight for the six rocks.

7.4.2.2 Rock Type

When the similar procedures were performed for relationship between rock type and the specific energy, it was found that rock B consumed the largest energy, and rock D consumed the least. The descending order of means of specific energy is:

$$SE(B) > SE(F) > SE(A) > SE(C) > SE(E) > SE(D)$$

or

$$11,633 > 10,038 > 3522 > 2676 > 1491 > 1288 \ (MJ/m^3)$$

Result of the Newman-Keuls test is tabulated in Table 7.12. By comparing the differences of mean specific energy with the corresponding critical values, it was found that the six rocks could be divided into two groups. One group included rocks B and F, which corresponded to the higher specific energy; while the other group included rocks A, C, D, and E and corresponded to the lower specific energy values.

7.4.3 Regression Analysis

7.4.3.1 Weight-on-bit

The specific energy was averaged according to six bit weights and plotted against weight-on-bit in Figure 7.6. The GLM and NLIN regression techniques were performed to correlate the specific energy with weight-on-bit, regardless of the effects of the rock type.

Table 7.12 Newman-Keuls Test for Rock Type on Specific Energy

No. of mean spanned	6	5	4	3	2
Least signifcant value (MJ/m^3)	7,609	7,494	7,332	7,148	6,802
Mean differences of the average specific energy (MJ/m^3)	10,345	10,142 8,750	8,957 8,547 2,234	8,111 7,362 2,031 1,388	1,595 6,516 846 1,185 203

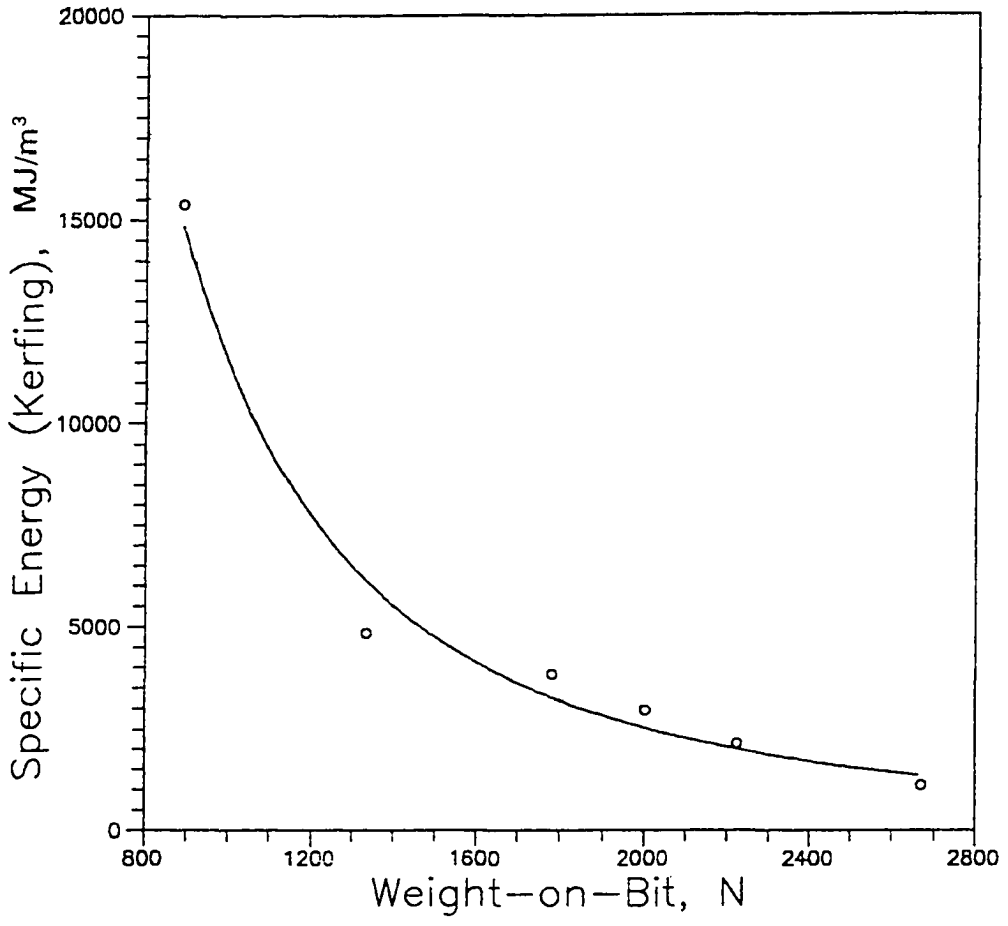

Figure 7.6: Specific energy (kerfing) vs. weight-on-bit in the Latin square drilling test

An inversed power equation was found to best fit the experimental data:

$$SE_k = 3.94 \times 10^{10} W^{-2.18} \qquad (7.8)$$

where SE_k is specific energy (kerfing) in MJ/m^3, and W is weight-on-bit in Newton.

7.4.3.2 Rock Type

The GLM and NLIN statistical analyses were performed on the specific energy with the uniaxial compressive strength of rock. An exponential equation was found to best present the experimental results. The equation is:

$$SE_k = 414.309 e^{0.0183\sigma_c} \qquad (7.9)$$

where σ_c is the uniaxial compressive strength in MPa. This relationship is also graphically illustrated in Figure 7.7.

7.4.3.3 Multi-variable Regression Analysis

The GLM and stepwise multi-variable regression procedures were performed to formulated the relationship between the specific energy and the influential factors. Again, the number of parameters used in the analysis were the same as those for the penetration rate and applied torque. Table 7.13 summarizes the results. The quadratic GLM model contained ten items, having a R^2 of 0.84 and F-value of 13.24. By backward eliminating, the stepwise statistical analysis generated an equation with seven parameters. The R^2 of the stepwise model (0.83) was slightly lower than it was for the quadratic GLM model. It had, however, a higher F-value (19.59) and higher *degrees of freedom for error*, and

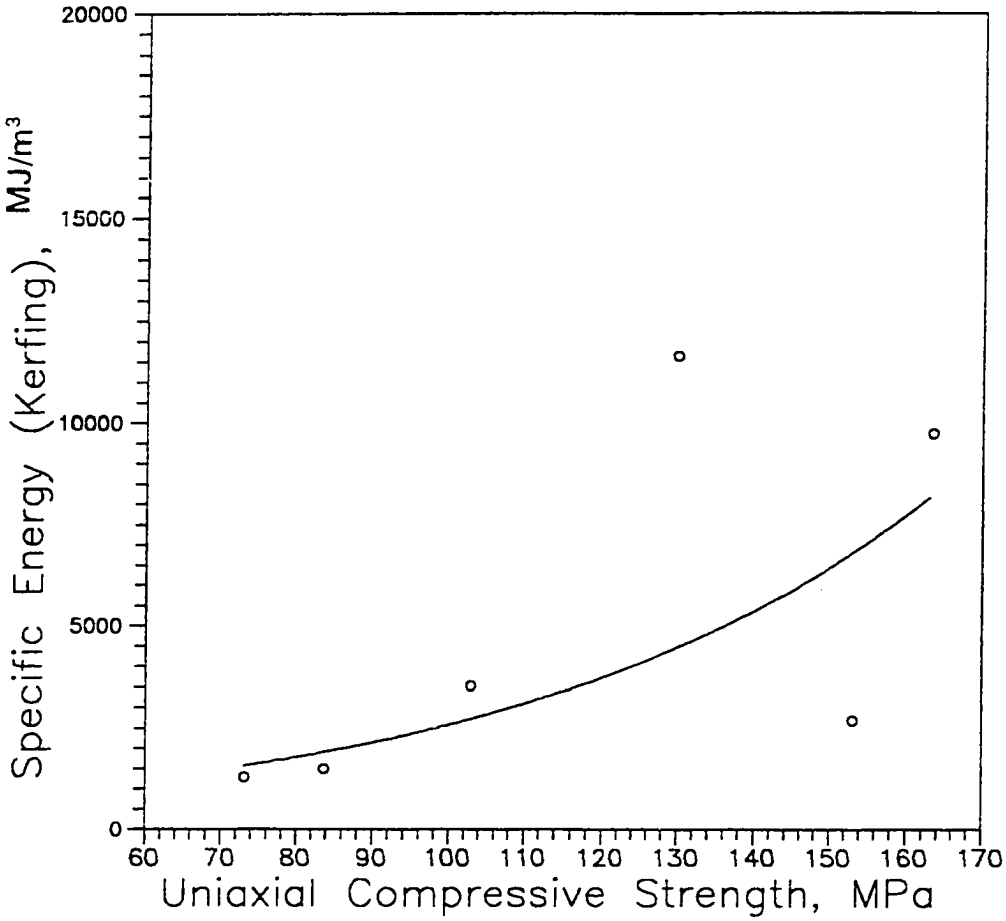

Figure 7.7: Specific energy (kerfing) vs. uniaxial compressive strength in the Latin square drilling test

Table 7.13: Summary of regression analysis for specific energy in Latin square drilling test

	GLM			Stepwise		
Factor	Coefficient	F	Pr>F	Cofficient	F	Pr>F
Intercept	-25606.307	n/a	n/a	-13515.742	0.82	0.3742
W	-2.046	41.36	0.0001			
N	87.142	6.87	0.0147	26.826	1.82	0.1877
UCS	440.063	33.17	0.0001	363.271	2.51	0.1241
W*W	0.132	9.49	0.0050	0.113	26.91	0.0001
N*N	-0.046	1.32	0.2613			
UCS*UCS	1.735	4.45	0.0451	1.823	4.88	0.0355
W*N	-0.049	1.26	0.2730			
W*UCS	-1.597	31.61	0.0001	-1.501	44.09	0.0001
N*UCS	-0.908	1.98	0.1714	-0.720	10.46	0.0031
W*N*UCS	0.002	0.86	0.3614	0.001	12.05	0.0017

W: Weight-on-bit, N
N: Rotational speed, rpm
UCS: Uniaxial compressive strength, MPa

was thus chosen to predict the specific energy. The equation is:

$$SE_K = -13515.742 + 26.826N + 363.271\sigma_c + 0.113W^2 + 1.823\sigma_c^2 - 1.501W\sigma_c - 0.720N\sigma_c + 0.001WN\sigma_c \quad (7.10)$$

where:

T is the applied torque in Nm,

W is the weight-on-bit in Newton,

N is the rotational speed in rpm, and

σ_c is the uniaxial compressive strength in MPa.

7.5 CHAPTER SUMMARY

1. The weight-on-bit usually was the most influential factor among the three parameters investigated (i.e., weight-on-bit, rotational speed, and rock type).
2. The rotational speed affected the penetration rate significantly, but had no effects on the applied torque and specific energy.
3. A higher penetration rate could be obtained by increasing weight-on-bit and rotational speed.
4. A higher weight-on-bit was corresponding to a higher torque.
5. The specific energy increased substantially as the weight-on-bit decreased.

CHAPTER 8

DRILLING PERFORMANCE PREDICTION AND ENGINEERING APPLICATIONS

8.1 PENETRATION RATE

Theoretical drilling models were developed in Chapter 2 assuming several different rock failure mechanics. Those models included: 1) Plastic deformation model (Equation 2.24), 2) Compressive crushing model (Elastic, Equation 2.25), 3) Fracture mechanics model without consideration of cutter spacing (Fracture 1, Equation 2.30), and 4) Fracture mechanics model with consideration of cutter spacing (Fracture 2, Equation 2.33).

It was noted that geometry constants were involved in those models, i.e., η in the plastic and elastic models and α_1 and α_2 in the fracture models. These geometry constants can only be determined from experiment. In this study, those geometry constants were calculated based on the data of the BQ1 bit. Table 8.1 presents the result. Those geometry constants were used in the theoretical equations to predict the penetration rate for another surface-set diamond bit, i.e., the AQ1 bit. The results are graphically presented in Figure 8.1. It was noted that the fracture model with consideration of cutter spacing (fracture model 2) predicted a better result than the fracture model without consideration of cutter spacing (fracture model 1). None of the two models, however, made a better prediction of the penetration rate than did the plastic and elastic models. Of the four models, the elastic model gave the best result.

Table 8.1: Geometry constants for the theoretical drilling models for BQ1 bit

Model	Plastic	Elastic	Fracture 1	Fracture 2
η	0.0135	0.1665	n/a	n/a
α_1	n/a	n/a	1.6×10^{-6}	17.36
α_2	n/a	n/a	n/a	17.36

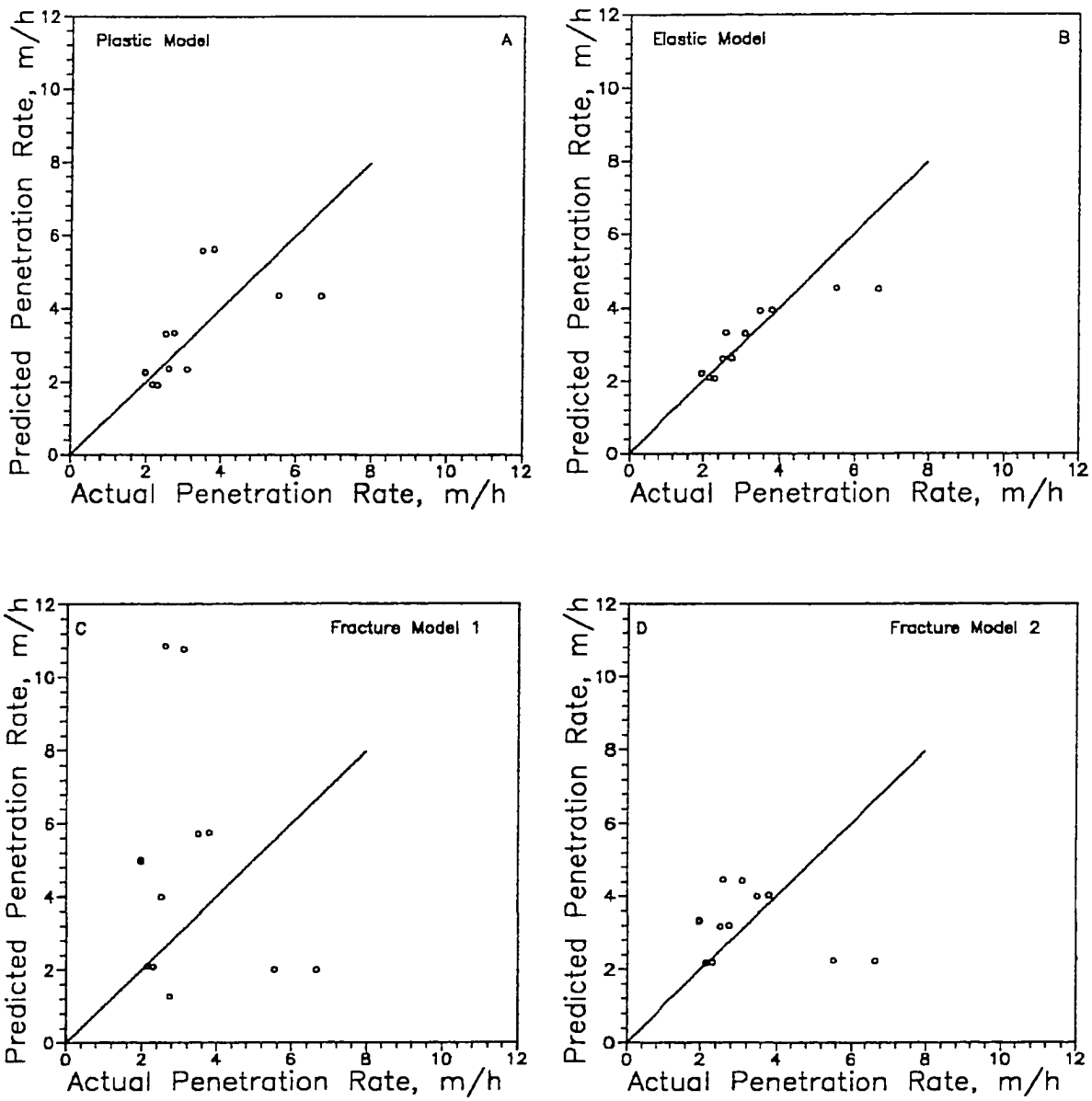

Figure 8.1: Penetration rate predicted by theoretical models vs. actual experimental data: (A) Plastic model, (B) Elastic model, (C) Fracture model 1 -- without consideration of cutter spacing, and (D) Fracture model 2 -- with consideration of cutter spacing

8.2 WEIGHT-ON-BIT

An effective cutting action of a diamond core drill on rock requires that the diamonds penetrate into the rock surface first, then shear or crack the rock in front of the diamonds and remove the chips away. To have a good penetration rate, there should be enough normal force acting on the rock surface by diamonds. If the normal stress under the diamond cutters is low, the diamond tip can only partially penetrate into rock surface. However, it cannot penetrate into rock surface at all when the diamond is worn out. In this case, the drilling operation is not taking the full advantage of the diamond cutters and the bit only slides across rock surface with little penetration.

On the other hand, stress under the diamonds cannot be so excessive that much of the pressure is acting on the bit matrix. This will result in a large friction between rock surface and bit matrix, which does not contribute to rock cutting and chips removal. It can also cause excessive heat and subsequently a quick bit wear. From the standpoint of a drill operator, there must be an optimum weight for each specific bit in a given environment. This optimum weight-on-bit is called *Maximum Effective Weight* (W_{eff}) in this study. Theoretically, this weight-on-bit occurs when all the diamonds are penetrated into rock surface, and the matrix of the bit just comes in contact with the formation.

There are many difficulties related to the determination of the Maximum Effective Weight. First, stress concentrations under diamond tips may occur. This stress concentration will cause a highly localized stress in the immediate region below the rock surface. It may cause plastic deformation or a crack in some very small area. Secondly, the actual normal force is not uniformly distributed among all diamonds of the bit. This

may cause different stress distribution under the tips of diamonds. Thirdly, the failure process of the rock below the contact points is not clear and is difficult to observe directly.

To simplify the problem, the following assumptions are made: 1) Diamonds protruded from the matrix are in the shape of a cone; 2) The diamonds in a bit are uniformly distributed in the cross-section of the cutting head; and 3) Weight-on-bit is uniformly distributed to each diamond particle. The models examined included: 1) Plastic model; 2) Elastic model (compressive crushing); 3) Fracture model 1 (without consideration of cutter spacing); and 4) Fracture model 2 (with consideration of cutter spacing).

The Maximum Effective Weight-on-bit predicted the four models in this study are presented in Figure 8.2. It was noted that the compressive crushing theory (elastic) predicted the highest W_{eff}, and it was the next highest from the plastic deformation theory. The results predicted by the two fracture theories were the smallest. However, results from the plastic deformation theory and the two fracture theories were very close.

Figure 8.3 shows the normalized penetration rate versus weight-on-bit for the BQ1 bit on granite rocks. The data in circles were from Longyear Company (1991). It was noted that when the weight-on-bit was lower than about 4,448 Newtons (1,000 lb), the penetration rate increased almost linearly with weight-on-bit, and it did not increase much beyond that bit weight. This result was very close to the W_{eff} predicted by the plastic deformation theory and the fracture models.

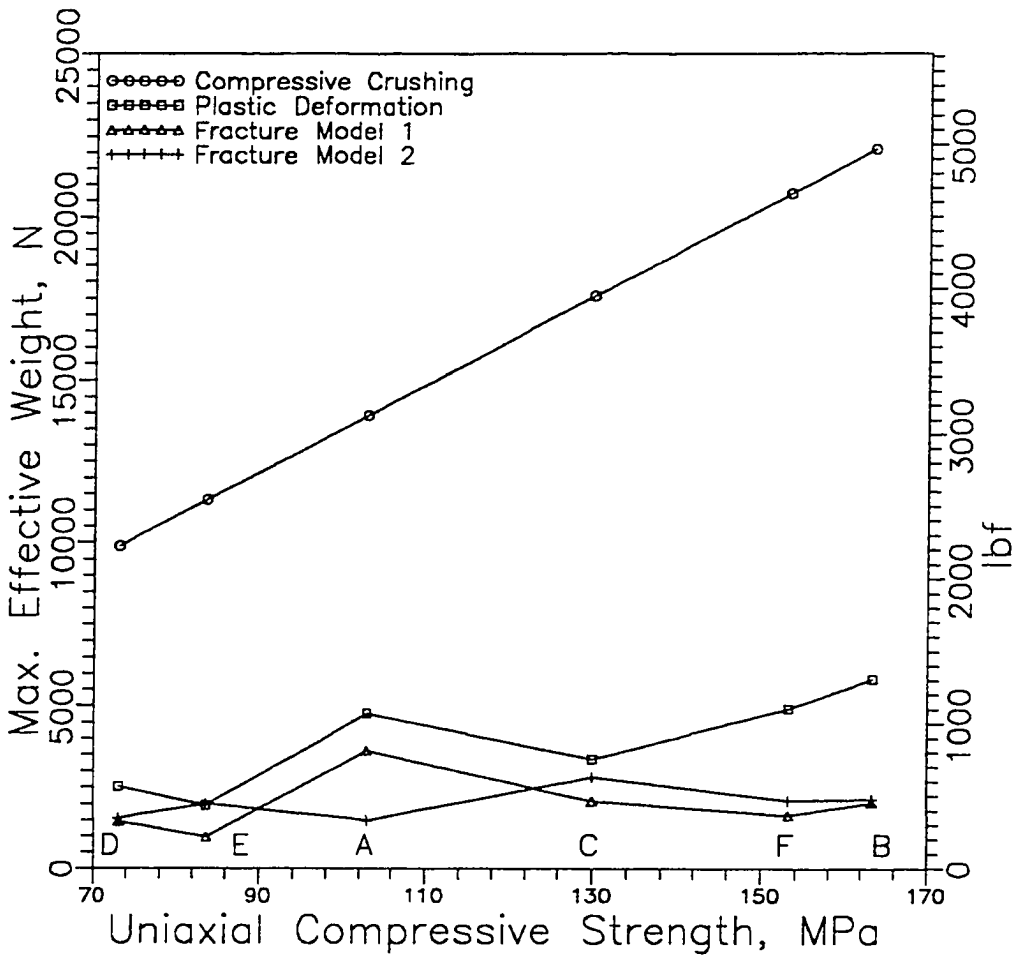

Figure 8.2: Maximum effective weight-on-bit vs. uniaxial compressive strength of rock

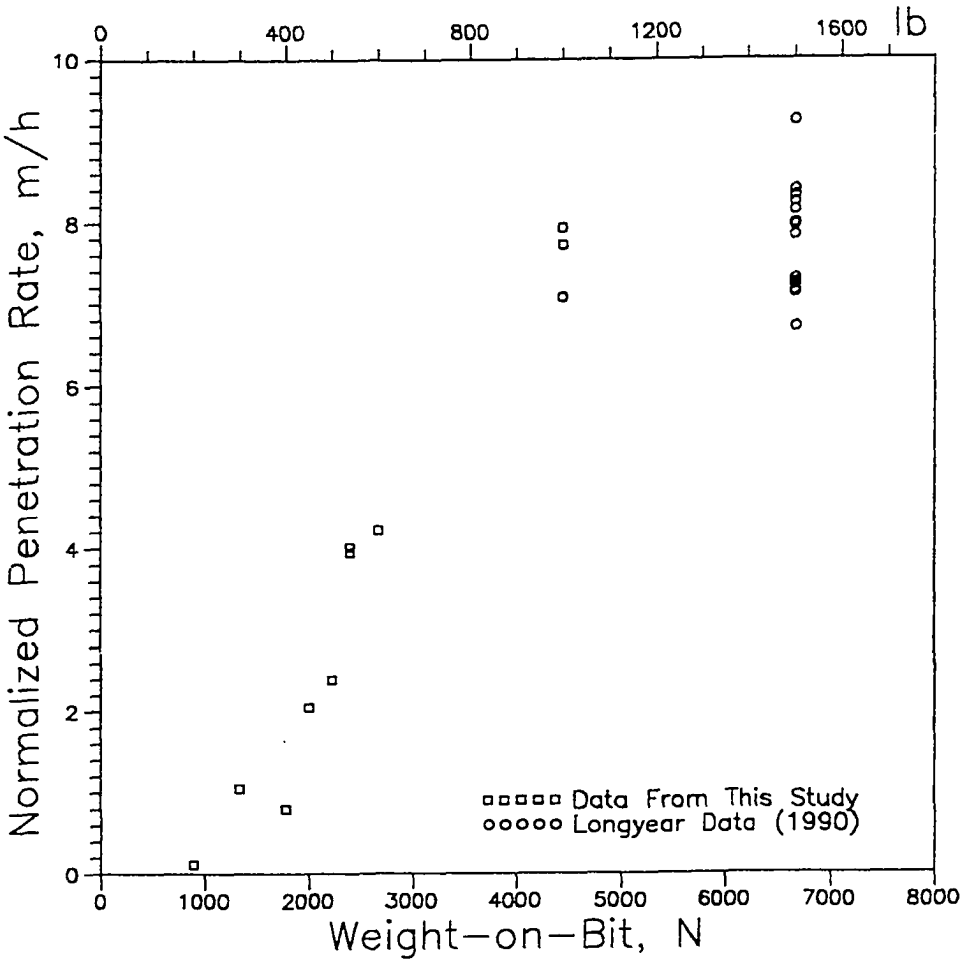

Figure 8.3: Normalized penetration rate vs. weight-on-bit for BQ1 bit on granite rock

8.3 ROTATIONAL SPEED

Usually the higher rotational speed will increase the penetration rate. However, the linear relationship between the penetration rate and rotational speed may not be true for all speeds. Higher speed is not always advantageous especially in hard rocks due to two major reasons. The first reason is that there must be sufficient time for each diamond to actually imbed into the rock surface, to penetrate and to chip away rock fragments by lateral force. The second reason is that a fast rotation will create shock loads and seriously damage the bit and drill string. These physical phenomena also impose an upper limit on the rotational speed in drilling practice.

The rotational speed is not only limited by the above physical and mechanical conditions, but also is limited by the available power and weight-on-bit. This rotational speed is the maximum possible speed a drill can achieve. For the BQ1 bit, this speed can be estimated by the following equation (Huang and Wang, 1992):

$$N=\frac{60\eta P}{W(0.756-0.187\log\sigma_c+\frac{1.42\times10^5}{W^2})r} \qquad (8.1)$$

where:

N is the rotational speed, rpm,

η is the power transfer efficiency to bit,

P is the available power for drilling, Watt,

W is the weight-on-bit, Newton,

σ_c is the uniaxial compressive strength of rock, MPa, and

r is the radius of the core bit, meter.

Figure 8.4 graphically illustrates this equation at η=80% for the BQ1 bit. It was found from the curves that at a constant weight exerted on a rock, higher speed can be obtained if the strength or hardness of the rock is higher.

8.4 GREENLAND UNDER ICE SHEET BEDROCK CORING

The Greenland Ice Sheet Program Two (GISP2) was an ice coring project conducted by the Polar Ice Coring Office (PICO) at the University of Alaska Fairbanks, under the contract of the National Science Foundation, Division of Polar Programs. It started in the 1989 summer season, and in the subsequent five seasons, drilling penetrated and cored the 3,051 meters of ice and reached the bedrock. Shortly after, it penetrated into the bedrock and produced 1.55 meters rock cores, the first pieces of rock ever obtained from underneath the continental ice sheet.

The GISP2 site was located at 72.58° North latitude, 38.48° West longitude and at an elevation of 3,207 m. The mean annual temperature at GISP2 is -31°C, and it often goes below -15°C during summer.

The drill used to recover the GISP2 ice core was developed by PICO at the University of Alaska Fairbanks. It was a cable-suspended electrical-mechanical drill. This drill was capable of retrieving continuous ice cores 13.2 cm (5.2 in) in diameter and 6 m (19.7 ft) long. It was designed to work in borehole filled with n-butyl acetate liquid, which has minimal health and environmental risks. The entire drill and core handling

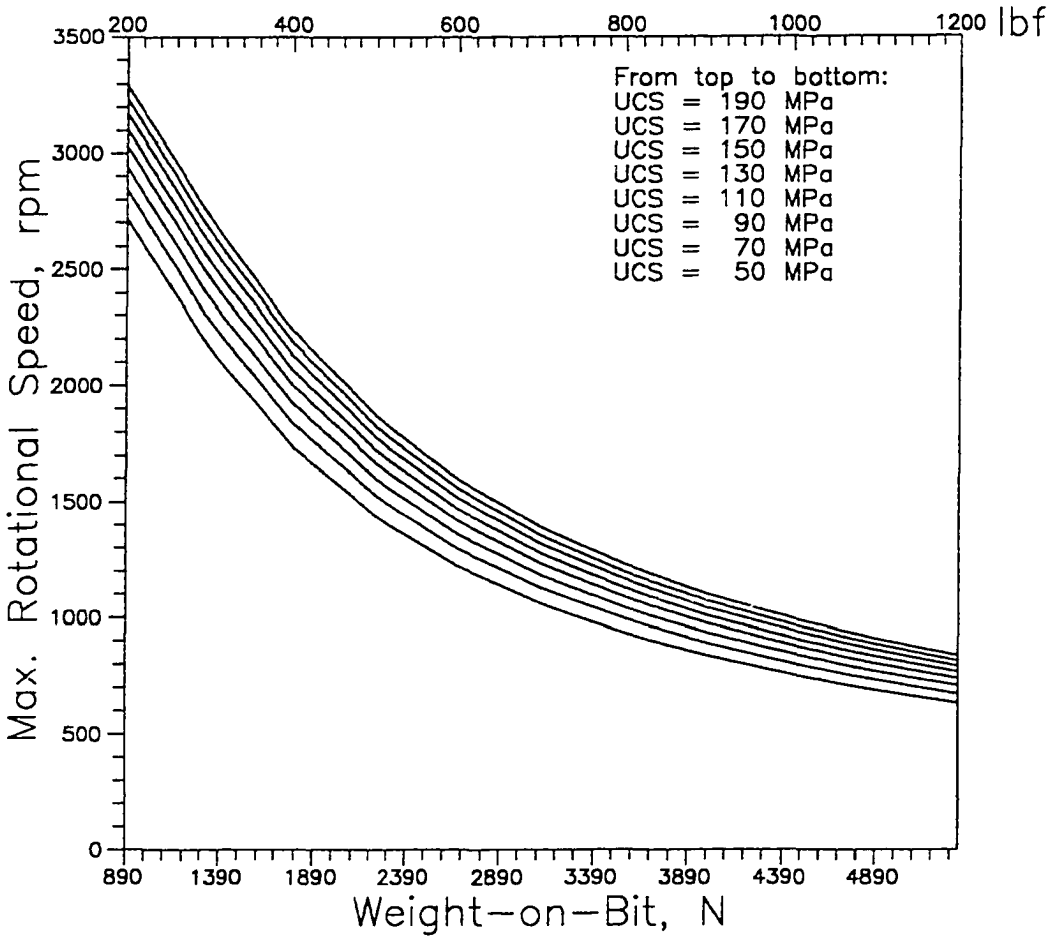

Figure 8.4: Maximum rotational speed vs. weight-on-bit for BQ1 bit

system were housed inside a 17 m diameter geodesic dome. This consisted of, among other things, a 33 m high twin tower assembly, a carousel drill handling system, fluid handling and recovery systems, a ventilation system, as well as a core-handling line where the ice cores were extracted and logged. Also installed was 77 m of the 25-cm diameter drill casing.

The drilling operation was controlled by a control panel along with an instrument package installed in the drill. The instrument package in the drill monitored sixteen parameters (e.g., weight, pressure, temperature, inclination, azimuth, rotational speed, current). It transmitted these data to the control panel which provided a digital readout of the measured parameters and depth. It also provided controlling of the speed and direction of the drill motor.

To drill and retrieve bedrock cores, a diamond core bit, Christensen thinkerf surface-set diamond bit was attached to the bottom of the drill when it reached the surface of bedrock. This bit was a surface-set diamond core bit, with only one diamond profile. The inner and outer diameters of this bit were 3.348 and 4.826 cm (1.318 and 1.900 in), respectively.

The data obtained from this rock coring were very limited due to the relatively short core length. During a continuous running period of 43 minutes, a depth of 1.8 meters rock was penetrated. Therefore, the penetration rate was 2.512 m/h. Table 8.2 summaries some of the parameters of this rock coring.

The drill unit plus cable weighed 5,160 Newtons (1,160 lb) in air, 3,736 Newtons (840 lb) in n-butyl acetates. The core breaking force of the rock was 7,117 Newtons

Table 8.2: Summary of drilling parameters of the GISP2 bedrock coring

Time	Depth (m)	Rotational speed (rpm)	Weight-of-Cable (lb)
10:30am	3051.4	650	690
	3052.7	540	430
11:13am	3053.2	472	338

(1,600 lb) in n-butyl acetate. Therefore, the true core break force was 3,380 Newtons (760 lb). The tensile strength of the Greenland bedrock at GISP2 was thus calculated as 557 psi (3.84 MPa). The uniaxial compressive strength of this rock estimated by Equation 5.5 was 49 MPa.

The weight-on-bit in this Greenland ice and rock coring was exerted by gravity acting on the drill unit. To control the weight-on-bit during coring, a tension force was exerted on the cable. At the beginning of rock coring (at the depth of 3,051.4 m), the weight-of-cable was 3,069 Newtons (690 lb). It reduced to 1,913 Newtons (430 lb) at the depth of 3,052.7 m, and further reduced to 1,503 Newtons (338 lb) at the depth of 3,053.2 m before the coring stopped. Meanwhile, the rotational speed started at 650 rpm. It decreased to 540 rpm at the depth of 3,052.7 m when the actual weight-on-bit increased, and further decreased to 472 rpm at the depth of 3,053.2 m. The average weight-on-bit and rotational speed during this drilling period were 1,575 Newtons (354 lb) and 554 rpm, respectively.

Based on the weight-on-bit, rotational speed, and uniaxial compressive strength of rock, the penetration rate was calculated by Equation 7.4. The result was 2.339 m/h, or 6.9% lower than the actual value (2.512 m/h).

Since the cross-section areas of the BQ1 bit and the Christensen thinkerf bit were different, the load density (weight-on-bit divided by cross-section area of the bit) on the two bits were different when a same magnitude of load was exerted on them. This difference can be compensated by substituting the weight-on-bit in Equation 7.4 with the load density. The predicted penetration rate was 2.742 m/h. This is 9.2% higher than the

actual value.

8.5 CONCLUSIONS

Several conclusions were drawn from above discussions:

1. The geometry constants involved in the theoretical drilling models were determined from experiment. The models developed from one bit could be used to predict drilling performance of another similar bit.
2. The fracture model with consideration of cutter spacing (fracture model 2) predicted a better result than the fracture model without consideration of cutter spacing (fracture model 1). Neither of the two models, however, made a better prediction of the penetration rate than did the plastic and elastic models. Of the four models, the elastic model gave the best result.
3. The maximum effective weight-on-bit (W_{eff}) was predicted by assuming different failure conditions of rock. The W_{eff} predicted by the elastic model (compressive crushing) was much higher than those predicted by other theories (i.e., plastic deformation, fracture mechanics). The W_{eff} predicted by the plastic theory and the two fracture models were close to each other and agreeable with the experimental observation.
4. Statistical drilling equation was used to predict penetration rate in Greenland under ice sheet bedrock coring. The variation between the predicted value and the experimental value was less than 10%.

BIBLIOGRAPHY

Alpan, H. S. (1950): Factors affecting the speed of penetration of bits in electric rotary drilling. *Trans. Inst. Min. Eng.*, v. 109, p.1119.

Barrett, J. L. (1962): Drilling research develops low-cost diamond bit. *Eng. and Min. J.*, v.163(5), May 1962, p.87-92.

Brook, N. (1985): The equivalent core diameter method of size and shape correction in point load testing. *Int. J. Rock Mech. Min. Sci. & Geotech. Abstr.*, v.22(2), 61-70.

Brook, N. (1977): The use of irregular specimens for rock strength tests. *Int. J. Rock Mech. Min. Sci. & Geotech. Abstr.*, v.14, 193-202.

Cargill, J. S. and Shakoor A. (1990): Evaluation of empirical methods for measuring the uniaxial compressive strength of rock. *Int. J. Rock Mech. Min. Sci. & Geotech. Abstr.*, v.27(6), 495-503.

Cheatham, J. B. and Gnirk, P. F. (1967): The mechanics of rock failure associated with drilling at depth. Proc. 8th Symp. on Rock Mechanics: In Failure and Breakage of Rock. University of Minnesota, C. Fairhurst (ed), 1967, 410-439.

Cherepanov, A. G. and Cherepanov, G. P. (1990): Cutting Resistance of Rocks. *Problemy Prochnosti*, No. 11, 57-72, Nov. 1990 (in Russian).

Clark, B. G. (1979): Principles of Rock Drilling. *Colorado School of Mines Quarterly*, v.79(2).

Davies, O. L. (1979): *The design and analysis of industrial experiments.* (Ed.), Longman

Group.

DeLucia, F. (1984): How diamond bits/system hydraulics affect downhole-motor drilling. *Oil and Gas Journal*, April 16, 1984. p.71-76.

Draper, N. R. and Smith, H. (1980): *Applied Regression Analysis*. 2nd edition. John Wiley & Sons, Inc.

Duklet, C. P. and Bates, T. R. (1981): Predicting diamond bit drilling rates. *World Oil*, v.192, April 1981, p.127-135.

Eronini, I. E. (1982): On dynamic fracture of rock under bit impact loads. *Trans. of ASME Journal of Energy Resource Technology*, 104(2), p.105-107.

Eronini, L. E., Somerton, W. H., and Auslander, D. M. (1982): A dynamic model for rotary rock drilling. Transactions of the ASME, Journal of Energy Resources Technology, v.104(2), p.108-120.

Evans, I. (1984): A theory of the cutting force for point attack picks. *Int. J. Min. Engng.*, v.2, p.63-71.

Evans, I. and Pomeroy, C. D. (1966): *The Strength, Fracture, and Workability of Coal*. Pergamon Press, London.

Fish, B. G. (1961): The basic variables in rotary drilling. Mine & Quarry Eng., January 1961, p. 29-34.

Fisher, R. A. (1990): *Statistical Methods, Experimental Design, and Scientific Interence*. A Re-issue of *Statistical Methods for Research Workers*, *The Design of Experiments*, and *Scientific Inference*. Edited by J. H. Bennett. Oxford University

Press.

Fivehouse, D. (1976): *The Diamond Drilling Industry*. Hancock House Publishers, Canada.

Göktan, R. M. (1991): Brittleness and micro-scale rock cutting efficiency. *Mining Science and Technology*, v.13, 237-241.

Göktan, R. M. (1990): Effects of cutting pick rake angle on the failure pattern of high-strength rocks. *Mining Science and Technology*, v.11, 281-285.

Goodrich, R. H. (1956): *High pressure rotary drilling machines*. Bull. Tech., Ser. 94, p.25-45.

Gyss, E. E. and Davis, H. G. (1927): The hardness and toughness of rocks. *AIME: Min. and Met.*, June 1927, p.261-266.

Harley, G. T. (1926): Proposed ground classification for mining purposes. Eng. and Min. J., v.122, no.11, p.413-416.

Hartman, H. L. (1962): Crater geometry relations in percussive drilling. *Mine and Quarry Eng.*, Dec. 1962, p.530-536.

Head, A. L. (1951): A drillability classification of geological formations. *World Oil*, Oct. 1951, pp.125-138.

Hibbs, Jr., L. E. and Sogoian, G. C. (1983): *Wear Mechanisms for Polycrystalline Diamond Compacts as Utilized for Drilling in Geothermal Environments-Final Report*. SAND82-7213.

Hoek, E. and Bray, J. W. (1981): *Rock Slope Engineering*. 3rd Ed., The Institution of

Mining and Metallury, Lodon.

Hoover, E. R. and Middleton, J. N. (1981): Laboratory evaluation of PDC drill bits under high-speed and high-wear conditions. *Journal of Petroleum Technology*, 33, p.2316-2321.

Hough, Jr., C. L. (1986): The effects of back rake angle on the performance of small-diameter polycrystalline diamond rock bits: ANOVA tests. *ASME Journal of Energy Resource Technology*. 108(4), p.305-309.

Hough, Jr., C. L., Das, B., and Rozgonyi, T. G. (1986): Life models for small- diameter polycrystalline diamond compact bits in hard abrasive media. *ASME Journal of Energy Resource Technology*, 108(4), p.310-314.

Howarth, D. F. (1986): Review of rock drillability and borability assessment methods. *Trans. Instn. Min. Metall. (Sect. A: Min. Industry)*. v.95.

Hucka, V. J. and Das, B. M. (1974): Brittleness determination of rocks by different methods. *Int. J. Rock Mech. Min. Sci.*, v.1, 389-392.

ISRM (Int. Soc. for Rock Mech.), Comm. on Testing Meths. (1985): Suggested Method for Determining Point Load Strength. *Int. J. Rock Mech. Min. Sci. & Geotech. Abstr.* v.22(2), 51-60.

ISRM (Int. Soc. for Rock Mech.), Comm. on Testing Meths. (1977): *Suggested Method for Determining Hardness and Abrasiveness of Rocks*. Committee on Laboratory Tests, Document No. 5.

Jaeger, J. C. and Cook, N. G. W. (1976): *Fundamentals of Rock Mechanics*. John Wiley

& Sons, Inc.

Karasawa, H. and Misawa, S. (1992): Development of new PDC bits for drilling of geothermal wells-Part I: laboratory testing. *ASME Journal of Energy Resource Technology*, 114(4), p.323-331.

Karasawa, H. and Misawa, S. (1992): Development of new PDC bits for drilling of geothermal wells-Part II: field testing. *ASME Journal of Energy Resource Technology*, 114(4), p.332-338.

Karfakis, M. G. and Heins, R. W. (1986): Laboratory investigation of bit bearing temperatures in rotary drilling. *ASME Journal of Energy Resource Technology*, 108(3), p.221-227.

Karpuz, C., Pasamehmetoglu, A. G., Dincer, T. and Muftupglu, Y. (1990): Drillability studies on the rotary blasthole drilling of lignite overburden series. *Int. J. Surface Min. & Reclamation* 4(2), 89-93.

Kinoshita, S. (1956): Studies on drillability of rocks by rotary drills. *Inst. Min. of Japan*, 1956, p.43-48.

Kragelskii, I. V. (1965): *Friction and Wear.* Butterworth and Co., Ltd., Lodon, 1965.

Lawn, B. R. and Swain, M. V. (1975): Review-indentation fracture: principles and applications. *J. Material Sciences*, v. 10, 1049-1081.

Long, A. E. (1960): *A Glossary of the Diamond-Drilling Industry*. BuMines Bull. 583.

Longyear Company (1990): *Drilling Test Report*, unpublished.

Ma, D. and Azar, J. J. (1986): A study of rock-bit interaction and wellbore deviation.

ASME Journal of Energy Resource Technology, 108(3), p.228-233.

Ma, D. and Azar, J. J. (1985): Dynamics of roller cone bits. *ASME Journal of Energy Resource Technology*, 107(4), p.543-548.

Mellor, M. *(1976): Mechanics of cutting and boring.* Part II: Kinematics of axial rotation mechines. CRREL Report 76-16.

Moore, M. A. (1978): *Materials in Engineering Applications*, v. 1, 97-111.

Moorhouse, W. W. (1959): *The Study of Rocks in Thin Section.* Happer & Row Publishers.

Mott, B. W. (1956): *Micro-indentation Hardness Testing.* Butterworth and Co., Ltd., Lodon, 1956.

Nishimatsu, Y. (1972): The mechanics of rock cutting. *Int. J. Rock Mech. Min. Sci.* v.9, p.261-270.

Ouchterlony, F. (1974): Fracture mechanics applied to rock blasting. *Proc. 3rd Congr. ISRM*, Denver, v. 2, 1377-1383.

Ozdemir, L. Miller, R., and Wang, F. D. (1977): Mechanical tunnel boring prediction and machine design. Annual Report. NSF IRA-770199, Colorado School of Mines, Golden.

Paone, J. and Madson, D. (1966): Drillability studies-impregnated diamond bits. *Rep. Invest. U.S. Bur. Mines 6776.*

Paone, J. and Bruce, W. E. (1963): Drillability studies-diamond drilling. Rep. Invest. U.S. Bur. Mines 6324.

Paone, J., Bruce, W. E., and Virciglio, P. R. (1966): Drillability studies-statistical regression analysis of diamond drilling. *Rep. Invest. U.S. Bur. Mines* 6880, 26p.

Pearse, G. (1985): Hydraulic rock drills. *Mining Mag.*, v.18, p.220-231.

Rinaldi, R. E., Koci, B. R. and Sonderup, J. M. (1990): *Evaluation of deep ice core drilling systems*. PICO TR-09-1.

Rostomyan, P. M. (1957): The process of rock penetration in drilling. *Heftyanoe Khoz.* No.7, p.9-13 (in Russian).

Roxborough, F. F. (1973): Cutting rock with picks. *Min. Eng.*, v.132, p.445-454.

Sanio, H. P. (1985): Prediction of the performance of disc cutters in anisotropic rock. *Int. J. Rock Mech. Min. Sci. & Geotech. Abstr.*, v.22(3), p.153-161.

Sasaki, K. N., Yamakado, N., Shiohara, F., and Tobe, M. (1962): Investigations of diamond core bit boring. *Ind. Diamond Rev.*, v.22, No.259, June 1962, p.178-186.

Shepherd, R. (1950): Physical properties and drillability of mine rocks. *Coll. Eng.*, Dec. 1950, pp.468-470.

Shimomura, Y. and Takato, A. (1958): Research on relations of physical properties of rocks and drilling rates of diamond bits. *Min. and Met. Inst. of Japan*, v.74, No. 844, Oct. 1958, p.852-860.

Simon, R. (1956): Theory of rock drilling. *Proc. 6th Ann. Drilling Symp.*, Univ. Minnesota, Minneapolis, 1956, pp. 1-14.

Sinkala, T. (1991): Relating drilling parameters at the bit-rock interface: theoretical and field studies. *Mining Science and Technology*, v.12, p.67-77.

Snowdon, R. A., Ryley, M. D., and Temporal, J. (1982): A study of disc cutting in selected British rocks. *Int. J. Rock Mech. Min. Sci.*, v.13, 311-319

Steel, R. G. D. and Torrie, J. H. (1980): *Principles and Procedures of Statistics--A Biometrical Approach*. 2nd edition. McGraw-Hill Book Company.

Tabor, D. (1951): *The Hardness of Metals*. Oxford, Clarendon Press.

Teale, R. (1965): The concept of specific energy in rock drilling. *Int. J. Rock Min. Sci.*, v.2(1), 57-73.

Tsoutrelis, C. E. (1969): Determination of the compressive strength of rock *in situ* or in test block using a diamond drill. *Int. J. Rock Mech. Min. Sci.*, v.6, 311-321.

Umez-Eronini, E. L. (1983): Rotary drill bit/rock model with cutter offset. *Trans. of the ASME Journal of Energy Resource Technology*. v.105(3), p.356-361.

Unger, H. F. and Fumanti, R. R. (1972): Percussive drilling with independent rotation. *U.S. Bur. Mines Rep. Invest*. No. 7692.

Whittaker, B. N. and Szwilski, A. B. (1973): Rock cutting by impact action. *Int. J. Rock Mech. Min. Sci. & Geotech. Abstr.*, v.9, p.659-671.

Wumkes, M. A. (1990): *Deep Drill Status Report*. PICO TR-90-2, 27p.

Zhao, X. L., Roegiers, J. C., and Passaris, E. K. S. (1994): Indentation fracture mechanics and rock disc cutting. *Proceedings of the 1st American Rock Mechanics*, at the University of Texas at Austin, June 1-3, 1994, 327-334.

Ziaja, M. B. (1982): Mathematical model of the diamond-bit drilling process and its practical application. SPE, p.911-922.

Appendix 1: F-distribution at $\alpha = 0.05$

	v1									
v2	1	2	3	4	5	6	7	8	9	10
1	161.40	199.50	215.70	224.60	230.20	234.00	236.80	238.90	240.50	241.90
2	18.51	19.00	19.16	19.25	19.30	19.33	19.35	19.37	19.38	19.40
3	10.13	9.55	9.28	9.12	9.01	8.94	8.89	8.85	8.81	8.79
4	7.71	6.94	6.59	6.39	6.26	6.16	6.09	6.04	6.00	5.96
5	6.61	5.79	5.41	5.19	5.05	4.95	4.88	4.82	4.77	4.74
6	5.99	5.14	4.76	4.53	4.39	4.28	4.21	4.15	4.10	4.06
7	5.59	4.74	4.35	4.12	3.97	3.87	3.79	3.73	3.68	3.64
8	5.32	4.46	4.07	3.84	3.69	3.58	3.50	3.44	3.39	3.35
9	5.12	4.26	3.86	3.63	3.48	3.37	3.29	3.23	3.18	3.14
10	4.96	4.10	3.71	3.48	3.33	3.22	3.14	3.07	3.02	2.98
11	4.84	3.98	3.59	3.36	3.20	3.09	3.01	2.95	2.90	2.85
12	4.75	3.89	3.49	3.26	3.11	3.00	2.91	2.85	2.80	2.75
13	4.67	3.81	3.41	3.18	3.03	2.92	2.83	2.77	2.71	2.67
14	4.60	3.74	3.34	3.11	2.96	2.85	2.76	2.70	2.65	2.60
15	4.54	3.68	3.29	3.06	2.90	2.79	2.71	2.64	2.59	2.54
16	4.49	3.63	3.24	3.01	2.85	2.74	2.66	2.59	2.54	2.49
17	4.45	3.59	3.20	2.96	2.81	2.70	2.61	2.55	2.49	2.45
18	4.41	3.55	3.16	2.93	2.77	2.66	2.58	2.51	2.46	2.41
19	4.38	3.52	3.13	2.90	2.74	2.63	2.54	2.48	2.42	2.38
20	4.35	3.49	3.10	2.87	2.71	2.60	2.51	2.45	2.39	2.35
21	4.32	3.47	3.07	2.84	2.68	2.57	2.49	2.42	2.37	2.32
22	4.30	3.44	3.05	2.82	2.66	2.55	2.46	2.40	2.34	2.30
23	4.28	3.42	3.03	2.80	2.64	2.53	2.44	2.37	2.32	2.27
24	4.26	3.40	3.01	2.78	2.62	2.51	2.42	2.36	2.30	2.25
25	4.24	3.39	2.99	2.76	2.60	2.49	2.40	2.34	2.28	2.24

Appendix 2: Newman-Keuls q-Values at $\alpha = 0.05$

	k								
df	2	3	4	5	6	7	8	9	10
1	18.00	27.00	32.80	37.10	40.40	43.10	45.40	47.40	49.10
2	6.09	8.33	9.80	10.90	11.70	12.40	13.00	13.50	14.00
3	4.50	5.91	6.83	7.50	8.04	8.48	8.85	9.18	9.46
4	3.93	5.04	5.76	6.29	6.71	7.05	7.35	7.60	7.83
5	3.64	4.60	5.22	5.67	6.03	6.33	6.58	6.80	7.00
6	3.46	4.34	4.90	5.30	5.63	5.90	6.12	6.32	6.49
7	3.34	4.17	4.68	5.06	5.36	5.61	5.82	6.00	6.16
8	3.26	4.04	4.53	4.88	5.17	5.40	5.60	5.77	5.92
9	3.20	3.95	4.42	4.76	5.02	5.24	5.43	5.60	5.74
10	3.15	3.88	4.33	4.65	4.91	5.12	5.31	5.46	5.60

Appendix 3
An example of data sheet from the 6-488B data acquisition system

BQ1 bit on rock E
00:00:01 08/23/92 STOP MODE

CH	CURRENT	UNITS
01	+0000.3	LB-FT
02	+00000	RPM
04	+0420.0	LBS
05	+03.861	INCHES

BQ1 bit on rock E
00:00:03 08/23/92 STOP MODE

CH	CURRENT	UNITS
01	+0007.8	LB-FT
02	+00205	RPM
04	+0765.0	LBS
05	+04.009	INCHES

BQ1 bit on rock E
00:00:05 08/23/92 STOP MODE

CH	CURRENT	UNITS
01	+0013.3	LB-FT
02	+00248	RPM
04	+1200.0	LBS
05	+04.070	INCHES

BQ1 bit on rock E
00:00:07 08/23/92 STOP MODE

CH	CURRENT	UNITS
01	+0018.4	LB-FT
02	+00502	RPM
04	+1368.0	LBS
05	+04.124	INCHES

BQ1 bit on rock E
00:00:09 08/23/92 STOP MODE

CH	CURRENT	UNITS
01	+0017.9	LB-FT
02	+00499	RPM
04	+1424.0	LBS
05	+04.251	INCHES

BQ1 bit on rock E
00:00:11 08/23/92 STOP MODE

CH	CURRENT	UNITS
01	+0024.4	LB-FT
02	+00501	RPM
04	+1496.0	LBS
05	+04.339	INCHES

BQ1 bit on rock E
00:00:13 08/23/92 STOP MODE

CH	CURRENT	UNITS
01	+0023.3	LB-FT
02	+00496	RPM
04	+1500.0	LBS
05	+04.460	INCHES

BQ1 bit on rock E
00:00:15 08/23/92 STOP MODE

CH	CURRENT	UNITS
01	+0021.9	LB-FT
02	+00499	RPM
04	+1480.0	LBS
05	+04.547	INCHES

BQ1 bit on rock E
00:00:17 08/23/92 STOP MODE

CH	CURRENT	UNITS

01	+0019.8	LB-FT
02	+00501	RPM
04	+1424.0	LBS
05	+04.635	INCHES

BQ1 bit on rock E
00:00:19 08/23/92 STOP MODE

CH	CURRENT	UNITS
01	+0016.9	LB-FT
02	+00501	RPM
04	+1496.0	LBS
05	+04.648	INCHES

BQ1 bit on rock E
00:00:21 08/23/92 STOP MODE

CH	CURRENT	UNITS
01	+0021.2	LB-FT
02	+00498	RPM
04	+01500.0	LBS
05	+04.662	INCHES

BQ1 bit on rock E
00:00:23 08/23/92 STOP MODE

CH	CURRENT	UNITS
01	+0022.4	LB-FT
02	+00500	RPM
04	+1504.0	LBS
05	+04.682	INCHES

BQ1 bit on rock E
00:00:25 08/23/92 STOP MODE

CH	CURRENT	UNITS
01	+0019.8	LB-FT
02	+00500	RPM
04	+1496.0	LBS

05 +04.709 INCHES

BQ1 bit on rock E
00:00:27 08/23/92 STOP MODE

CH	CURRENT	UNITS
01	+0021.6	LB-FT
02	+00498	RPM
04	+1488.0	LBS
05	+04.817	INCHES

BQ1 bit on rock E
00:00:29 08/23/92 STOP MODE

CH	CURRENT	UNITS
01	+0023.8	LB-FT
02	+00498	RPM
04	+1484.0	LBS
05	+04.900	INCHES

BQ1 bit on rock E
00:00:31 08/23/92 STOP MODE

CH	CURRENT	UNITS
01	+0024.1	LB-FT
02	+00496	RPM
04	+1480.0	LBS
05	+04.908	INCHES

BQ1 bit on rock E
00:00:33 08/23/92 STOP MODE

CH	CURRENT	UNITS
01	+0023.3	LB-FT
02	+00498	RPM
04	+1484.0	LBS
05	+05.001	INCHES

BQ1 bit on rock E
00:00:35 08/23/92 STOP MODE

CH	CURRENT	UNITS
01	+0024.1	LB-FT
02	+00495	RPM
04	+1504.0	LBS
05	+05.014	INCHES

Appendix 4

The Basic program used to extract peer data from the data logger

```
10    DIM C1$(10)
100   OPEN "C:\DRILLING\TEST1.DAT" FOR INPUT AS #1
105   OPEN "C:\CALCULT\TEST1.DAT" FOR OUTPUT AS #2
110   LINE INPUT#1, C1$(I)
120   FOR K=1 TO 1000
130   FOR I=1 TO 4
140   LINE INPUT#1, C1$(I)
150   NEXT I
160   INPUT#1, CH1, CH2
170   INPUT#1, TORQUE
180   INPUT#1, UNIT0$
190   INPUT#1, RCH1
200   INPUT#1, RPM
210   INPUT#1, UNIT1$
220   INPUT#1, TCH1
230   INPUT#1, WEIGHT
240   INPUT#1, UNIT2$
250   INPUT#1, DCH1
260   INPUT#1, DEPTH
270   INPUT#1, UNIT3$
280   PRINT TORQUE, RPM, WEIGHT, DEPTH
290   PRINT#2, TORQUE, RPM, WEIGHT, DEPTH
300   LINE INPUT#1, C$
310   NEXT K
320   END
```

Appendix 5: Result of the preliminary rock coring test

Bit	Rock	RPM	Bit Weight (lb)	Torque (lb-ft)	PR (in/min)
AQ1	A	507	540	9.35	1.703
AQ1	A	503	540	10.30	2.023
AQ1	B	501	540	10.66	1.509
AQ1	B	507	540	10.53	1.416
AQ1	C	502	540	9.68	1.646
AQ1	C	506	540	10.51	1.796
AQ1	D	490	540	11.20	4.368
AQ1	D	492	540	13.20	3.627
AQ1	E	487	540	13.33	2.291
AQ1	E	490	540	13.89	2.491
AQ1	F	498	540	8.99	1.288
AQ1	F	502	540	8.61	1.288
AQ2	A	501	540	8.06	0.669
AQ2	A	504	540	7.87	0.892
AQ2	B	501	540	6.31	0.173
AQ2	B	501	540	6.20	0.106
AQ2	C	499	540	6.24	0.187
AQ2	C	502	540	6.16	0.173
AQ2	D	499	540	10.70	1.158
AQ2	D	501	540	9.90	1.087
AQ2	E	507	540	11.78	1.126
AQ2	E	507	540	11.23	0.922
AQ2	F	504	540	6.61	0.321
AQ2	F	506	540	6.47	0.233

(cont'd)

Bit	Rock	RPM	Bit Weight (lb)	Torque (lb-ft)	PR (in/min)
BQ1	A	496	540	11.23	2.419
BQ1	A	492	540	13.26	3.804
BQ1	B	497	540	12.29	1.538
BQ1	B	503	540	12.13	1.648
BQ1	C	498	540	11.45	2.152
BQ1	C	519	540	12.09	1.999
BQ1	D	500	540	13.30	2.376
BQ1	D	505	540	13.00	2.284
BQ1	E	505	540	13.45	1.755
BQ1	E	494	540	15.69	1.680
BQ1	F	499	540	12.13	1.546
BQ1	F	495	540	12.13	1.618
BQ2	A	507	540	7.65	0.465
BQ2	A	489	540	6.35	0.133
BQ2	B	502	540	6.98	0.067
BQ2	B	501	540	7.26	0.070
BQ2	C	499	540	6.86	0.116
BQ2	C	488	540	6.81	0.104
BQ2	D	507	540	10.20	0.943
BQ2	D	507	540	10.40	0.915
BQ2	E	497	540	12.39	0.611
BQ2	E	502	540	11.55	0.489
BQ2	F	504	540	6.76	0.168
BQ2	F	504	540	6.75	0.113

Appendix 6: Result of the Latin square rock drilling test

Rock	RPM	Bit Weight (lb)	Torque (lb-ft)	PR (in/min)
A	204	200	4.85	0.017
A	300	500	8.44	0.447
A	395	600	11.21	1.262
A	455	300	6.39	0.214
A	501	450	7.75	0.568
A	607	400	7.38	0.477
B	201	450	7.81	0.040
B	301	300	7.13	0.034
B	402	400	8.33	0.095
B	452	200	7.52	0.022
B	498	500	8.59	0.191
B	596	600	8.69	0.798
C	202	300	5.92	0.065
C	303	400	7.22	0.157
C	398	500	8.48	0.340
C	454	450	7.93	0.363
C	496	600	9.45	1.118
C	605	200	5.23	0.181
D	203	500	11.40	0.662
D	300	600	12.28	0.921
D	399	300	8.55	0.445
D	445	400	10.33	0.843
D	502	200	8.73	0.446
D	598	450	10.04	1.176
E	202	600	13.51	0.654
E	301	450	10.31	0.613
E	401	200	6.84	0.237
E	445	500	12.35	0.912
E	506	400	10.78	0.791
E	600	300	8.20	0.664
F	201	400	6.62	0.038
F	301	200	4.59	0.008
F	400	450	7.80	0.194
F	452	600	8.99	0.473
F	503	300	5.91	0.125
F	602	500	8.32	0.419